الجمهورية الجزائرية الديمقراطية الشعبية
People's Democratic Republic of Algeria
وزارة التعليم العالي و البحث العلمي
Ministry of Higher Education and Scientific Research

Mohamed Khider University - Biskra
Faculty of Science and Technology
Department: Civil and Hydraulic Engineering
Reference: .....

جامعة محمد خيضر بسكرة
كلية العلوم و التكنولوجيا
قسم : الهندسة المدنية و الري
المرجع: .....

Thesis submitted for obtaining the degree of

Doctorate in Civil Engineering

Specialty: Geo-Mechanics and Structures in Interaction

Elaboration et caractérisation d'un bio-composite destiné à la construction

---

Elaboration and characterization of a bio-composite destined for construction

By

Oussama Benaimeche

Thesis defended publicly on: 21 /11 /2019

The jury is composed of:

Mr. Abdelhamid Guettala	Professor	President	University of Biskra
Mr. Mekki Mellas	Professor	Supervisor	University of Biskra
Mr. Miloud Beddar	Professor	Examiner	University of M'sila
Mr. Larbi Belagraa	Lecturer	Examiner	University of M'sila

Acknowledgements

This thesis is the result of four years of work and I am using this opportunity to express my gratitude to everyone who supported me throughout the course of this experience.

I would like to express my deepest appreciation and thanks to my supervisor Professor Mekki Mellas for his guidance and support during these years, his expertise, understanding, and patience added considerably to my research study experience.

I would like to thank professors Andrea Carpinteri and Sabrina Vantadori from university of Parma for their special hospitality and collaboration.

I would also like to acknowledge Pr. Ahmed Bouaziz, Dr. Bouzidi Mezghiche, Dr. Bachir Taallah, Pr. Abdelhak Mabrouki and all the members of civil engineering laboratory of Mohamed Khidher University of Biskra.

A very special gratitude goes to my colleague Nadhir Toubal Seghir for his pieces of advice and precious discussions, we have had long path passed through these years.

I am also grateful to the president of jury Pr. Abdelhamid Guettala who honored me with his presence and chairing the defense jury.

I would also like to express my sincere thanks to the jury members Pr. Miloud Beddar and Pr. Larbi Belagraa for the honor they have offered me, beside devoting their precious time to examine my humble work.

Last but not least, I would like to thank the most priceless persons in my life whose i look up to: my mother and my father, for giving birth to me and supporting me spiritually throughout my life.

Oussama

Education

Is the passport to the future,

For tomorrow belongs to those

who prepare for it today

Malcolm X

ملخص

تستمر صناعة المواد المركبة في التطور والنمو من خلال إدخال مواد وتقنيات جديدة. كبديل للمواد المعدنية، بدأ استخدام المواد ذات المنشأ الطبيعي (خاصة النباتية منها). نظرًا لخصائصها المرغوبة مثل التأثير البيئي المنخفض، التكلفة المنخفضة، القابلية للتحلل الحيوي، الكثافة المنخفضة والخصائص الميكانيكية الجيدة، فقد تم استخدام الألياف النباتية على نطاق واسع كتعزيز في المواد المركبة القائمة على الأسمنت. من بين عائلة الألياف النباتية، تمثل ألياف النخيل المتولدة من الحصاد السنوي لأشجار النخيل كمية كبيرة من الألياف النباتية التي تعتبر عادة نفايات أو تستخدم لتطبيقات الحياة اليومية في نسب قليلة مقارنة بالكميات المتواجدة. تعد ألياف النخيل الشبكية أحد الأنواع التي تنتمي إلى هذه الألياف، وهي عبارة عن حصيرة منسوجة من الالياف تحيط بساق نخيل التمر. تعتبر عملية تثمين قيمة ألياف النخيل الشبكية خطوة رئيسية نحو إنتاج مواد صديقة للبيئة من الأسمنت وخفيفة الوزن وتخفيض تكاليف المواد المخصصة لقطاع البناء.

تقدم رسالة الدكتوراه الحالية بحثًا تجريبيًا حول استخدام ألياف النخيل الشبكية كتدعيم للمواد الإسمنتية. لهذا الغرض، تمت دراسة تأثير إدراج ألياف النخيل الشبكية بكميات متعددة على خصائص المواد الاسمنتية في الحالة السائلة. علاوة على ذلك، تمت دراسة الأداء الميكانيكي لمركبات المواد الاسمنتية من خلال التحقق من سلوكيات الانضغاطية والانثناء والكسور.

تظهر النتائج التي تم الحصول عليها أن الخصائص السائلة للملاط الأسمنتي مع استعمال الياف النخيل الشبكية لم تتأثر من خلال اعتماد عمليات خلط تكون فيها الياف النخيل الشبكية في حالة رطبة. أظهرت الخصائص الفيزيائية والميكانيكية المختارة للمركبات القائمة على الأسمنت و المدعمة بألياف النخيل الشبكية انخفاض مع زيادة تدريجية في محتوى الألياف. ومع ذلك، فإن إدراج ألياف النخيل الشبكية بشكل عام يحسن سلوك ما بعد الذروة، ليونة وتأخير انهيار مركبات الملاط الإسمنتية مقارنة مع عينات الملاط الغير مدعمة. وقد أظهرت هذه الدراسة أيضا خصائص مهمة في نتائج الكسر التي تم الحصول عليها لمحتوى منخفض من ألياف النخيل الشبكية (وهو، 2% من حيث الحجم)، قيمة صلابة كسر مشابهة لما هو مذكور في الدراسات السابقة للمواد الاسمنتية.

الكلمات المفتاحية : الملاط القائم على الإسمنت، ألياف النخيل الشبكية، مقاومة الضغط، مقاومة الانثناء، صلابة الكسر، نموذج المعاملين المعدل

Abstract

The composite materials industry evolves and grows continuously by introducing new materials and technologies. As an alternative for mineral materials, materials of natural origin (especially vegetable) started to be used. Due to their desirable characteristics such as low environmental impact, low cost, biodegradability, low density and good mechanical properties, the vegetable fibers have been extensively used as reinforcement in cement-based composite. Among the vegetable fibers family, date palm fibers (DPF) generated from the annual crop taking of date palm trees represent a considerable amount of vegetable fibers which normally considered as a waste or it is used for applications of daily life in low values of the total products. Date palm mesh fibers (DPMF) is a type that belong to these fibers, it is a cross mat of single fibers surrounding the stem of the date palm tree. The valorization of the DPMF is a major step toward the production of green lightweight cement-based materials and reducing the cost of materials destined for construction sector.

The present thesis exposes an experimental investigation on the use of DPMF as reinforcement for cementitious materials. For this purpose, the influence of the DPMF's inclusion with multiple fractions on the fresh properties of a cement mortar was studied. Furthermore, the mechanical performance of cement mortar composites has been examined through investigating the compressive, flexural and fracture behaviors.

The results obtained show that the fresh properties of the reinforced mortar composites were not influenced after adopting such a mixing process in which the DPMF were introduced in wet state. The selected physical and mechanical properties of the cement-based mortar composites showed a decrease with the gradually increase of fibers content. Nevertheless, the inclusion of DPMF improves the post-peak behavior,

the ductility and delays the failure of cementitious composites compared with plain mortar specimens. Also this study has shown an interesting fracture properties obtained for low content of DPMF (2% by volume). Previous research works reported a similar fracture toughness value.

Keywords: Cement-based mortar, Date palm mesh fibers (DPMF), Compressive strength, Flexural strength, Fracture toughness, Modified two-parameter model.

Résumé

L'industrie des matériaux composites continue d'évoluer et de se développer en introduisant de nouveaux matériaux et technologies. En guise d'alternative aux matériaux minéraux, les matériaux d'origine naturelle (et notamment végétale) commencent à être utilisés. En raison de leurs caractéristiques souhaitables, telles que faible impact environnemental, faible coût, biodégradabilité, faible densité et bonnes propriétés mécaniques, les fibres végétales ont été largement utilisées comme renfort dans les composites à base de ciment. Parmi les fibres végétales, les fibres de palmier dattier issues de la récolte annuelle de palmiers dattiers représentent une quantité considérable de fibres végétales normalement considérées comme des déchets ou utilisées pour des applications de la vie quotidienne à des valeurs faibles de ces produits. Les fibres à mailles de palmiers dattiers sont un type de fibres appartenant à ces fibres, c'est un tapis corsé tissé entourant le tronc du palmier dattier. La valorisation du fibres à mailles de palmiers dattiers constitue une étape majeure dans la production de matériaux à base de ciment légers et écologiques et permet de réduire les coûts des matériaux destinés au secteur de la construction.

La thèse actuele représente une recherche expérimentale sur l'utilisation de fibres à mailles de palmiers dattiers comme renforcement pour les matériaux à base de ciment. À cette fin, l'influence de l'inclusion de fibres à mailles de palmiers dattiers à fractions multiples sur les propriétés fraîches d'un mortier de ciment a été étudiée. En outre, les performances mécaniques des composites de mortier de ciment ont été étudiées en étudiant les comportements de compression, de flexion et de rupture.

Les résultats obtenus montrent que les propriétés fraîches du mortier de ciment en incluant des fibres de datte n'ont pas été influencées, par l'adoption d'un tel processus

de mélange dans lequel les fibres à mailles de palmiers dattiers était introduit à l'état humide. Les propriétés physiques et mécaniques choisies des composites de mortier à base de ciment ont montré une diminution avec l'augmentation progressive du contenu en fibres. Néanmoins, l'inclusion de fibres à mailles de palmiers dattiers améliore généralement le comportement post-pic, la ductilité et retarde la défaillance des composites à base de ciment par rapport aux échantillons de mortier ordinaire. Cette étude a également montré les propriétés de fracture croisées obtenues pour une faible teneur en fibres à mailles de palmiers dattiers (ce qui correspond à 2% en volume), une valeur similaire de ténacité à la rupture été rapportée dans la littérature.

Mots-clés: Mortier à base de ciment, Fibres à mailles de palmiers dattiers, Résistance à la compression, Résistance à la flexion, Ténacité, Modèle modifié à deux paramètres

Contents

List of Figures

List of Tables

Frequently Used Symbols and Abbreviations

Symbol	Explanation
α	Crack length
β	Constant related to the geometry of the specimen
Δ_F	Displacement of any value of force
ρ	Apparent density
σ	Applied stress
σ	Far-field stress
θ	Crack kinking angle
$\underline{a}$	Effective crack length
$F_{c,\max}$	peak load due to compression
G_{IC}	Critical strain energy release rate
K_{IC}	Critical stress intensity factor
K_I	Stress intensity factor
R_c	Compressive strength
R	Crack growth resistance
U_T	Total strain energye
U	Elastic energy release by the system
$V(\alpha_0)$	Geometrical parameter
W	Energy required for a crack to propagate
A	Crack area

a_0	Initial crack length
$a_1 + a_2$	Total length of the deflected crack
B	Depth of the specimen
C_i	Initial compliance
C_u	Compliance at the maximum load
d	Distance
dA	Infinitesimal increase of the crack area
E	Young's modulus
F	Virtual force
G	Total energy release rate
G_f	Fracture energy
H	Humidity rate
I_t	Toughness index
$K^s_{(I+II)C}$	Critical stress-intensity factor under mixed mode
K^S_{IC}	Mode I critical Stress intensity at the tip of the effective crack
$K_{IF,0}$	Mode I SIF of a straight crack under a pair of virtual forces
$K_{IF,1}$	Mode I SIFs of a kinked short branch crack under a pair of virtual forces
$K_{IF,2}$	Mode I SIFs of a kinked long branch crack under a pair of virtual forces
K_{IF}	Mode I SIF due to the virtual forces
$K_{IIF,1}$	Mode II SIFs of a kinked short branch crack under a pair of virtual forces
$K_{IIF,2}$	Mode II SIFs of a kinked long branch crack under a pair of virtual forces
K_{IIF}	Mode II SIF due to the virtual forces
$K_{IIP,1}$	Mode II SIF of a kinked short branch crack under bending loades
$K_{IIP,2}$	Mode II SIF of a kinked long branch crack under bending loades
K_{IIP}	Mode II SIF due to the loading force
$K_{IP,0}$	Mode I SIF of a straight crack under bending loades
$K_{IP,1}$	Mode I SIF of a kinked short branch crack under bending loades
$K_{IP,2}$	Mode I SIF of a kinked long branch crack under bending loades
K_{IP}	Mode I SIF due to the loading force
m	Prescribed multiplier

P	Load applied
P_f	Peak load due to bending
P_{max}	Peak load
R_f	Flexural strength
S	Loading span
v	Poisson's ratio
V_0	Volume of the dry specimen
V_h	Volume of the specimen corresponding to Hummidity rate
w	Opening width of the notch
W	Width of the specimen
z	Generic integration variable

Abbreviation	Explanation
CCM	Cohesive crack model
CBM	Crack band model
CMOD	Crack mouth opening displacement
CTOD	Crack tip opening displacement
DPF	Date palm fibers
DPMF	Date palm mesh fibers
C_2S	Dicalcium silicate (Belite)
DGFM	Double-G fracture model
DKFM	Double-K fracture model
ECM	Effective crack model
FRC	Fiber reinforced concrete
FCM	Fictitious crack model
FPZ	Fracture process zone
GGBS	Ground granulated blast furnace slag
JFRCC	Jute fibers reinforced cementitious composite
LEFM	Linear elastic fracture mechanics
MTPM	Modified two parameter model
NF	Natural fibers
NEFM	Non-linear elastic fracture mechanics
PM	Plain mortar
PC	Portland cement
PFA	Pulverized fly ash
ROI	Region of Interest
RM	Reinforced mortar
SPF	Saturation point of the fibers
SCB	Semi-circular bend
SEM	Size-effect model
SIF	Stress intensity factor
C_4AF	Tetracalcium aluminoferrite (Ferrite)

C_3A	Tricalcium aluminate (Aluminate)
C_3S	Tricalcium silicate (Alite)
TPM	Two parameter model
VF	Vegetable fibers

CHAPTER 1

Introduction

1.1 Research Background

During the last years, problems related to the environmental issues led scientific researchers to look for suitable ways to introduce the production wastes in manufacturing the materials of construction. In this context, synthetic fibers as steel, plastic, carbon fibers and glass fibers were extensively used in various domains of industry such as automotive, construction, aerospace and sport, these fibers have been utilized regarding their low cost, simple methods of production, interesting mechanical performances, moreover, the abundant biomass in nature created a serious environmental problem due to disposing a large amount of bio-sourced wastes. Generally, the latter is neutralized through burning, consequently, it leads to raise the dioxide emission rate. New social awareness has brought more attention toward valorizing these wastes in order to eliminate their bad impact on the environment and improve its economic value, which pushed many researchers to look for characterizing the physical and the mechanical properties in order to study the feasibility of reinforcing such construction materials.

Natural fibers (flax, jute, sisal, coir and bamboo fibers) have been proposed as a convenient alternative for classical synthetic fibers due to their desirable characteristics such as biodegradability, low cost, ability to be recycled, zero carbon footprint and low density **[1]**.

Since the cement-based materials have a low tensile and fracture properties, the addition of fibers is one of the effective ways in order to improve the strength and the toughness of these materials, the latter behavior is directly related to the capability of

material resistance against the crack propagation which is called the fracture toughness. In fracture mechanics, concrete and metals need different approaches. For both concrete and metallic materials, fracture mechanics is considered as nonlinear because of the nearness of such a zone in front of stress-free crack tip, in which the material exhibits a nonlinear behavior. Such a zone is known as the plastic zone in brittle and ductile metals, it is for the most part described by either perfect yielding or hardening plasticity of the materials, while such a zone is known as fracture process zone (FPZ) in the concrete and it experiences a softening damage (tearing).

Concrete just as rocks and numerous different materials, are usually known under the name of quasi-brittle materials. Generally, in ductile materials, the applied energy is dispersed as plastic energy to shape plastic zones, in this case, the Nonlinear Elastic Fracture Mechanics (NEFM) can be utilized for the determination of fracture behavior. Whereas, in brittle materials, the applied energy is devoured as a surface energy to shape new broken surfaces **[2]**, with the surface energy being essentially more prominent than the plastic energy, in this case, the Linear Elastic Fracture Mechanics (LEFM) can be applied to investigate the crack propagation and the fracture process. Furthermore, in quasi-brittle materials, energy is responsible for the formation of the fracture process zone **[3]**.

Among vegetable fibers, those obtained from date palm (Phoenix Dactylifera, one of the most cultivated palm around the world) have been proved to be a good alternative for reinforcement of cement-based composites. The date palm tree is composed of: (a) a long trunk; (b) a mesh, surrounding the trunk; (c) leaves; (d) reproductive organs; (e) fruit bunches. The mesh is characterized by a fibrous structure, which creates a natural woven mat of crossed fibers of different diameters and is considered as a lignocellulosic material. The date palm is commonly found in North Africa, Middle East, India and USA. There are about 100 million date palm trees in the world, and each tree can grow for more than 100 years **[4]**.

In Algeria, there are more than 18.7 million trees, and the annual trimming operations produce enormous quantities of agricultural wastes, which are usually thrown away, except small quantities used for traditional products. Such wastes can represent an abundant source of low-cost raw material for industrial purposes. Therefore, the development of cement-based composites reinforced with this agricultural material represents an excellent solution for an efficient utilization of such wastes as a renewable resource **[5]**.

1.2 Objectives

The objective of the present thesis is to study the feasibility of using date palm mesh fibers as reinforcement for cement based materials. In particular, the research aims are to study:

- The effect of the DPMF on the fresh properties of the cement based-materials by examining the workability and the consistency of cement mortar prepared by multiple fractions of DPMF.
- The effect of the DPMF on the density and the compactness properties of the cement-based materials.
- The affected mechanical behavior including tests of compressive and three-point bending applied on a cement-based material prepared by multiple fractions of DPMF.
- The influence of the DPMF on the fracture properties of cement-based materials by examining the fracture toughness of notched beam specimens prepared by cement mortar reinforced by multiple fractions of DPMF.
- The effect of DPMF addition on the energy absorption capability of the cement-based material by measuring the toughness index which is determined through the analysis of the Load-CMOD curves.

1.3 Layout of the Thesis

In order to achieve the aforementioned objectives, the present thesis is structured as follows:

- **Chapter 1** presents a general introduction in which it states the area of the present research study and the intended objectives to be achieved.
- **Chapter 2** presents an overview of the previous studies on the utilization of Vegetable fibers (VF) in cementitious materials. In particular, the chemical, physical and mechanical characterization of vegetable fibers have been reviewed. The fresh properties of cementitious materials reinforced by different varieties of vegetable fibers have been shown. Furthermore, the mechanical properties of cementitious material reinforced with VF have been also presented. Finally, the research gap in which it resumes the present work is exposed.

- In **Chapter 3**, a theoretical background on the available fracture mechanics approaches is presented. The earlier linear elastic fracture mechanic (LEFM) applied for metallic material and its feasibility of application on cementitious materials has been shown. The most powerful nonlinear fracture mechanic models for the fracture study of cementitious materials have been presented such as fictitious crack model (FCM), Two parameter model (TPM) and the modified version (MTPM) which includes the possibility of the crack deflection.

- **Chapter 4** is devoted to the characterization of the used materials in this study, and the methods used in the experimental campaign. The chemical, physical and mineralogical properties of the used matrix containing cement and sand are presented, the mechanical and physical characteristics of the used DPMF are also presented. Moreover, the tests procedures according to the available recommendations of the workability on the flow table, the compressive test and three-point bending test on unnotched and notched specimens were demonstrated.

- The results obtained from the experimental program and their discussions are reported in **Chapter 5**. Firstly, the fresh properties of cement based mortar composites is presented and discussed. Then the hardened properties of the cement based mortar composites including the flexural behavior, the compressive strength are mentioned. Moreover, the fracture properties results of the cement based mortar are examined by the determination of the fracture toughness, the toughness index related to the absorbed energy of different mortars are presented.

- A general conclusion is given at the end that summarizes the main results of the present research study. Also the perspectives and future work outcomes from this study are suggested.

CHAPTER 2

State of the art

2.1 Introduction

The use of vegetable fibers (VF) as a raw material returns to old civilizations vanished centuries ago. For instance, 3000 years ago in Egypt, walls were built by reinforcing clay with straw. Recently, a new social awareness has pushed the scientific community to look for suitable solutions for the environment and to reduce the depletion of petroleum resources. Thus, since the second half of the twentieth century, VFs have been extensively used as a suitable reinforcement in many fields of industry **[6]**. During the last few years, a significant effort has been made by scientists and engineers to provide a technical database for the various types of VF. The reinforcement of polymeric materials with VF as an alternative to conventional synthetic reinforcement can thus become a reality, and contribute to the increase of the economic value of VF wastes. Furthermore, the production of low cost and eco-friendly composite materials that have some advantages for particular applications such as thermal and acoustic insulation is a very possible concept **[7]**. The reinvention of natural fibers and their combination with polymers has given rise to a new class of materials that can compete with or replace synthetic materials for some structural, but mostly for nonstructural and semi-structural applications.

The introduction of VFs in cementitious matrices started in the beginning of eighties (1980s). More recently, housing construction has seen an increase in the application of VF in various non-structural and some structural building elements in both exterior and interior applications such as walls, floors, roofing, siding, external cladding, internal lining, building boards, bricks, bracing and fencing. VF composites are also found

in the construction of decks, as well as in the building of roads and bridges **[6]**.

The mechanical behavior of VF reinforced cementitious composites varies according to the origin of the fibers and the type of cementitious matrix. Generally, the utilization of VF in lightweight cementitious composites has shown interesting results due to the compatibility between the fiber and the matrix. Lightweight cementitious materials have mechanical properties close to that of VFs, meaning that they can stop the matrix from breaking the fibers, guarantee a good adhesion and reduce the pullout phenomena of fibers inside the matrix. Furthermore, VF could support the matrix by exhibiting more tensile strength to the lightweight cementitious matrix, which is basically a brittle material, therefore improving the cracking resistance of cementitious materials.

The chapter reviews the recent research papers which focused on the utilization of VF in the reinforcement of cementitious materials. Firstly, it represents a general overview on the availability of VFs and their properties. Thereafter, the selected mechanical behavior of various types of cementitious materials is summarized.

2.2 Short introduction on vegetable fibers

2.2.1 Overview

Natural fibers can be classified according to their origin into animal, mineral and vegetable fibers (VF). The latter one, which are also known as lignocellulosic fibers due to their main components being cellulose, hemicellulose, and lignin **[8]** are classified according to their chemical composition as wood and non-wood fibers. Wood fibers have a higher amount of lignin when compared with non-wood fibers, and can be divided into either softwood or hardwood fibers. Softwood fibers can be found in pines, firs, etc..., and hardwood fibers are found in birch, eucalyptus, beech, etc... Non-wood fibers cover four major categories according to which part of the plant the fibers are located (e.g., bast, seed, leaf, stalk and reed fibers) **[1]**. Figure 2.1 shows examples of natural fibers and their classification based on **[9]**.

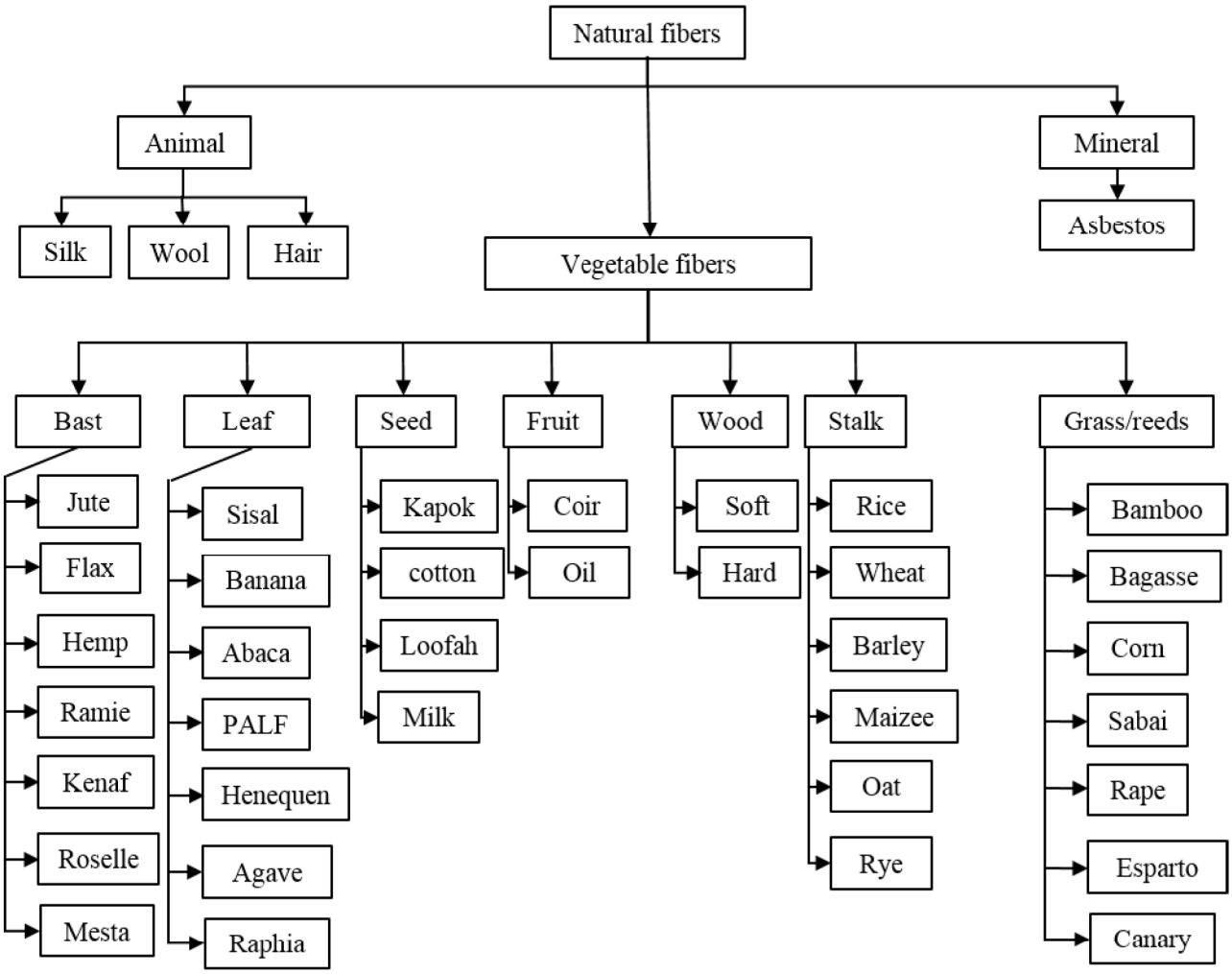

Figure 2.1: Classification of natural fibers **[8, 9]**

The actual trend of the waste generation process from abundant in nature agro-based materials such as VF has found a wide application in multiple fields of industry, as shown in Table 2.1 (based on **[10]**). The annual worldwide production of VF derived from wood and non-wood fibers is presented in Figure 2.2, based on the studies of **[10, 11, 12]**.

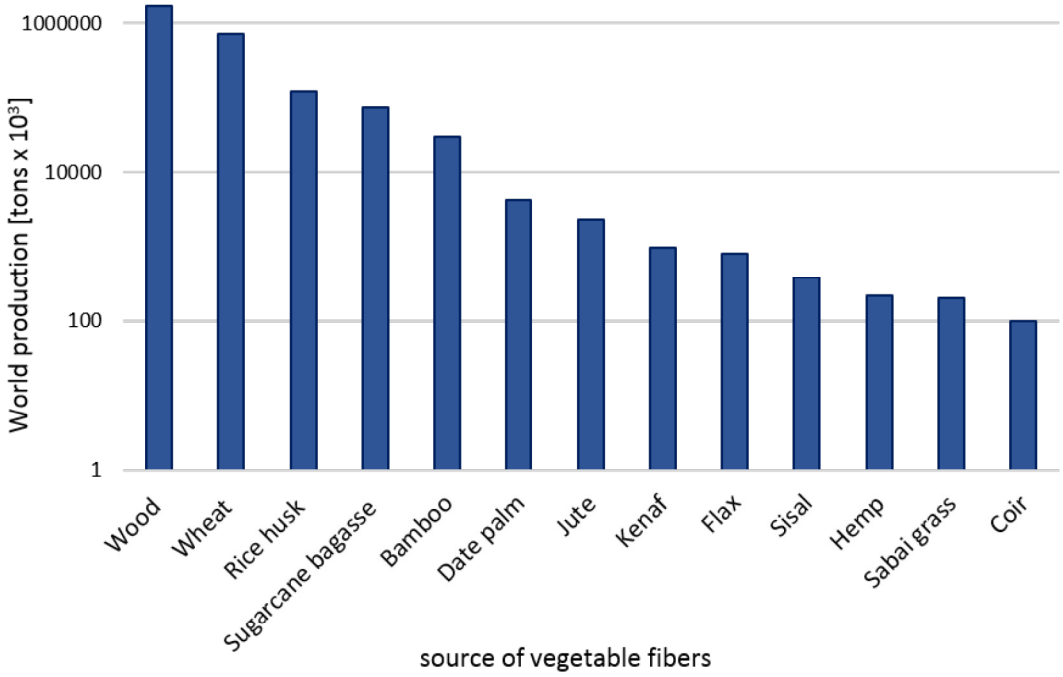

Figure 2.2: Annual production of VF **[10, 11, 12]**.

Table 2.1: Fields of application and the market of natural fiber composites **[10]**.

Application field	Part in market
Construction and building	15%
Electrical and electronic	4%
Agriculture	3%
Functional	2%
Automotive and transports	16%
Textiles	18%
Consumer goods	18%
Packaging-flexible	9%
Packaging-rigid (incl. Food service-ware)	15%
Other	1%

The price of VF when compared with the price of synthetic fibers is very low, for example, the price of glass fibers varies between 1200 and 1800 $/ton. Whereas, VF costs between 200 and 1000 $/ton **[1, 13]**. Moreover, the price of VF varies depending on the available amount and the market demands of these fibers. For instance, the yearly product of date palm and hemp fibers is 4200000 tons and 214000 tons, respectively.

This difference in the production ratio makes the date palm fibers 60 times cheaper than hemp fibers, with a price value of about 20 $/ton **[10]**. More details concerning the price of some VFs are shown in Figure 2.3. The structure of plant fiber is compa-

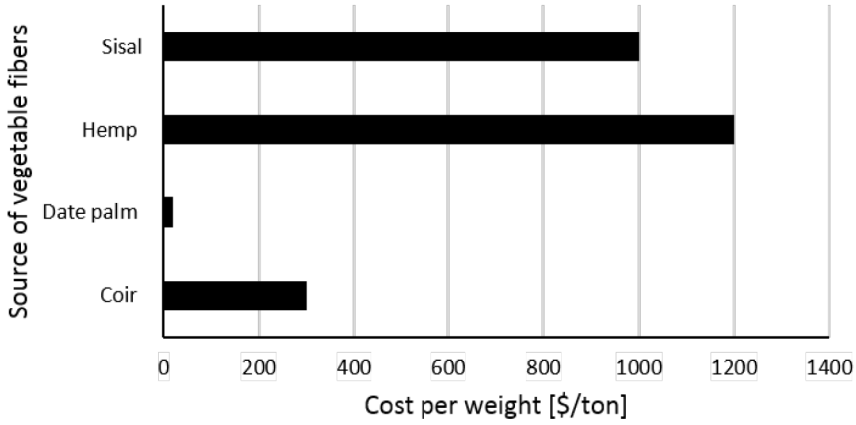

Figure 2.3: Price of selected VF products.

rable to a stack of composite folds, whose structure is detailed in Figure 2.4 (based on **[14]**).

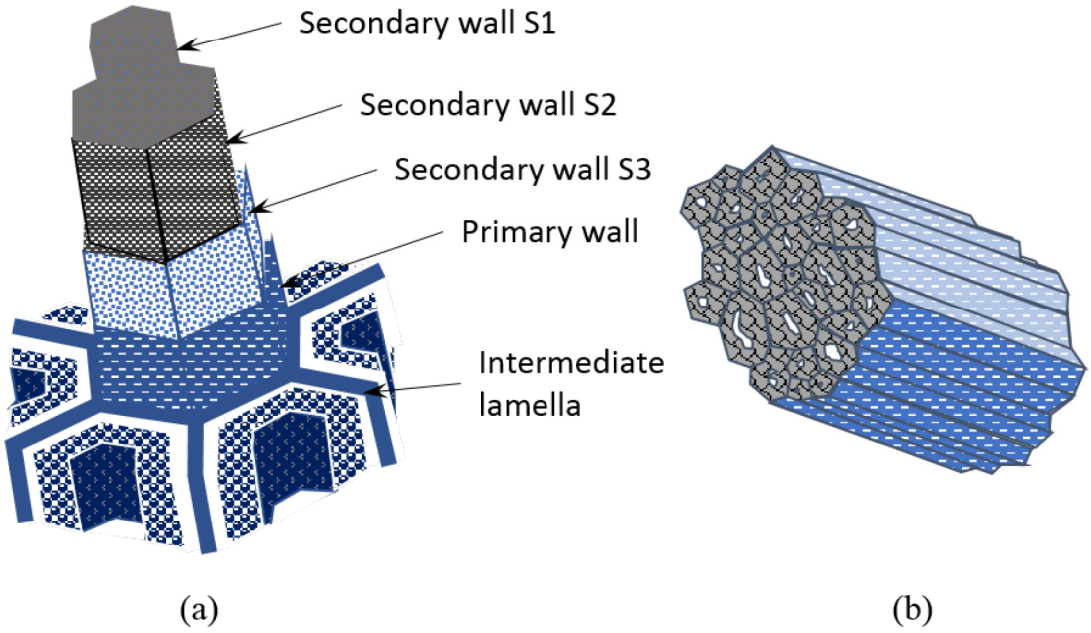

Figure 2.4: (a) Complete structure of hemp fiber in a bundle. (b) Fibrillar structure of hemp fiber.

The fiber consists of a primary and a secondary wall, with the secondary wall consisting of the 3 layers S1, S2, and S3. The S2 layer is the thickest one and sets the behavior of the whole fiber. This multilayer structure imparts anisotropy to the material. In a plant, the fibers are usually assembled in the form of a bundle, which in turn forms their polygonal shapes. The primary and secondary walls contain a frame formed of cellulose microfibrils that is surrounded by a matrix containing hemicellulose and lignin.

2.2.1.a The cellulose

Cellulose is a natural polymer and is the most available biopolymer on earth. It can be found in many fields of industry, such as packaging, textiles and paper, as well as being used as a food additive. Cellulose consists of long chains of glucose anhydride unit molecules of up to 15000 molecules. The glucose anhydride particles are linked together by beta bonds [β(1,4)]. The cellulose molecule has a linear formation due to this bonding configuration (see Figure 2.5). The degree of polymerization (d.p) determined by scientists, which is based on counting the glucan residues, is about 10000 for wood cellulose **[11]**.

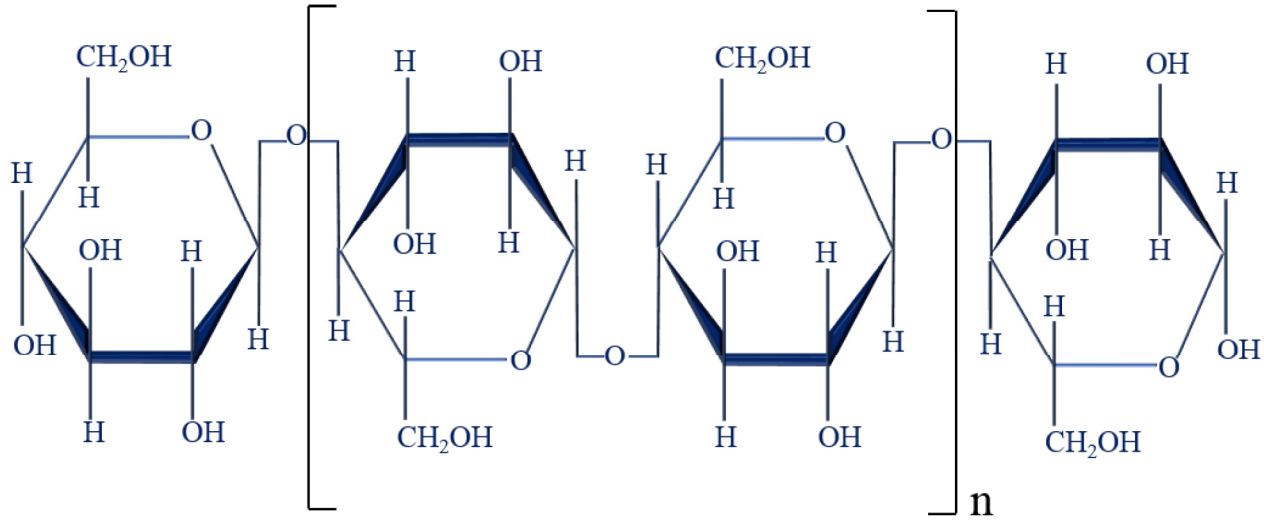

Figure 2.5: Cellulose molecule.

The cell unit form of cellulose is known in literature by different names, such as microfibrils, elementary fibrils, and protofibrils. Such a configuration of different cellulose components is shown in Figure 2.6 (based on **[10]**).

2.2.1.b The hemicellulose

Hemicellulose is a natural polymer like cellulose, consisting of carbohydrate monomers. However, hemicellulose consists of a variety of carbohydrate monomers, unlike homopolysaccharide cellulose. Thus, the monomers that hemicellulose consists of are arabinose, mannose, galactose, glucose, and xylose. Since, hemicellulose has considerable side-branch groups, its structure is more open and non-crystalline. Hemicellulose is more hygroscopic than cellulose and attracts more water molecules due to its open structure. The degree of polymerization of hemicellulose in wood is about 100 to 200, which is very low when compared to that of cellulose of 10000. The difference between wood and non-wood fibers does not appear in the content of cellulose, however, it does appear in the contents of hemicellulose and lignin. Non-wood fibers such

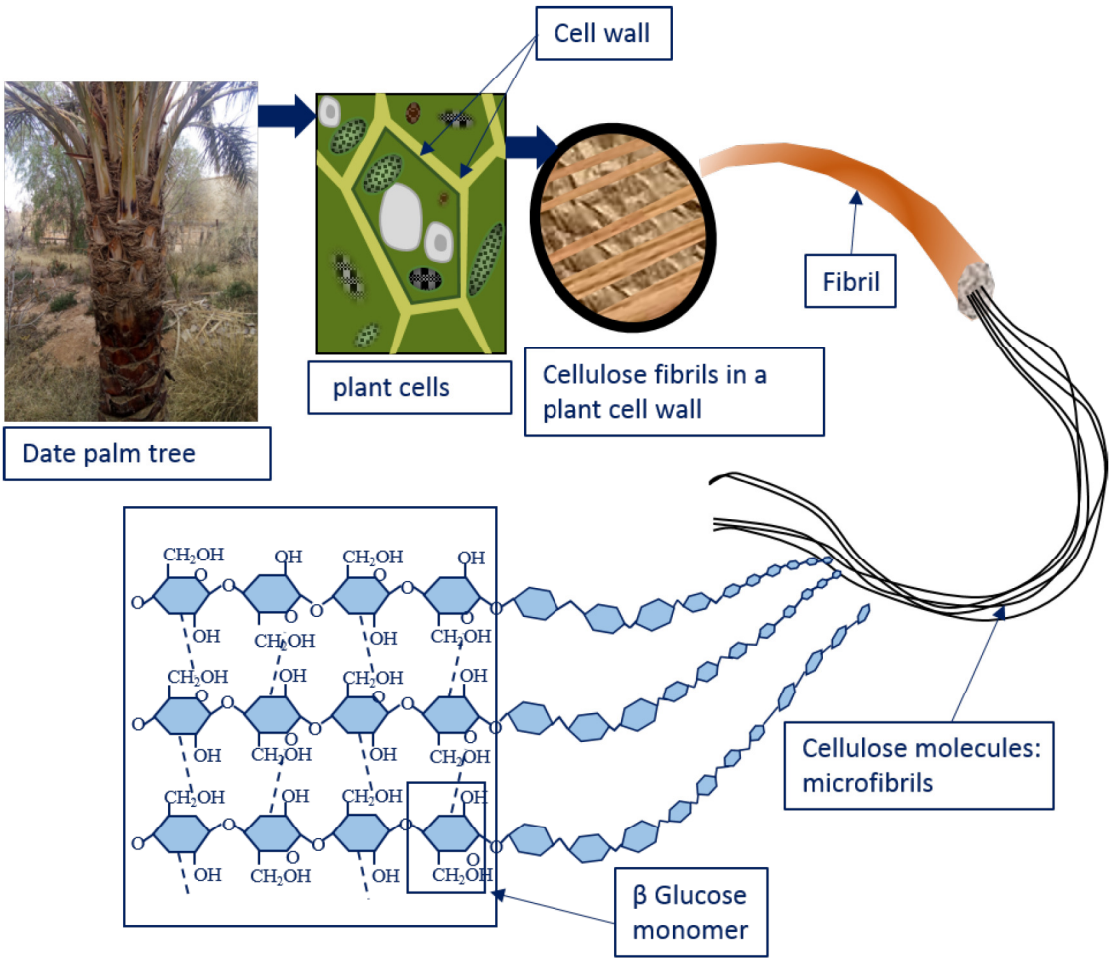

Figure 2.6: Organization of cellulose components in the cell wall of a typical plant fiber.

as grasses (wheat, corn and rice) contain up to 40% of the major hemicellulose found in grasses, whereas wood fibers are composed of 25-35% of hemicellulose by dry weight. Figure 2.7 illustrates a typical hemicellulose molecule found in a type of wood fiber named Arabinoglucuronoxylan (xylan) **[11]**.

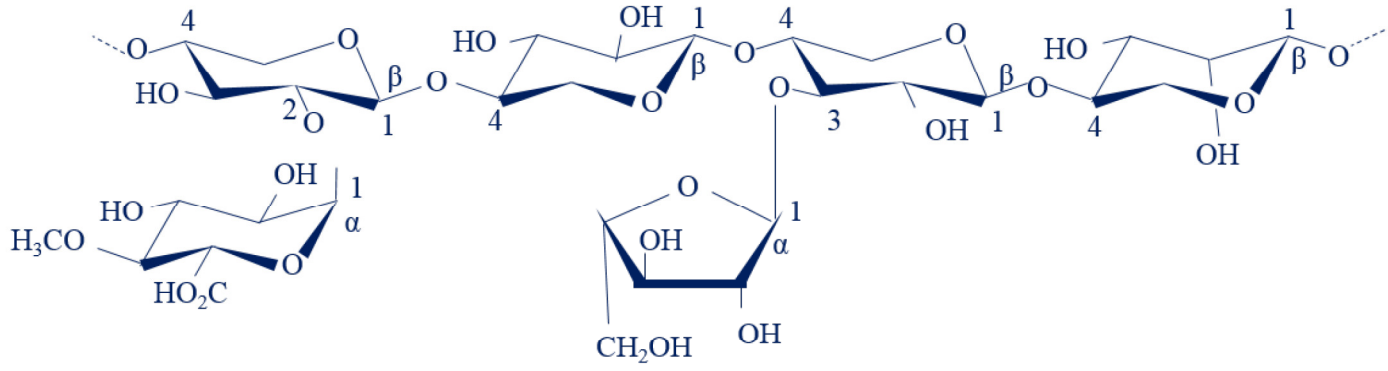

Figure 2.7: Structure of hemicellulose (xylan) consisting of a xylopyranose backbone, with glucuronic acid (1→2) and arabinofuranose (1→3) side branches.

2.2.1.c The lignin

Lignin is an extremely heterogeneous macromolecule that represents about 30% of the organic carbon in the biosphere. Lignin is totally amorphous, and unlike the other carbohydrate-based cellulose and hemicellulose, it contributes to the protection of the cell walls by working as the glue that holds the cells. Lignin has an aromatic structure represented by three precursors: p-coumaryl, sinapyl, and coniferyl alcohol (see Figure 2.8 (based on **[11]**)). The contents of lignin in a vegetable fiber vary from 2% to up to 45% **[10, 11]**.

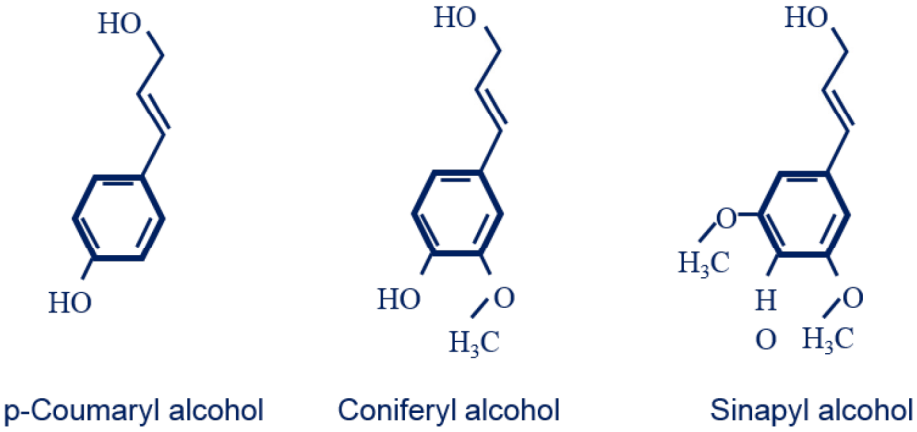

Figure 2.8: Structure of lignin precursors.

2.2.2 Mechanical properties of vegetable fibers

Vegetable fibers (cotton, jute, hemp, flax, sisal, kenaf, coconut, abaca, wood, etc...) have biological structures mainly composed of cellulose, hemicelluloses and lignin. Cellulose is a polymer that, unlike the other components of fiber that have an amorphous structure, it has a largely crystalline structure with a modulus of elasticity of about 136 GPa compared to that of 75 GPa for glass fibers. Vegetable fiber is comparable to a composite material reinforced with fibrils of cellulose. The matrix is mainly composed of hemicellulose and lignin. The cellulose fibrils are helically oriented at an angle called the "microfibrillar angle". This angle is located in between the fibrils and the axis of the fiber. The degree value of the microfibrillar angle is conditioning the stiffness of the fiber. The properties of natural fibers are often subject to discussion due to the fact of the techniques used to cultivate, extract or separate the fibers vary significantly, which may modify their behavior. For instance, the factors that can affect the properties of VF could be attributed to the variety, the conditions of cultivation (soil, treatment, climate), maturity, degree of preparation (retting, scutching, combing ...), moisture content, crystalline structure (degree of crystallinity, degree of polymerization, cellulose type ...), and morphology (cell diameter, microfibrillar angle, lumen

size), etc. Usually, the amount of reinforcement and the orientation of fibers in a composite material set the elastic and rupture characteristics. Similarly, in a plant fiber, the physical properties of natural fibers are mainly determined by the chemical and physical composition, structure, the percentage of cellulose, the micro fibrillar angle, the aspect ratio L/ d (length / diameter: which is an important parameter allowing the load transfer between the fibers and matrix), the transversal section, and the degree of polymerization. To simplify, for a given percentage of cellulose, the microfibrillar angle will be weak and the strength of the fiber will be higher; moreover, the microfibrillar angle will be significant and the elongation at breakage will be important. The complexity of physical, mechanical or thermal property measurements makes the characterization of VF more delicate. These dispersions follow the structural differences observed in the fibers. For example, the size of cells not only depends on the variety of the fiber to which they belong, but also on their maturation stage, their "meteorological history" and their location in the plant. The mechanical properties of different fibers from different origins of plants used for the reinforcement of common composite materials are shown in Figure 2.9 (based on **[12, 15]**). By taking into account the natural behavior of these fibers, some dispersions can be noticed.

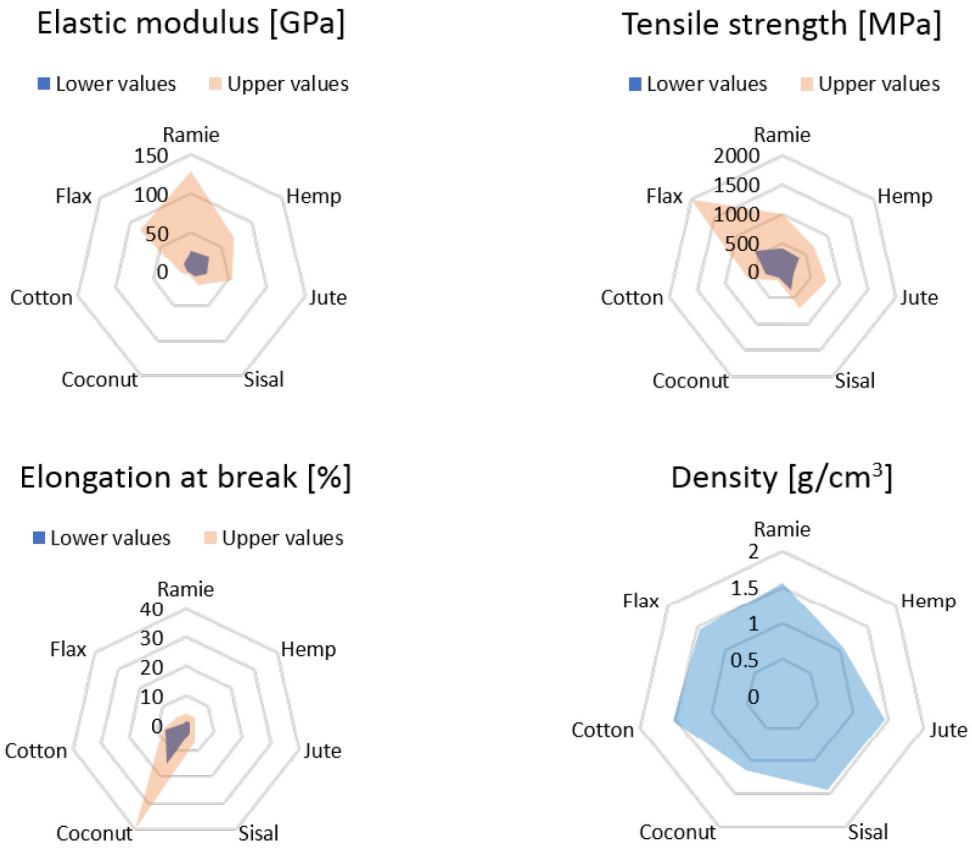

Figure 2.9: The average mechanical properties of different types of VF.

2.2.3 Chemical properties of vegetable fibers

The main constituents of VF are cellulose, hemicelluloses and lignin. Other products like proteins, pectin, starch, and inorganic salts are present in smaller amounts **[16]**. The chemical composition of VF depends on its origin, but in general, cellulose is always predominant with percentages by weight ranging from 22% for Sabai fibers to 85% for linters of cotton (see Figure 2.10 (based on **[12, 17]**). Lignin concentrations vary from 7 to 24% by weight, and those of hemicelluloses from 12 to 27% by weight. These compounds are heteropolymers, which exhibit a great variability in its chemical composition according to their origin. The inorganic compounds, are characterized by their ash content, also vary depending on the nature of the fiber. Thus, this content is about 1% by weight for wood lignocellulosic fibers and of the order of 14% for fibers from rice.

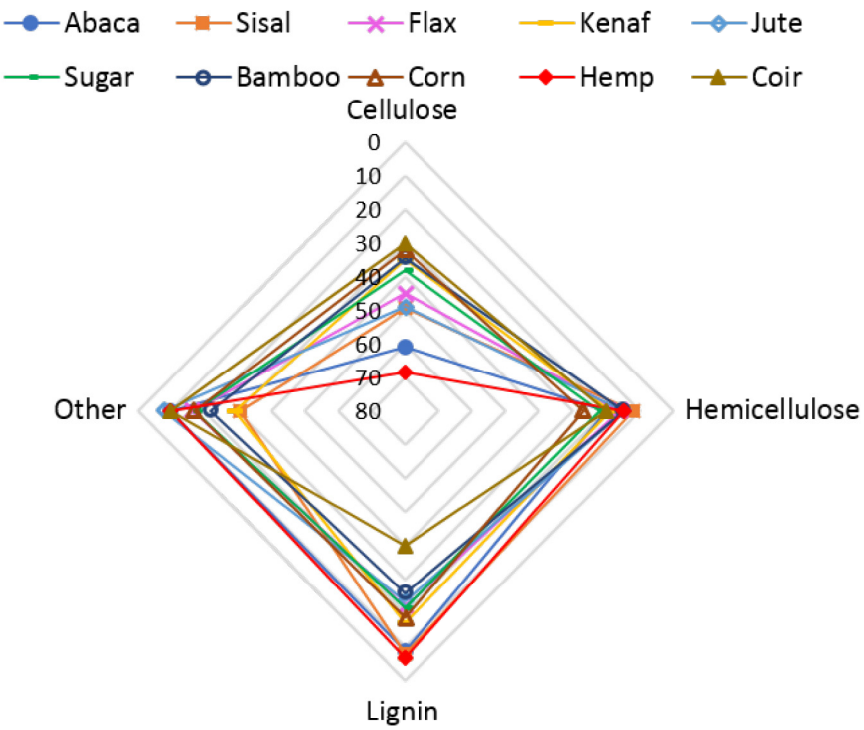

Figure 2.10: Chemical analysis of some VFs.

2.2.4 Physical properties of vegetable fibers

2.2.4.a Hygroscopic properties of vegetable fibers

The dimensional instability with respect to moisture is the main property of wood, which makes its use more delicate. When a tree is alive, it contains water that flows through its cells. The wood material, therefore, contains a certain rate of humidity, depending on the weather conditions. Water plays the role of plasticizer for the polymer chains constituting the cell walls, which is the reason behind the fact that the moisture content and diffusion phenomena govern all the characteristics of the wood. If not for the constituent water, represented by the atoms of hydrogen and oxygen composing the molecules of the polymer's structure, water is found in two forms:

- Free water: it fills the cells and the vessels, is held by capillary forces and is not involved in dimensional variations.
- Bound water: it is fixed on the polymers structure by physisorption or chemisorption. The forces involved are electrostatic or of the type of hydrogen bonds with hydroxyl groups.

The dimensional variation of hygroscopic material is mainly due to the water content, with the amount of water (bound water and free water) contained in the wood being characterized by a parameter called "moisture content of wood", which is defined as the ratio:

$$M(\%) = \frac{(W_h - W_0)}{W_0} \times 100 \tag{2.1}$$

Where;

W_h: the humid weight of specimen

W_0: the anhydrous weight of the specimen

During the wood drying process, it is the free water that evaporates first. The fiber saturation point of the wood is reached when the moisture content is about $M = 30\%$. By continuing the drying process, it is the bound water which begins to evaporate. Dry wood in the air has a moisture content of 13 to 17% according to the seasons. It can have a drier state when artificially dried; in particular, it reaches an anhydrous state after a dry cycle for several hours in an oven at a temperature of 100 to 105 °C. Therefore, it is conceivable that there is a moisture content threshold for which the adsorption sites

are saturated (cell walls have the maximum amount of bond water). When there is no free water, the fiber saturation point (FSP) is reached. The moisture content at the FSP is very variable depending on the species, but is between 25 and 35% of moisture content for most types of fibers. Generally, it is more suitable to give a value of 30%, which corresponds to the behavior of the majority of species.

The moisture content of some types of VF is significantly different, as shown in Figure 2.11 (based on the studies of **[18, 19]**). This difference is related to the hydrogen bonding of cellulose and the amount of hemicellulose.

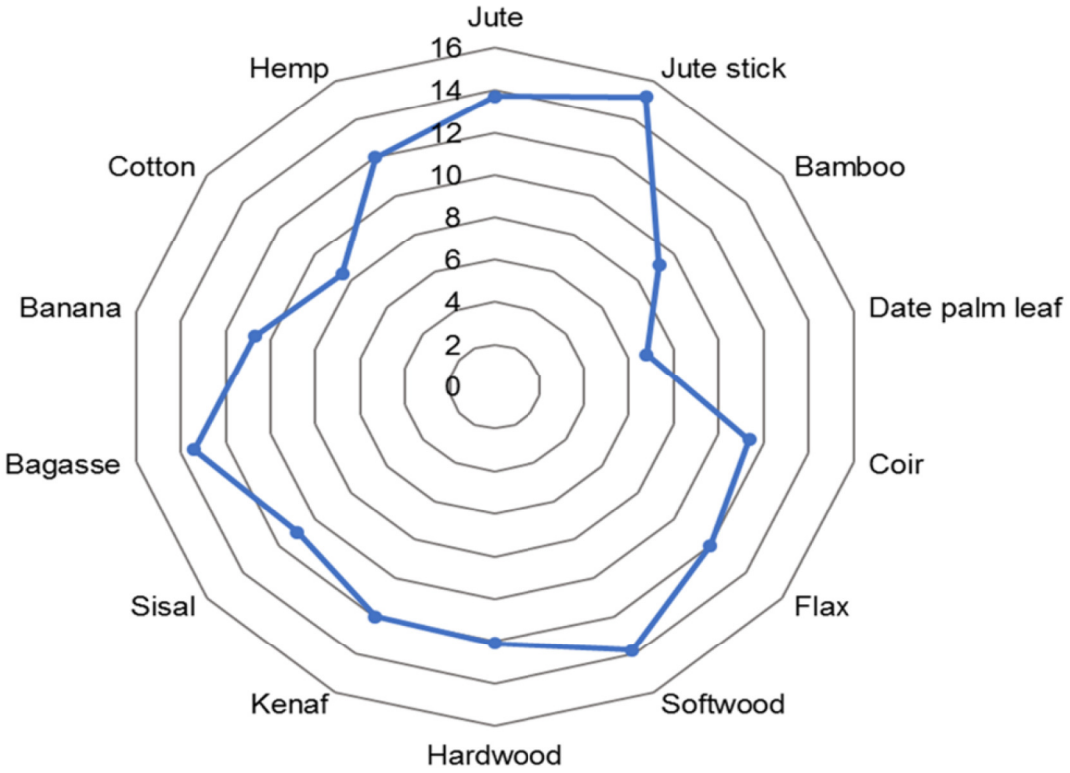

Figure 2.11: Moisture content of some selected VFs.

By submerging VF in water, the moisture content in this case, will be beyond the FSP, including both the bond and the free water. In this context, as mentioned in the research study of Benmansour et al **[20]**, the properties of moisture depend on the aspect ratio of fibers again. In this study, the authors evaluated the water absorption of date palm fibers as a function of immersion duration. They found that the fibers with a small surface absorb more water compared to those with a larger surface (see Figure 2.12).

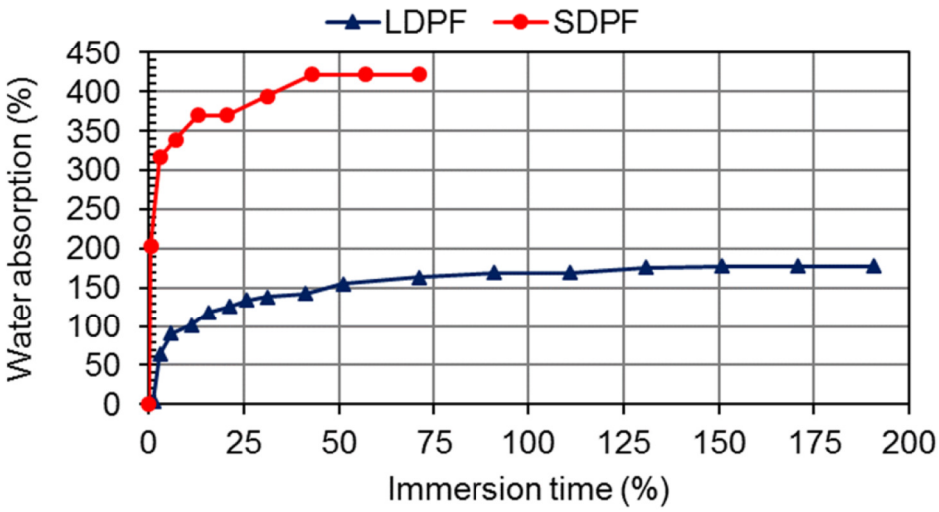

Figure 2.12: Water absorption ratio of date palm fibers as a function of immersion time.

2.3 Effects of VF on the fresh properties of cement-based materials

The incorporation of VF leads to a significant decrease in the workability. This is due to the water absorbed by the VF. However, the mixture needs to have sufficient flowability for the casting process. A mixture that is too dry could lead to a final product that is insufficiently compacted, which would probably contain more voids. Conversely, a mixture that is too wet will lead to a decrease in mechanical strength.

The other important aspect of workability is the formation of fiber pellets, which is also known as the agglomeration of the fibers together during the mixing process. The degree of agglomeration depends on the type and length of fibers used, the volume fraction of fibers, and the size of aggregates in the cementitious composite **[21]**. Fiber agglomeration should be avoided as it has a detrimental effect on mechanical strength. Some arrangements can be made during mixing to minimize the agglomeration effect. Normally, the progressive addition of fibers at the end of the mixing operation, when the other components are completely mixed, reduces this agglomeration effect. The utilization of a water-reducing plasticizer likewise makes it conceivable to significantly expand the workability without affecting the mechanical properties of the composite **[22]**. Moreover, according to Aziz et al (Aziz, Paramasivam and Lee, 1981), the reduction of the granular dosage also makes it possible to limit the formation of pellets **[23]**.

The flow ability of reinforced fresh mortar was negatively affected by the presence of fibers in the study of Çomak et al **[24]**. This reduction (see Figure 2.13) was attributed to the increase of water absorption by the increase of the fiber content. Nevertheless,

the length of fibers has no effect on the flowability of cementitious materials **[24]**.

Another aspect has a significant influence on the workability of fresh mortar, namely, the methodologies adopted to mix the VF homogeneously in the mortar matrix. In this context, Chakraborty et al **[25]** tested three different processes of preparing the cement mortar composite by including 5 different fractions of jute fibers (0.5, 1, 2, 3 and 4%).

The first mixing process, which is termed as PS1, was conducted as follows: the slurry was made with 50% of the total quantity of cement and water, the fraction of chopped jute fibers was then added continuously during 10 min of mixing time, the remaining part of cement was mixed with the required quantity of sand separately for 5 min, the dry mix (sand and cement) was then added to the slurry (jute fibers, water, and cement) and mixed for 5 min, and finally, the remaining quantity of water (50%) was added into the slurry (Sand, cement and jute fibers).

The second type of mixing, which is termed as PS2, was similar to PS1. The difference in this process was in the phase which the fibers were incorporated, the jute fibers were first submerged in 50% of the total quantity of water, then after 50% of the total quantity of cement was added and the slurry was mixed for 10 min. The remaining part of cement was dry mixed with sand and the dry mix was added to the slurry. Finally, the remaining part of water was added to the slurry.

The third mixing process, which was termed as PS3, was performed as follows: the chopped jute fibers were immersed in water for 24 h until reaching full saturation, the saturated fibers were mixed with 50% of the total quantity of cement and water, and then the required amount of sand and remaining quantities of cement and water were added to the slurry.

The highlight of the results obtained (see Figure 2.13 (based on **[24, 25]**)), showed that the workability decreased by using process PS1 and PS2 in the preparation of mortar due to the hydrophilic nature of the jute fiber. Nevertheless, the third type of mixing process, PS3, showed flowability values similar to that of the control mortar specimen. The reasons behind this difference can be explained by the fact that in preparation processes PS1 and PS2, the jute fibers were added dry into either the cement slurry (PS1) or into the water (PS2). In both cases, (PS1) and (PS2), the amount of water required for hydration of the cement was reduced by the presence of the jute fibers, which, as mentioned earlier, have a hydrophilic nature. Therefore, the significant reduction of workability by using preparation processes PS1 and PS2 is due to the incomplete hydration process of the cement mortar.

In process PS3, however, the jute fibers were already saturated. The required amount of water for cement hydration was not affected by the presence of fibers since they are wet. Therefore, the workability of the mortar mixture prepared using process PS3 showed similar workability as that measured for the control mortar specimen.

The key factors that affect the reduction of the workability in cement mortars are the aspect ratio and the volume fraction of the fibers. The reduction of the workability could be remedied by the pre-treatment of fibers to reduce the chemical components that absorb the water. The VF could be pre-wetted before inclusion in the mixture. Otherwise, the absorption rate of fibers could be considered when preparing fiber reinforced mortar mixtures by adding a determined extra amount of water **[26]**.

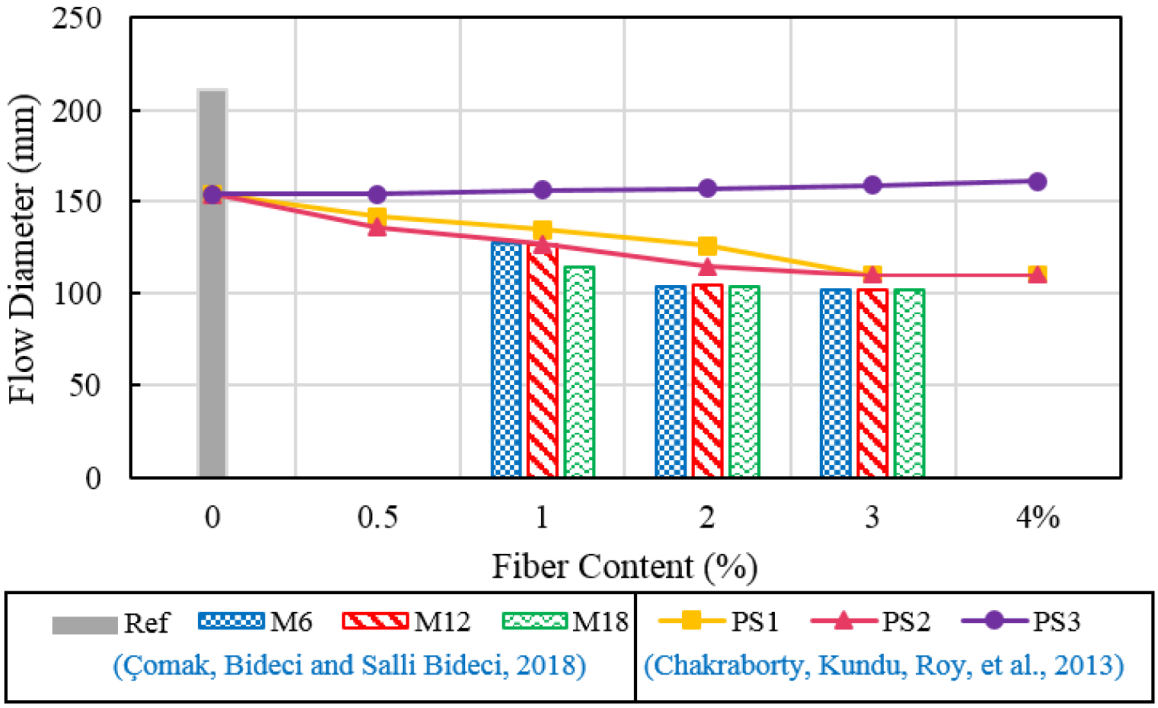

Figure 2.13: Workability of cement mortar reinforced with: (i). Jute fibers (0, 0.5, 1, 2, 3 and 4%) using three different mixing process (PS1, PS2 and PS3), (ii). Hemp fibers (0, 1, 2 and 3%) with different lengths (Ref:0mm, M6:6mm, M12:12mm and M18:18 mm).

2.4 Effects of VF on the mechanical behaviors of cement-based materials

The mechanical properties of VF reinforced cementitious materials, as with other fiber-reinforced concrete (FRC), are affected by a large number of factors **[27]**, mainly;

- Type of fibers: sisal, hemp, jute, coir, date palm, etc.
- Morphology of fibers: length, diameter, transversal section.
- Type of fiber's inclusion: single fibers, bundle, strand.
- Fiber surface: smooth, rough, coating agent.
- Matrix properties: type of cement, size of aggregates, admixtures.
- Proportions of the different constituents: W/C ratio, fiber content, proportion of aggregates.
- Mixing process: type of mixer, sequence of constituent's addition, method of fiber incorporation, period and speed of mixing.
- implementation method: vibration standard, extrusion.
- Curing condition: air, water.

In this section, the mechanical behavior of cementitious composites reinforced with VF will be discussed based on the previous studies available in the literature. More precisely, the mechanical behavior will be analyzed in terms of compressive and flexural strength.

2.4.1 Compressive strength

According to many researchers **[28, 29, 30, 31, 32, 33, 34, 35]**. The compressive strength of cementitious materials is negatively affected by the inclusion of VF. For instance, Kriker et al **[31]** mentioned in their study that the compressive strength decreased by increasing both the content of fibers and their length. The compressive strength of the concrete specimen reinforced with 2% by volume of date palm fibers in which the fiber length is 15 mm represents 90% of the compressive strength when compared to the unreinforced concrete specimen. However, the specimen reinforced with 3% of fibers of 60 mm length represents 55% of the compressive strength of plain concrete. The authors attributed this decrease to the increase in the number of defects and the non-uniformity of fiber distribution.

In a similar study, Tioua et al **[28]** investigated the compressive strength of a self-compacting concrete reinforced with two volume fractions of date palm fibers (0.1 and 0.2% by volume) of two different lengths (1 and 2 cm). In this study, two different curing conditions were utilized (laboratory and hot-dry climate). The authors concluded that specimens cured in a hot-dry climate had a higher strength when compared to those cured in the laboratory after 1 day of being cured. This was due to the accelerating effect of the temperature on the hydration rate. Moreover, the specimens cured in the laboratory had a larger compressive strength after 7 and 28 days of being cured. However, in both curing conditions, the specimens containing date palm fibers had a lower compressive strength compared to the control specimen. The authors attributed this decrease to the increase of the porosity introduced by the date palm fibers.

Other parameters, such as the saturation degree of the fibers, could influence the compressive strength of cementitious composites reinforced with VF, which was indicated by Hamzaoui et al **[33]** in a study on the mechanical behavior of modified mortar using dry and wet hemp fibers. In this study, the compressive strength decreased in both cases when using dry or wet hemp fibers. Moreover, the dry hemp fibers caused a significant decrease when compared to wet hemp fibers.

A new green composite material containing a high amount of fly ash (fixed to cement at a rate of 1.6) and reinforced with three different volumes of bagasse fibers (3, 8, and 12% by volume) was mechanically investigated by Tian et al **[34]**. By increasing the content of bagasse fibers, a significant reduction of the compressive strength in early age could be noticed. When, at the age of 7 days, the composite reinforced with 3% of bagasse fibers showed a compressive strength value of 24.24 MPa. This value dropped by 51.7% and by 43.52% for composites reinforced with 8% and 12% of bagasse fibers, respectively. The authors indicated that this high reduction in early age is related to the unsaturated hydration of cementitious composites, which is influenced by the uneven

distribution of water due to the hydrophilic nature of bagasse fibers. Nevertheless, the change in the compressive strength of the composites at the age of 28 days became more stable.

Some studies mentioned that the addition of low quantities of VF could lead to beneficial results in compressive strength **[24, 30, 36]**.

Ozerkan et al **[30]** noticed in a study related to the mechanical performance of cement mortar reinforced with date palm fibers that inclusion of 0.5% of date palm fibers has the desired effect on the compressive strength of cement mortar. This result was found due to the high compaction between the mortar matrix and the fibers, which led to a good homogeneity of this mix.

Andiç-Çakir et al **[36]** tested cement mortar composites prepared with the use of fine aggregates and coir fibers with an addition ratio of 0.4, 0.6 and 0.75% by weight of the total mixtures. The authors indicated that the increase of coir fibers led to an increase in compressive strength, and this increase varied between 3.64% and 14.25% for the reinforced specimens with untreated coir fibers. Moreover, an increase varying between 9% and 17.94% was achieved for specimens containing alkali-treated coir fibers.

A similar result was obtained in the experimental study performed by Çomak et al **[24]**, in which the authors mentioned that VF could have a good effect on the compressive strength of cementitious materials. In this study, cement-based mortar incorporating hemp fibers with a fiber content ratio of 1, 2, and 3% with different lengths of 6, 12 and 18 mm was investigated. The authors recorded an increase in the compressive strength of up to 30%. The authors considered that the long fibers' orientation to sample length was found to be better and contributed to a much bigger increase in compressive strength. The results obtained from different studies concerning the effect of VF reinforcement on the compressive strength of cementitious materials are summarized in Table 2.2.

Table 2.2: Various compressive strength results of different cementitious materials blended with different VF reinforcements.

References	Type of fibers	Type of cementitious matrix	Dosage [%] (Length of fibers[cm])	Compressive Strength [MPa]
Al-Rifaie et al **[29]**	Date palm	Plaster	2, 4, 6, 8 and 10	A gradual decrease with the increase of fibers
Belakroum et al **[32]**	Date palm	Lime	20, 35 and 50	A gradual decrease with the increase of fibers
Kriker et al **[31]**	Date palm	Concrete	0, 2,and 3 (15 and 60)	A gradual decrease with the increase of both dosage and length of fibers
Ozerkan et al **[30]**	Date palm	Cement mortar	0, 0.5, 1 and 2	Appropriate with 0.5 % of fibers, decreased after 0.5 % of fibers
Tian et al **[34]**	Bagasse	green composite	3, 8 and 12	A gradual decrease with the increase of fibers
Tioua et al **[28]**	Date palm	SCC	0.1 and 0.2 (1 and 2 cm)	A gradual decrease with the increase of fibers
Hamzaoui **[33]**	Dry and wet hemp	Cement mortar	1.1, 2.1 and 3.1	Reduced
Çomak et al **[24]**	Hemp	Cement mortar	1, 2, and 3 (6, 12 and 18)	improved
Andiç-Çakir et al **[36]**	Coir	Cement mortar	0.4, 0.6 and 0.75	A gradual improvement with the increase of fibers

2.4.2 Flexural strength

The studies carried out on the flexural behavior of the VF reinforced cementitious composites were highlighted. The plain matrix of cementitious composite presented a brittle linear behavior in flexural strength. On the other hand, The bio-composite samples presented non-brittle behavior and continued to support a significant load after the maximum load. Sedan **[37]** compared the mechanical properties of cement paste and cement matrix incorporating hemp fibers (16% by volume). For this purpose, three-point bending tests were carried out on these two materials after 28 days of being cured in water.

The author distinguishes that the bending behavior of the cementitious composite has three phases(see Figure 2.14):

- Phase I: Quasi-linear behavior close to that of the cement paste specimen. In this phase, the efforts are mainly supported by the matrix.
- Phase II: Appearance of the first crack in the matrix just before reaching the peak load. Then, the forces are transformed to the fibers that support the load and in turn limit the propagation of the crack by their bridging effect.
- Phase III: Beyond the peak load (post-peak phase), the load decreases in a controlled manner, unlike the cement paste which breaks suddenly. The author associates this phase with a progressive rupture of the fiber/matrix interfaces, followed by the fibers pull-out.

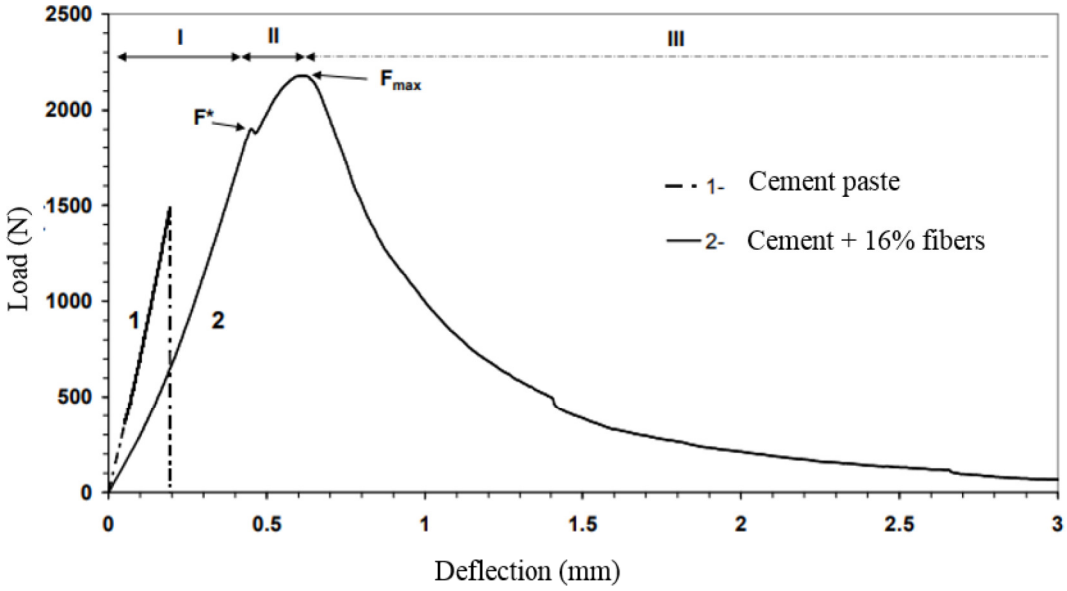

Figure 2.14: Load-Deflection curve of cement paste specimen and cement composite specimen reinforced with hemp fibers based on the study of **[37]**

The transition from a brittle matrix to a ductile composite material exhibiting controlled post-peak behavior is noted by all authors. However, this behavior transformation is not always accompanied by an improvement in flexural strength **[31]**.

By analyzing the research studies carried out on the flexural behavior of cementitious materials reinforced with VF, it is noticed that the flexural behavior of these composites is related to the nature and the dimensions (aspect ratio) of fibers, the type of cementitious matrices, the dispersion of fibers in the matrix, and also to the preparation process that was adjusted to prepare the VF (raw, wet, treated). Some of the results obtained by different researchers are shown in Figure 2.15 (based on **[25, 38, 39]**).

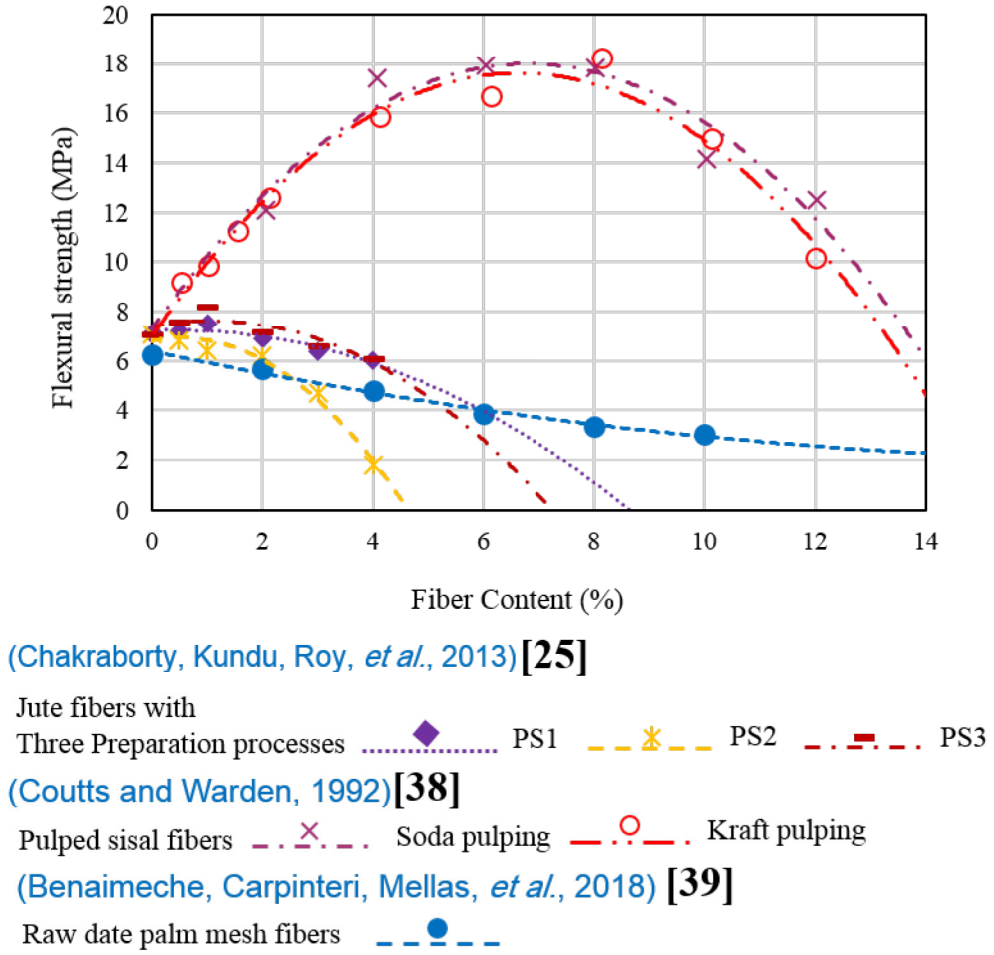

Figure 2.15: Various flexural strength results of different VF-reinforced cementitious materials.

Chakraborty et al **[25]** studied the mechanical influence of jute fibers with 4 volume fractions (0.5, 1, 2, 3 and 4%) by using three different processes (PS1, PS2 and PS3) of preparing the fibers, which was described in section 2.3.
The authors concluded that using processes PS1 and PS3 contributed to an increase of the flexural strength with a corresponding increase of the amounts of jute fiber up to 1%. However, using more than 1% leads to a gradual decrease in flexural strength (see Figure 2.15).
Regarding process PS2, the flexural strength was gradually decreased with the increase of fiber inclusion. The authors attributed this decrease to the agglomeration phenomena of fibers when using this process in the preparation (PS2). Among all the processes used, the PS3 process exhibited the best fiber dispersion. Therefore, the mortar specimens prepared according to PS3 showed the highest value of flexural strength, in which it was improved by 16% for 1% of jute fiber reinforcement when compared to the control specimen.

In the recent study performed by Benaimeche et al **[39]**, the mechanical behavior of cement mortar reinforced with date palm mesh fibers as a raw material was investigated. The authors indicated that a reinforced mortar specimen with 10 % of DPMF

leads to a decrease of about 50 % in flexural strength. Therefore, it can be concluded that the addition of date palm fibers as a raw material does not have a beneficial effect on flexural strength.

In the research studies performed by Coutts et al **[38]**, flexural strength was found to be improved when using up to 8% of fibers (see Figure 2.15). This may be explained by the specific processes of the fiber's preparation, such as the Kraft and pulping process, as well as due to the casting process of the specimen by using a dewatering method to remove the extra amount of water.

Although the fiber's dosage had a significant influence on the flexural performance of the cementitious composites, the length of the fibers was also a parameter of influence. Le Hoang **[40]** studied cement mortars reinforced with flax fibers (see Figure 2.16). The authors mentioned that the flexural performances of the composite are directly related to the length of the flax fibers. Initially, the increase in fiber length resulted in an increase in flexural strength. However, from a length value of 30 mm, which is considered as a critical value, the strength no longer increases and instead begins to decrease. Nonetheless, it is still higher than that of the control cement mortar.

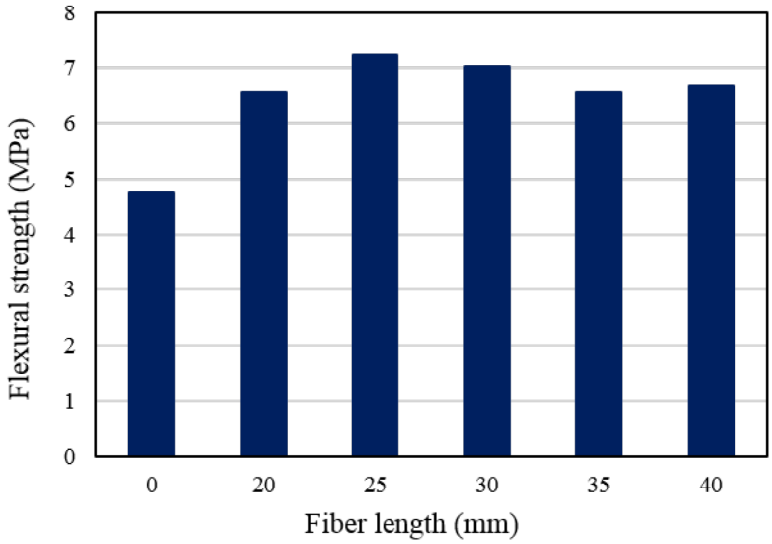

Figure 2.16: Influence of the fiber's length on the flexural strength of cement mortars reinforced with flax fibers **[40]**.

2.4.3 Fracture toughness

In fracture mechanic, the fracture toughness is considered as a material property, which determines the cracking resistance and the energy absorption capacity of materials **[41]**. It is generally associated with the stress intensity factor of materials. Therefore, it is a vital property to be evaluated for design purposes.

In literature, there is a very limited number of research papers published on fracture behavior of cementitious materials reinforced with vegetable fibers.

Zhou et al **[42]** conducted an experimental investigation on the fracture behavior of jute fibers reinforced cementitious composite (JFRCC). This composite material was based on concrete and reinforced with jute fibers, there were two types of binder used for concrete matrix: Portland cement (PC) with ground granulated blast furnace slag (GGBS), and PC with pulverized fly ash (PFA). The jute fiber reinforcement was at a fiber ratio of 0.5% by volume. The fracture toughness was determined according to the two parameter model and presented in Figure 2.17. The authors found that fracture toughness was largely increased in JFRCC with GGBS at all curing ages 7, 14, and 28 days, compared to plain mortar, this increase was attributed to the fact of the increase in the critical strain energy release rate. It was mentioned also that the combination of GGBS and PC results in a very strong bond between cement matrix and fiber.

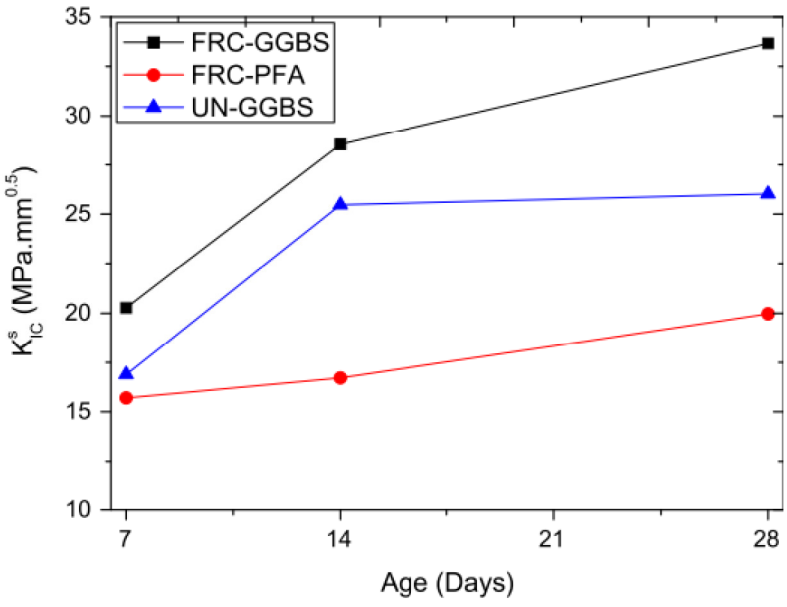

Figure 2.17: Stress intensity factor for various concretes at various ages **[42]**.

Razmi et al **[43]** investigated three different percentages of jute fibers (0.1%, 0.3% and 0.5% by weight) in the reinforcement of concrete. The authors used the Cracked semi-circular bend (SCB) to obtain fracture toughness under mixed mode I/II. The authors found that the effects of the fiber percentages on the mixed mode fracture toughness are very significant, it was found that adding jute fibers to concrete mix-

ture improves the fracture toughness about 45% under mixed mode loading. For the purpose of showing the effect of the fiber content and the mixed mode loading, the fracture locus for the mixed mode fracture toughness of concrete composites is shown in Figure 2.18, the area surrounded by the vertical and the horizontal axes, and each curve presents a safe zone area. It can be observed that the safe zone area increases as the fiber content increases.

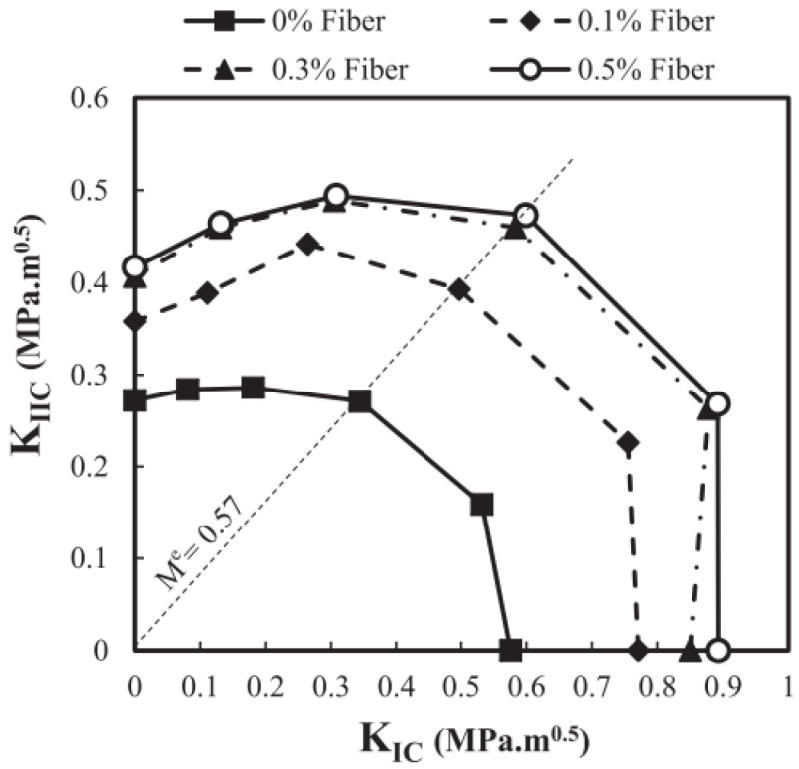

Figure 2.18: Fracture diagram for jute fiber-reinforced concrete at different fiber contents **[43]**.

The variance in the species of the vegetable fibers has an effect on the fracture toughness of the cementitious composites. For instance, Reis **[44]** investigated three types of vegetable fibers (coconut, banana and sugar can bagasse) in the reinforcement of polymer concrete prepared by mixing the sand with the epoxy resin, the fibers used for this study were natural (without any chemical treatment) at a fiber ratio of 2% by weight. Figure 2.19 presents the calculated fracture toughness results for each type of fibers. As can be seen, Sugar can bagasse fiber-reinforced polymer concrete presents the best performance in terms of fracture toughness with an increase rate of 17.8% compared to plain polymer concrete. An increase of about 15.7% was noticed for coconut fibers-reinforced polymer concrete. While, a decrease of 22.2% was observed for banana pseudo-stem fiber reinforcement.

In addition, the surface modification of vegetable fibers has a less significant effect on fracture toughness of the cementitious materials, in a similar study, Reis **[45]** investigated the incorporation of sisal fibers in the polymer concrete matrix by modifying the sisal fiber´s surface using different types of chemical treatment (5% of NaOH, 10%

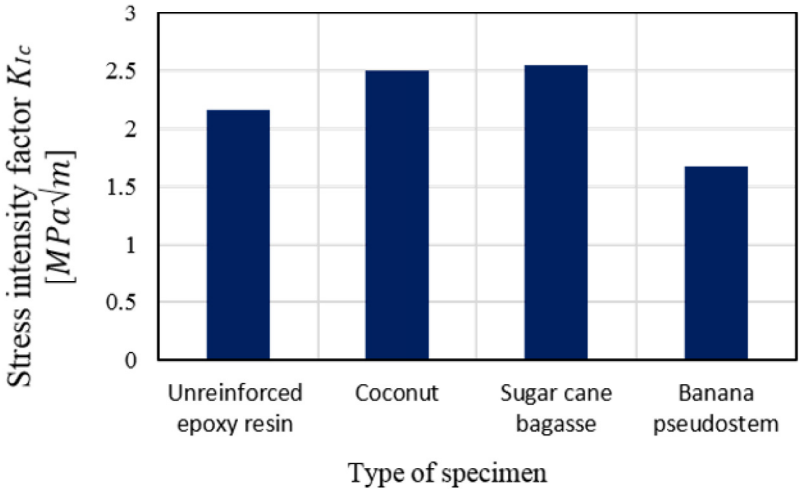

Figure 2.19: Stress intensity factor of different polymer concrete composites **[44]**.

of NaOH and 20% of acetic acid). The chopped sisal fibers were used at a fiber ratio of 1% by weight. Figure 2.20 shows the effect of the chemical treatment on the stress intensity factor of the polymer concrete composites. It can be seen that untreated sisal fibers contributes better than treated fibers to improve the fracture toughness of concrete polymers. Nevertheless, all reinforced specimens presented better performance in terms of fracture toughness.

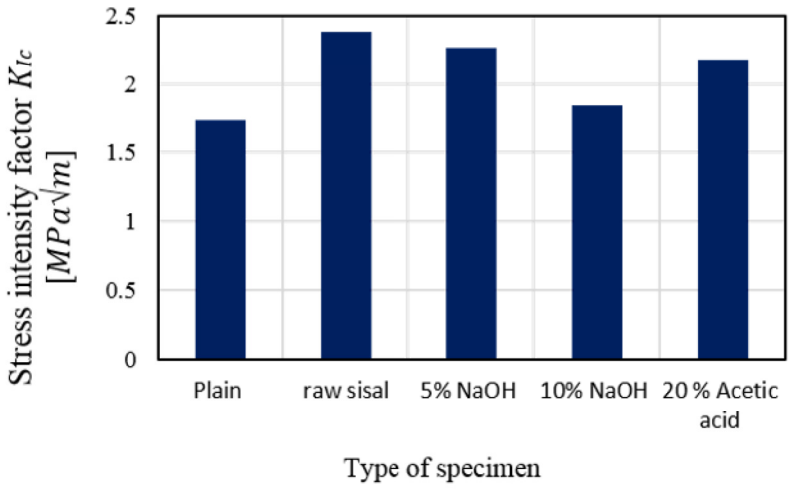

Figure 2.20: Stress intensity factor of untreated and treated polymer concrete composites Reis **[45]**.

2.5 Digital image correlation technique

The digital image correlation (DIC) is one of the optical techniques used for the measurement of the displacement field **[46]**. The DIC has been one of the most versatile methods due to the applicability advantage in which it can be used at any scale of observation **[47, 48, 49]**. DIC measurement is based on using a distinctive pattern on the surface of the image to inspect the displacement field between two or more recorded images. The pattern can be the natural texture or consists of the application of paint speckles. The measurement of the displacement field relies on the premise of the conversation of gray level in the examined domain **[50]**. DIC now knows a widespread use in academia and industry after its start origins as an academic technique **[48, 51, 52, 53]**. The DIC has been used during the application of the three point bending test to determine the displacement fields of the cementitious composites prisms **[54, 55, 56, 57, 58, 59, 60]**. The DIC has proven to be a powerful optical-numerical tool to measure the fundamental parameters used for the study of the fracture behavior of the cement-based materials such as: Crack Tip Opening Displacement (CTOD), Crack Mouth Opening Displacement (CMOD) and the crack extension (Δa), the determination of these parameters through the theoretical models and the DIC technique allows to have more accurate results.

Nunes and Reis **[54]** used the DIC technique in the evaluation of the fracture behavior of chopped glass fiber reinforced polymer mortars. The DIC was applied to the determination of the CTOD and Δa instead of using the clip gage. Moreover, the H-displacement fields for different load application were obtained (Figure 2.21). It was noted that the crack length increases as the applied load increased.

The DIC technique found to be a good tool in the identification of the displacement fields during different stages of load application. Das et al **[56]** used the DIC technique for the evaluation of the displacement fields of mortars contain different additions of limestone, fly ash and metakaolin. The crack visibility , the distinct displacement-jump at the tip of the notch and the CTOD were estimated using the colored images (Figure 2.22), based on treated DIC images inspected by a commercial software (Vic 2D).

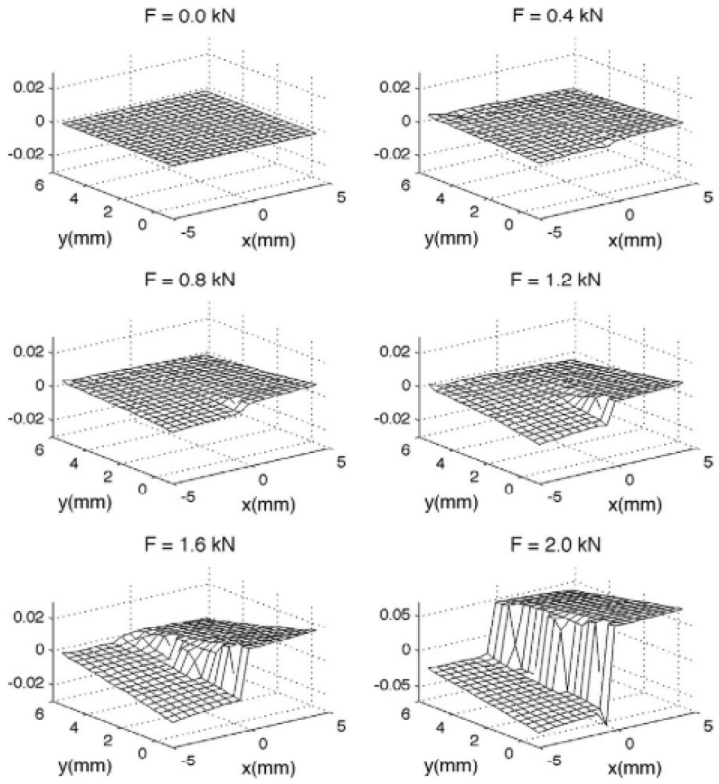

Figure 2.21: H-displacement (mm) for different applied loads **[54]**.

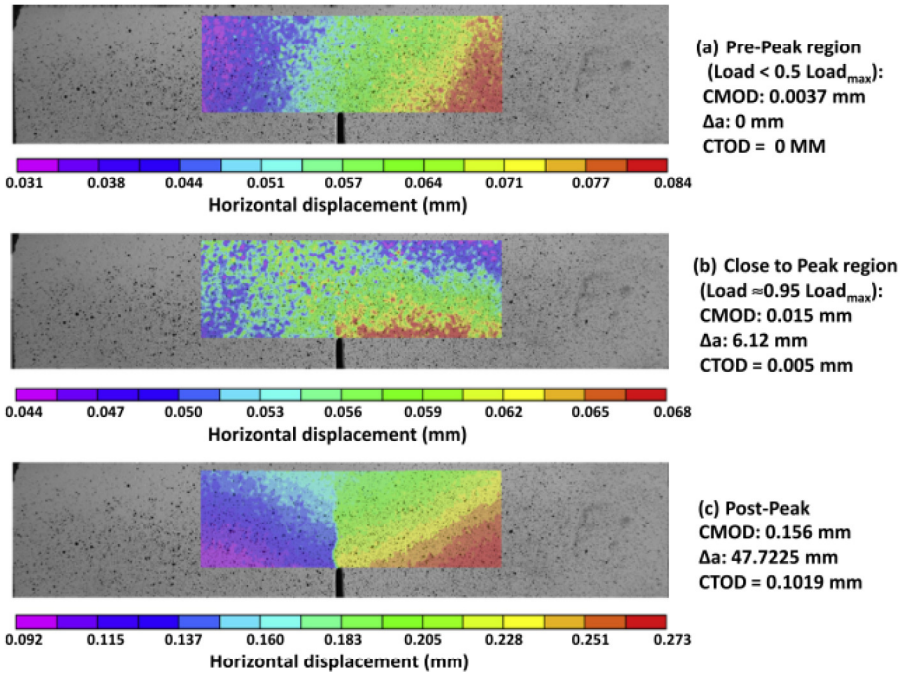

Figure 2.22: Horizontal displacement fields at: (a) pre-crack stage, (b) stable crack growth stage, and (c) unstable crack-propagation stage **[56]**.

2.6 Conclusion

The first part of the literature review's section has tackled the the properties of the vegetable fibers. The latter one are renewable resources abundant in the nature and available in the local region. Their production do not affect the environment compared with the synthetic fiber's production, which makes them sustainable reinforcement for the choice of composite materials that are updated and being important to reduce the ecological footprint of man on the environment. Moreover, the vegetable fibers demonstrated such mechanical properties are close to some properties of synthetic fibers such as glass fibers. However, it presented also some disadvantages such as a weak heat resistance, a high sensitivity to water moisture and also a wide range of the physical and mechanical properties.

Thereafter, the state of the art on the cementitious materials reinforced with such vegetable fibers has been reviewed. The incorporation of the vegetable fibers in the cementitious materials was mentioned with the aim of delaying the first crack and controlling the crack propagation for getting such a ductile material. A composite material reinforced with fibers continues to support more load even after failure. Furthermore, the vegetable fibers could improve such mechanical behavior such as flexural, fracture and the fatigue. The improvement of such behavior is directly related to the volume fractions, the nature and the mechanical behavior of fiber itself.

Taking this literature review into consideration, the vegetable fibers can be regarded as a promising alternative for the traditional synthetic fibers. These fibers have multiple beneficial advantages such as low cost, environmental impact and its incorporation could improve the cost and satisfy the mid-range requirement for the flexural and fracture behavior and also impact resistance.

On the highlights of what has been mentioned previously, for the suitable valorization of the local materials, and for the best knowledge of authors, no studies related to the fracture behavior of cement-based composites reinforced with DPMF are available in the literature. Consequently, an investigation on the utilization of date palm fibers in cementitious materials is required. Therefore, the present work deals with the mechanical and physical properties of a cement-based mortar reinforced with short DPMFs including the fracture, flexural and compressive strength.

CHAPTER 3

Theoretical background

3.1 Introduction

The "Fracture" term defines the local separation of material attachment in a solid body. It concerns a procedure that either partially distort the body which prompts the advancement of initial cracks or entirely devastates it. The actual fracture process appears in the body by means of elementary failure mechanisms on the microscopic level of a material which can be defined by the physical and micro-structural properties as it is shown in Figure 3.1. The worldwide type of appearance of the fracture on a naturally macroscopic level comprises in the development and spread of one or various cracks in the body, whereby the material is totally splitting. On this dimension, the methods of solid mechanics and mechanics of materials can effectively describes the fracture process of the material. The fracture phenomena is well known in nature and engineering by everyone. For instance, the fracture of stone and ice are very impressive cracks in the nature, particularly in the appearance of the incredible geological formations such as rock failures, crevasses and earthquakes, (see Figure 3.2 **[61]**).

Several centuries earlier, Leonardo da Vinci conducted experiments which provided some keys to the root causes of fracture. After measuring the strength of iron wires, da Vinci found that the strength related inversely with wire lengths, he concluded that the flaws in materials controlled the strength, these results were in qualitative manner. Thereafter, it was reported in the paper was published by Griffith in 1920 **[2]** that the relation between the fracture stress and the flaw size was determined in quantitative manner. Griffith applied the stress analysis model performed by Inglis

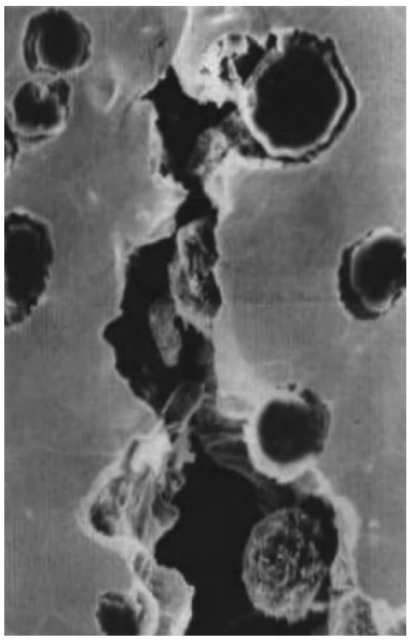

Figure 3.1: Micro-crack in the structure of ductile cast iron **[61]**.

Figure 3.2: Macro-crack (crevasse) in the Frundel glacier, Switzerland **[61]**.

[62] in 1913 for an elliptical hole to the unstable propagation of a crack. The author used the first law of thermodynamics to formulate the fracture theory which is based on the energy balance. This theory describes the strain energy change that is produced from the increase in crack growth is sufficient to overcome the surface energy of the material. This model was correctly predicting the connection between strength and flaw size in glass specimens only. Two decades after, the Griffith theory was extended to metals by Dr. G.R. Irwin, who included the energy dissipated by local plastic **[63]**. In 1956, Irwin **[64]** developed the concept of the energy release rate, which is related to the Griffith theory but is in a form that more useful for solving engineering problems. Shortly afterward, Irwin **[65]** used the Westergaard approach **[66]** that was released in

1938 which deals with the stress analysis in front of the sharp crack, the author explained the stresses and displacements near to the crack tip by a constant which is related to the energy release rate, this parameter later started to be known as the stress intensity factor **[67]**.

3.2 Linear elastic fracture mechanics (LEFM)

The early theories of fracture mechanics that were found prior to 1960 are fitting only with the mechanical behavior of materials that are governed by the Hooke's law. Despite the modifications suggested in the early of 1948 which are dedicated for small scale plasticity, the application of these suggestions were limited to structures which have linear elastic global behavior. From 1960, after the development of the fracture mechanics concepts, the extension of the Linear elastic fracture mechanics (LEFM) were accounted for different types of nonlinear material behavior as well as dynamic effects **[67]**.

Supposing that an elastic material body includes a crack is loaded in the opening mode (mode I), the full stress field in the vicinity of the crack tip is totally described if the stress intensity factor K_I is known. Therefore, the K_I is the parameter which define the intensity of the elastic stress field in front of the crack(see figure 3.3). When a material is supplied by a sufficient energy, the intensity of the stresses close to the crack tip reach critical values and the crack propagates in an unstable manner which leads the material to a brittle fracture. In this stage, the stress intensity factor attributed to the fracture toughness of the material K_I is being critical and it is denoted K_{IC}. Consequently K_{IC} is a material property used to define the toughness of the material. For instance, a material with higher K_{IC} is tougher and can bear a longer crack. The analysis of the

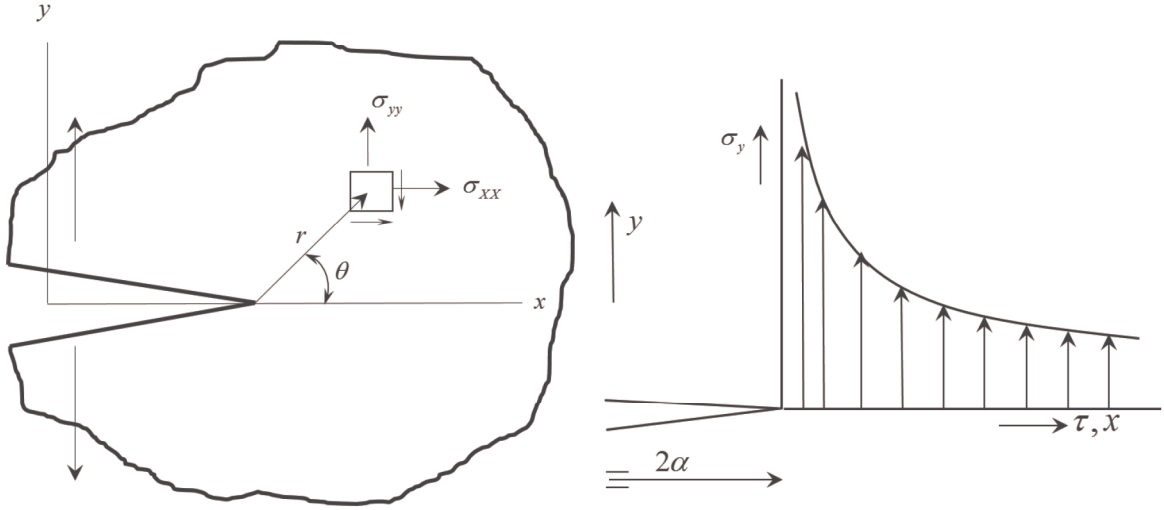

Figure 3.3: Elastic stress field in the vicinity of a crack tip **[68]**.

crack propagation is based on two primary approaches for predicting brittle fracture.

The first one is based on the amplitude of the stress intensity factor K. K is assigned to as Linear elastic fracture mechanics, which is still valid since the process zone which has inelastic deformations, in front of the crack tip, stays small and neglected in comparison with the specimen dimensions. In the handbook of Tada and Paris 1985 **[69]**, equations to determine K_I are mentioned for many different geometries of specimens. For instance, if we consider an infinite plate containing a crack of length 2α The K_I explained by the following equations **[70]**.

$$K_I = \sigma\sqrt{\pi\alpha} \quad \text{While for all other cases,} \quad K_I = \beta\sigma\sqrt{\pi\alpha} \tag{3.1}$$

Where:

β is a constant related to the geometry of the specimen
σ is the far-field stress
α is length of the crack

K_I has dimensions of $stress \times length^{(1/2)}$, usually it is $MPa\sqrt{m}$

The second approach is based on the energy balance concept which is proposed by Griffith. In this approach, The unstable crack growth propagation of a length α is supposed to occur just if the energy release rate by the system is equal or greater than the energy necessary for the crack to propagate. Thus, failure appears when **[70]**:

$$G_{IC} = \frac{\partial U}{\partial \alpha} = \frac{\partial W}{\partial \alpha} = R \tag{3.2}$$

Where:

G_{IC} is the critical strain energy release rate
R is the Crack growth resistance
U is the elastic energy release by the system
W is the energy required for a crack to propagate

In the application of LEFM, the correlation between the stress intensity factor, K_I and the strain energy release rate, G_I is expressed by

$$K_I^2 = E'G_I \quad \text{and it is expressed at unstable propagation, by} \quad K_{IC}^2 = E'G_{IC} \tag{3.3}$$

Where

$E' = E$ for plane stress
$E' = E/(1-v^2)$ for plane strain

3.3 Fracture mechanism in concrete

Concrete is considered neither as a brittle material like the glass and ceramic nor as a ductile material like metals. However, the sub-critical damage in concrete results in non-linear stress-strain response classified concrete as quasi-brittle material. Therefore, The strength of material approach has demonstrated insufficient in performing concrete design because the fracture strength of concrete is related to the size effect. This size effect is linked with the non-linear deformation which caused by the sub-critical cracking instead of concrete plasticity. The first attempts to use fracture mechanics approach to designing concrete were based on Linear elastic fracture mechanics (LEFM). These attempts were unsuccessful since the LEFM approach is not taking account the process zones that occurs around the macroscopic cracks **[67]**.

One of theses earlier attempts was the study of Kaplan **[71]**. When the author measured the critical strain energy release rate of notched concrete beams tested under three-point bending and four-point bending. he found that concrete mix proportion, type of loading, relative size of initial notch length, and specimen dimension are parameters influencing the critical strain energy release rate. It was indicated that the slow crack growth prior to fast fracture could be used in the fracture analysis. However, this process which is based on Griffith concept of critical energy rate maybe applicable to concrete after certain edition in the experimental and the analytical procedures. Thereafter, in the 1960s, researchers used LEFM related to the experimental determination of critical stress intensity factor K_{IC} in metals to the cementitious materials.

Some of the earlier investigations on the fracture process of cementitious materials and presented in the table 3.1, these studies are reviewed in the handbook of kumar **[72]**.

Table 3.1: Selected studies related to fracture mechanics models for cementitious materials **[72]**.

Reference	Case of the study	Results
Glucklich (1963) **[73]**	Application of fracture mechanics approach on concrete	The increase of the micro-cracked zone and the heterogeneity of the composite materials contribute to the relatively high value of the strain energy release rate.
Naus and Lott (1969) **[74]**	The effect of several concrete parameters : water-cement ratio, air content, sand-cement ratio, curing age, and size and type of aggregates on the fracture toughness	A regular dependency of the effective fracture toughness was observed with the variation of concrete parameters.
Shah and McGarry (1971) **[75]**	Study on notched specimens of hardened cement paste, mortar, and concrete.	Unlike mortar and concrete which are less notch-sensitive material, the cement paste are a notch-sensitive material to The critical length for mortar and concrete depends on the volume, type, and size of aggregates.
Walsh (1971) **[76]**	Geometrically similar notched concrete beams tested under three-point bending	The results did not follow the straight line of the slope, which concluded that the LEFM was not applicable to concrete. The author suggested to apply the LEFM depends upon the size of the specimen
Brown (1972) **[77]**	The effective fracture toughness of cement pastes and mortars were measured for notched-beam and double-cantilever beam	The crack growth is not influenced by the fracture toughness of cement whereas the toughness of mortar increases with the crack propagation
Kesler et al. (1972) **[78]**	The feasibility of LEFM in the study of cracked specimens of cement paste, mortar, and concrete	The LEFM cannot be applied directly to cementitious materials having sharp cracks
Brown and Pomeroy (1973) **[79]**	The effect of size and aggregates quality on the effective fracture toughness was experimentally studied	The addition of aggregates caused a progressive increase in toughness with crack growth
Walsh (1976) **[80]**	The effect of specimen size on the fracture strength parameter	If the specimen is quite large, the zone of stress disturbance which is surrounded by an area is small, thus the LEFM can be applied. Otherwise, if the specimen is small compared to the micro-cracking zone, the LEFM cannot be applied.

3.4 Nonlinear fracture mechanics for concrete

The non-linear zone in front of the crack tip which is composed of fracture process zone and hardening plasticity. These zones define the main difference between the application of fracture fundamentals in different kinds of materials (see figure 3.4. The application of LEFM is possible in materials containing very small fracture zone (see figure 3.4a) and this is the first case. In the second case of ductile material which has non-linear behavior, the hardening plasticity zone is large, while the fracture zone is small (figure 3.4b). Figure 3.4c presents the third case which is devoted for cementitious materials that have non-linear behavior in which the fracture zone is large and hardening plasticity is small **[72]**. The non-linear fracture models can be classified in

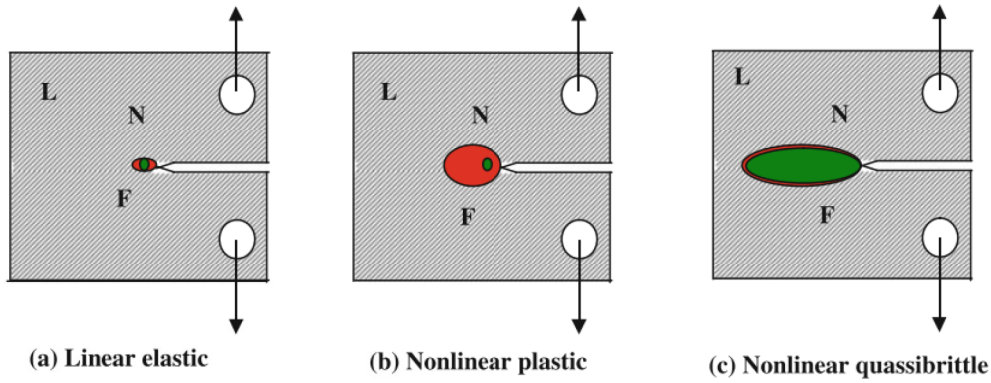

Figure 3.4: Types of nonlinear zones in different types of materials, L denotes linear elastic, N denotes the nonlinear material behavior due to plasticity, and F denotes the fracture process zone **[72]**.

two categories based on their basic approaches. The first approach uses the finite element method or the boundary element method. The second approach uses the modified LEFM concept. For instance, the first category included the fictitious crack model (FCM) and the crack band model (CBM). Whereas, the later category contained:

- Two-parameter model (TPM)
- Size-effect model (SEM)
- Effective crack model (ECM)
- Double-K fracture model (DKFM)
- Double-G fracture model (DGFM).

3.4.1 The fictitious crack model (FCM)

The fictitious crack model was first proposed by Hillerborg 1976 **[81]** which carried out the numerical simulation of the softening damage of concrete structures. It was the extended application of the cohesive crack model (CCM) proposed by Barenblatt **[82, 83]**. The hypothesis of this model is that the process zone is cramped into a narrow

band of line crack where the total fracture energy, G_f is consumed. Therefore, it can be represented the process zone as an extension of the actual crack, the fictitious crack, and is simulated as a tied crack which transmits the normal stress and this stress $\sigma(x)$ is also in a function of opening width w(see Figure 3.5)

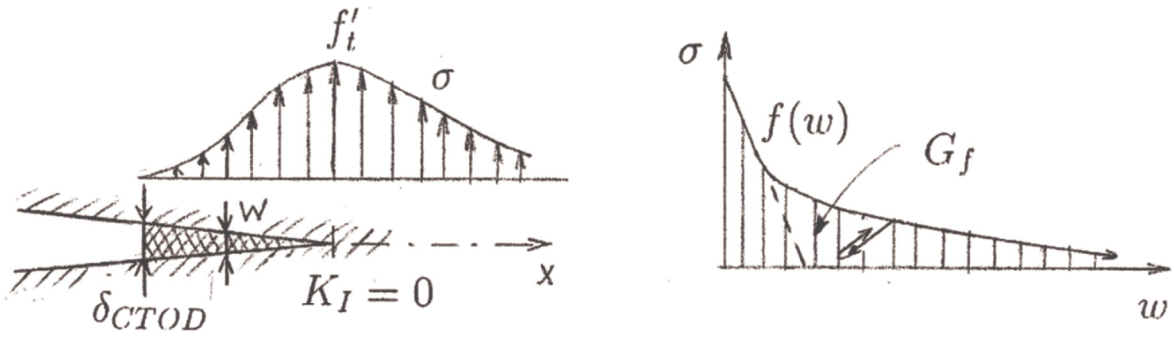

Figure 3.5: Cohesive crack model for quasi-brittle materials **[84]**.

Calculations are usually performed by means of numerical methods. Of course, difficulties arise from performing stable uniaxial tension tests and non-linear stress vs. displacement relationships complicate the computations. To avoid both problems, Hillerborg proposed to measure the fracture energy, G_f, with a three-point bending test using notched beam specimens and to assume a linear or bi-linear relationship for the closing pressure(HTLLERBORG, 1983) **[81]**. A draft recommendation of the fracture energy determination method has been made by the International Union of Testing and Research Laboratories for Materials and Structures (RILEM, 1985) **[85]**. Hillerborg (1980) **[86]** also extended his fictitious crack model to fiber reinforced concrete, and proposed that the closing pressure is a function of fiber length, fiber diameter and interfacial bond strength.

3.4.2 Two parameter model (TPM)

The model developed by Jenq and Shah **[87]** consists in an extension of the linear elastic fracture mechanics (LEFM) theory to include non-linear effects in concrete fracture. In fracture mechanics testing, the three-point bending test using notched-beams is a common method to evaluate the fracture toughness, K_{IC}, of a material. When such a test is used, LEFM applies only if the recorded load P vs. crack mouth opening displacement (CMOD) relationship is linear up to the maximum load (Figure 3.6).In such a case, K_{IC} is calculated using the peak load, P_{max}, and the length of the notch, a_0.

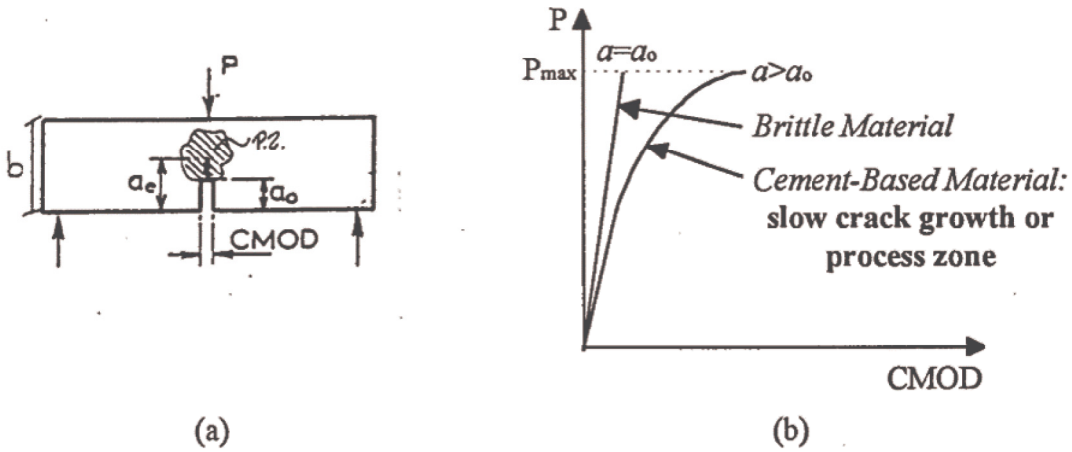

Figure 3.6: (a).Notched beam specimen under three-point bending and (b). Subcritical crack growth in cement-based materials **[87]**.

However, because of the process zone formation (or pre-critical crack growth), in a notched beam, substantial nonlinearity prior to the maximum load is observed. As a result, the effective length of the crack corresponding to the maximum load, referred to as the critical crack length, is longer than a_0.
Since in cement-based materials, there is no well defined crack tip but, most likely, a combination of a tortuous and bridged main crack accompanied by a damaged zone of considerable size, it is impossible to determine the exact length of the critical crack by direct observations. To evaluate this parameter, Jenq and Shah (1985) **[87]** assumed that after the precritical crack growth, the specimen behaves roughly as an elastic specimen containing a traction free crack referred to as the elastically equivalent crack or effective crack length. With this assumption, the available LEFM equations can be used. The effective crack length is obtained from compliance measurements using the following procedure (illustrated in Figure 3.7). For a notched beam specimen under three point bending the compliance, The initial compliance, C_i , is used to calculate the elastic modulus, E (Tada et al. (1985) **[69]**):

$$E = \frac{6Sa_0V(\alpha_0)}{C_iW^2B} \tag{3.4}$$

where S , W and B are loading span, width and depth of the specimen, respectively, a_0 is the notch length, C_i is the linear elastic compliance. Further, the parameter $V(\alpha_0)$ is expressed as follows (Tada et al.1985) **[69]**:

$$V(\alpha_0) = 0.76 - 2.28\alpha_0 + 3.87{\alpha_0}^2 - 2.04{\alpha_0}^3 + \frac{0.66}{1-{\alpha_0}^2} \quad \text{with} \quad \alpha_0 = \frac{a_0}{W} \tag{3.5}$$

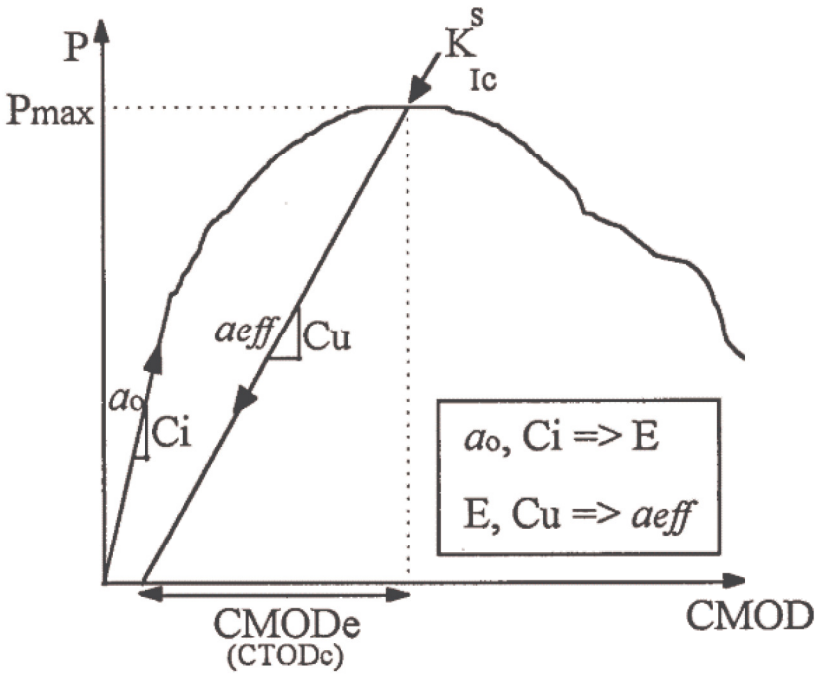

Figure 3.7: Determination of the effective crack length using compliance measurements **[87]**.

The graphical determination of the initial compliance of the specimen, C_i, along with the knowledge of the initial crack length (notch), a_0, allows for the calculation of the modulus of elasticity of the material, E, using Eq.(3.4). When performing the test, the specimen is loaded and unloaded just before reaching the maximum load, (95% of P_{max}). The compliance at the maximum load, C_u, can therefore be calculated using the maximum load and the elastic component of the CMOD, denoted CMOD_e.

Using Eq. (3.4) and the values of E obtained previously, the length of the crack which leads to a compliance C_u is calculated and referred to as the effective crack length, $\underline{a}$. The stress intensity at the tip of the effective crack is calculated using P_{max} and $\underline{a}$ using Eq. (3.6) and is denoted K_{IC}^S, as following:

$$K_{IC}{}^S = \frac{3P_{\max}S}{2WB}\sqrt{\pi\underline{a}}f(\alpha) \tag{3.6}$$

Although, experimental results obtained from beams with different dimensions showed that K_{IC}^S was size independent, $\underline{a}$ appeared however to be dependent on the size of the beams.

A crack shape was therefore assumed and, for a given effective crack length, the opening displacement of the crack located at the tip of the initial notch was determined (Fig 3.8). The resulting opening displacement is referred to as the critical crack tip opening displacement and is denoted as CTOD_c. According to the authors, the CTOD_c values appeared to be independent of the size of the specimen.

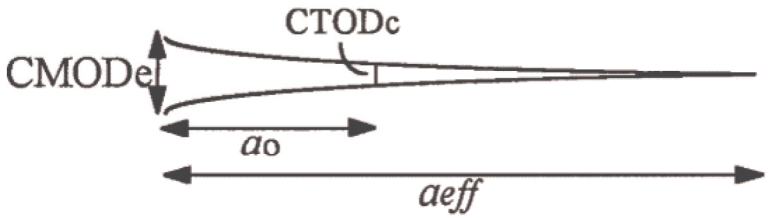

Figure 3.8: Determination of the crack tip opening displacement, CTOD.

The Two-Parameter Fracture Model consists, therefore, in fracture being defined by the two parameters: K_{IC}^{S} and CTOD$_c$ which, given their size independence, are considered to be material properties (Figure 3.9). It was therefore concluded that if these properties and the modulus of elasticity, E, are known for a given material, then one can predict the maximum load for a structure of any size and/or geometry.

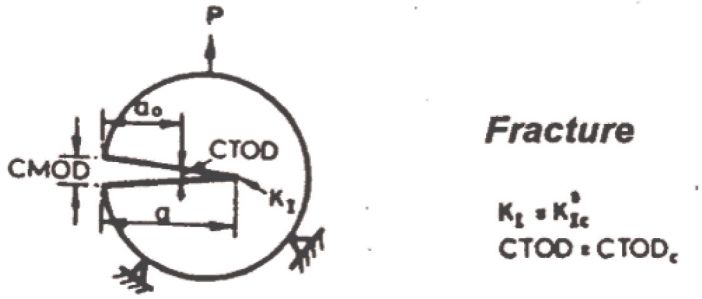

Figure 3.9: Two Parameter Fracture Model **[87]**.

The Two Parameter Fracture Model was tentatively recommended as a standard testing method to determine the fracture properties of quasi-brittle materials by the International Union of Testing and Research Laboratories for Materials and Structures. As per the draft recommendation **(RILEM, 1991) [88]**, the compliance corresponding to the maximum load, C_u, can be approximately calculated using the secant compliance method i.e. by assuming that the unloading path returns to the origin. However, it is pointed out that if such a method is used, the values of K_{IC}^{S} and CTOD$_c$ obtained are about 10 to 25% higher than those calculated using the actual unloading compliance, Therefore, ignoring permanent deformations leads to an overestimation of the toughness of the material and, eventually, to an overestimation of the design load carrying capacity of structures.
Finally, the authors of the model reported unique, constant values of K_{IC}^{S} and CTOD$_c$ using only notched beam specimens. However, years later, Ratanalert and wecharatana **[89]** conducted a series of experiments using two types of specimen (notched beam and compact tension) with different dimensions indicated that K_{IC}^{S} and CTOD$_c$ values are unique only to the notched beam specimen, the same two parameters were found to be 10 times larger for the compact tension specimens.

The Two-Parameter Fracture Model has also been extended to model fiber reinforced concrete (JENQ and SHAH, 1986) **[87]**. Here the crack propagation in the matrix is described by the same parameters described previously and requires the availability of experimental load versus slip relationship obtained from pull-out tests on single fibers.

3.4.3 Modified Two parameter model (MTPM)

A modified procedure is hereafter proposed by **[90]** when crack propagates under mixed mode loading (Mode I together with Mode II).
Specimens geometry and experimental test procedure are equal to those presented in the previous Section. The elastic modulus, E, is determined through Eqs (3.4) and (3.5). If the crack propagates under mixed mode loading, the effective critical crack length is obtained by following the procedure hereafter described. Let us consider a body loaded by both a loading force, P, and a pair of virtual forces, F, in equilibrium for any distance, d (Figure 3.10). The Castigliano theorem states that the displacement of any value of F (in its own direction) may be computed as follows **[69]**:

$$\Delta_F = \left(\frac{\partial U_T}{\partial F}\right)_{F=0} \tag{3.7}$$

where the total strain energy U_T can be obtained by adding the strain energy due to the applied forces with no crack and that introducing the crack while holding constant the applied forces:

$$U_T = U_{NoCrack} + \int_0^A \frac{\partial U_T}{\partial A} dA \tag{3.8}$$

being dA an infinitesimal increase of the crack area A (Figure 3.10). By assuming a

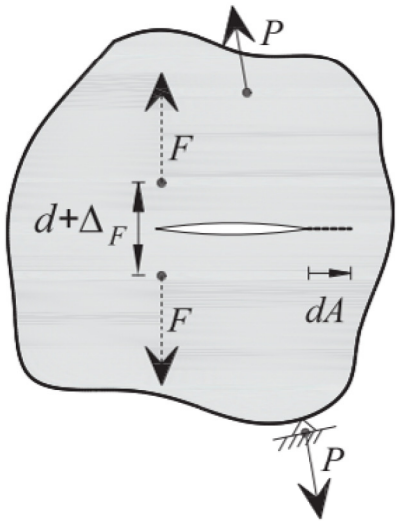

Figure 3.10: Body loaded by both a loading force P and a pair of virtual forces F, in equilibrium for any distance d.

constant loading force, P, the total energy rate, G, is equivalent to the rate of increase of the total strain energy, that is:

$$G = \frac{\partial U_T}{\partial A} \tag{3.9}$$

and the relative displacement of crack surfaces, Δ_F, given by the virtual forces can be computed as follows:

$$\Delta_F = \left(\frac{\partial U_{NoCrack}}{\partial F}\right)_{F=0} + \int_0^A \left(\frac{\partial G}{\partial F}\right)_{F=0} dA \tag{3.10}$$

By considering a prismatic body specimen including a kinked crack exposed to both three-point bending loading and a couple of virtual forces (applied in the lower part of the beam) perpendicular to the crack faces (Figure 3.11). For this situation, the main term on the right-hand side of Eq. (3.10) is equal to zero, since it relates to the displacement produced by the pair of virtual forces (in their own direction) in an uncracked beam, whereas the subsequent term is an element of the Stress-Intensity Factors (SIFs) for each loading mode, which are due to both the loading force P and the virtual forces F. For such a setup, the total energy rate G is given by:

$$G = G_I + G_{II} = \frac{K_I^2}{E} + \frac{K_{II}^2}{E} = \frac{1}{E}\left[(K_{IP} + K_{IF})^2 + (K_{IP} + K_{IF})^2\right] \tag{3.11}$$

where K_{IP} and K_{IIP} are the Mode I and the Mode II SIFs due to the loading force, respectively, whereas K_{IF} and K_{IIF} are the Mode I and the Mode II SIFs due to the virtual forces, respectively. By substituting Eq. (3.11) in Eq. (3.10), we obtain:

$$\begin{aligned}\Delta_F &= \frac{1}{E}\int_0^A \left[\frac{\partial}{\partial F}\left(2K_{IP}K_{IF} + 2K_{IIP}K_{IIF}\right)\right]_{F=0} dA \\ &= \frac{2}{E}\int_0^A \left[K_{IP}\left(\frac{\partial K_{IF}}{\partial F}\right)_{F=0} + K_{IIP}\left(\frac{\partial K_{IIF}}{\partial F}\right)_{F=0}\right] dA\end{aligned} \tag{3.12}$$

Each SIF term in Eq. (3.12) can be expressed as a function of the corresponding Mode I SIF of a straight crack having length equal to the projected length of the actual kinked crack, and the crack tip location is identified by the coordinate x shown in Figure 3.11 Since the SIF expressions of K_{IP}, K_{IIP}, K_{IF}, and K_{IIF} depend on the x-coordinate, the integral over the cracked area A (Eq. (3.12)) can be replaced by the following three integrals along a vertical line:

$$\Delta_F = \frac{2}{E}\left\{ \begin{array}{l} \int_0^{a_0} K_{IP,0}\left(\frac{\partial K_{IF,0}}{\partial F}\right)_{F=0} dx + \int_0^{a_0+a_1\cos\theta} \left[K_{IP,1}\left(\frac{\partial K_{IF,1}}{\partial F}\right)_{F=0} + K_{IIP,1}\left(\frac{\partial K_{IIF,1}}{\partial F}\right)_{F=0}\right] dx \\ + \int_{a_0+a_1\cos\theta}^{a_0+(a_1+a_2)\cos\theta} \left[K_{IP,2}\left(\frac{\partial K_{IF,2}}{\partial F}\right)_{F=0} + K_{IIP,2}\left(\frac{\partial K_{IIF,2}}{\partial F}\right)_{F=0}\right] dx \end{array} \right\} \tag{3.13}$$

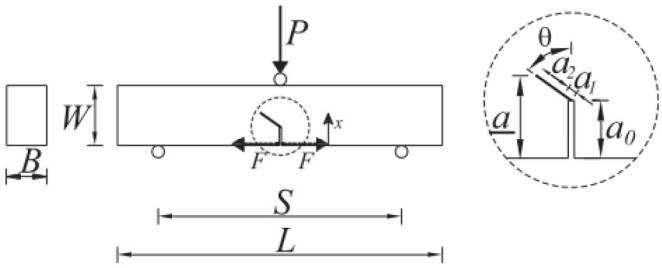

Figure 3.11: Geometrical and testing configuration of specimen according to the modified Two-Parameter Model.

being θ the crack kinking angle, and $a_1 + a_2$ the total length of the deflected crack, as is detailed in Figure 3.11. All the SIF terms in Eq. (3.13) can be expressed as a function of the Mode I SIFs at the crack tip of a straight crack under three-point bending ($K_{IP,0}$) and under a pair of virtual forces ($K_{IF,0}$) **[69]**:

$$K_{IP,0} = \frac{3PS}{2W^2B}\sqrt{\pi x}\, f(\alpha)$$
$$\text{with} \quad f(\alpha) = \frac{1}{\sqrt{\pi}} \frac{1.99 - \alpha(1-\alpha)(2.15 - 3.93\alpha + 2.70\alpha^2)}{(1+2\alpha)(1-\alpha)^{3/2}} \quad \text{and} \quad \alpha = \frac{x}{W} \tag{3.14a}$$

$$K_{IF,0} = \frac{2F}{\sqrt{\pi x}} g(\alpha)$$
$$\text{with} \quad g(\alpha) = \frac{0.46 + 3.06\alpha + 0.84(1-\alpha)^5 + 0.66\alpha^2(1-\alpha)^2}{(1-\alpha)^{3/2}} \tag{3.14b}$$

The Mode I and Mode II SIFs at the crack tip of a kinked crack characterized by a short branch, under three-point bending ($K_{IP,1}$, $K_{IIP,1}$) and under a pair of virtual forces ($K_{IF,1}$, $K_{IIF,1}$) can be evaluated following the approximated procedure proposed by Cotterell and Rice for a deflected crack characterized by a short branch in a centrally cracked infinite plate **[91]**:

$$K_{IP,1} = K_{IP,0}\cos^3\frac{\theta}{2} \tag{3.15a}$$

$$K_{IIP,1} = K_{IP,0} \sin\frac{\theta}{2}\cos^2\frac{\theta}{2} \tag{3.15b}$$

$$K_{IF,1} = K_{IF,0}\cos^3\frac{\theta}{2} \tag{3.15c}$$

$$K_{IIF,1} = K_{IF,0} \sin\frac{\theta}{2}\cos^2\frac{\theta}{2} \tag{3.15d}$$

The approximation is acceptable for $a_1/a_0 \leq 0.3$. The Mode I and Mode II SIFs at the crack tip of a kinked crack characterized by a long branch ($a_1/a_0 \leq 0.3$), under three point bending ($K_{IP,2}$, $K_{IIP,2}$) and under a pair of virtual forces ($K_{IF,2}$, $K_{IIF,2}$) can be evaluated following the approximated procedure proposed by Kitagawa et al. For a deflected crack characterized by a long branch in a centrally cracked infinite plate **[92]**:

$$K_{IP,2} = K_{IP,0}\cos^{3/2}\theta \tag{3.16a}$$

$$K_{IF,2} = K_{IF,0}\cos^{3/2}\theta \tag{3.16b}$$

$$K_{IIP,2} = K_{IP,0} \sin\theta\cos^{1/2}\theta \tag{3.16c}$$

$$K_{IIF,2} = K_{IF,0} \sin\theta\cos^{1/2}\theta \tag{3.16d}$$

By substituting Eqs. (3.14)-(3.16) in Eq. (3.13), we obtain:

$$\Delta_F = \frac{2}{E}\left\{\begin{array}{l} \int_0^{a_0} K_{IP,0}\left(\frac{\partial K_{IF,0}}{\partial F}\right)_{F=0} dx \\ + \left[\left(\cos^3\frac{\theta}{2}\right)^2 + \left(\sin\frac{\theta}{2}\cos^2\frac{\theta}{2}\right)\right]\left[\int_0^{a_0+a_1\cos\theta} K_{IP,0}\left(\frac{\partial K_{IF,0}}{\partial F}\right)_{F=0} dx - \int_0^{a_0} K_{IP,0}\left(\frac{\partial K_{IF,0}}{\partial F}\right)_{F=0} dx\right] \\ + \left[\left(\cos^{3/2}\theta\right)^2 + \left(\sin\theta\cos^{1/2}\theta\right)^2\right]\left[\begin{array}{ll} \int_0^{a_0+(a_1+a_2)\cos\theta} & K_{IP,0}\left(\frac{\partial K_{IF,0}}{\partial F}\right)_{F=0} dx \\ & - \int_0^{a_0+a_1\cos\theta} K_{IP,0}\left(\frac{\partial K_{IF,0}}{\partial F}\right)_{F=0} dx \end{array}\right] \end{array}\right\} \tag{3.17}$$

It can be noticed that all integrals are formally equal, changing only the integral extremes. An empirical solution can be employed according to that proposed by Tada et al. **[69]**:

$$\frac{2}{E}\int_0^z K_{IP,0}\left(\frac{\partial K_{IF,0}}{\partial F}\right)_{F=0} dz = \frac{6PSz}{EW^2B}V(\alpha)$$

$$V(\alpha) = 0.76 - 2.28\alpha + 3.87\alpha^2 - 2.04\alpha^3 + \frac{0.66}{1-\alpha^2} \quad \text{with} \quad a = \frac{z}{W} \tag{3.18}$$

being z a generic integration variable. Therefore, once each integral of Eq. (3.17) is empirically resolved and the unloading compliance C_u (equal to Δ_F/P) is taken into

account, we can explicit the elastic modulus from Eq. (3.17):

$$E = \frac{6S}{C_u W^2 B}\left\{\begin{array}{l} a_0 V\left(\frac{a_0}{W}\right) + \left[\cos^6\frac{\theta}{2} + \sin^2\frac{\theta}{2}\cos^4\frac{\theta}{2}\right]\left[(a_0 + a_1\cos\theta)\, V\left(\frac{a_0+a_1\cos\theta}{W}\right) - a_0 V\left(\frac{a_0}{W}\right)\right] \\ + \left[\cos^3\theta + \sin^2\theta\cos\theta\right]\left[\begin{array}{l}(a_0 + a_1\cos\theta + a_2\cos\theta)\, V\left(\frac{a_0+a_1\cos\theta+a_2\cos\theta}{W}\right) \\ - (a_0 + a_1\cos\theta)\, V\left(\frac{a_0+a_1\cos\theta}{W}\right)\end{array}\right] \end{array}\right\} \tag{3.19}$$

Now a_2 can be obtained from Eq. (3.19) by employing an iterative procedure. Therefore, the effective critical crack length is equal to $\underline{a} = a_0 + (a_1 + a_2)\cos\theta$ with $a_1 = 0.3a_0$. As it is shown in Figure 3.11, the kinked crack branch consists of the two segments, named a_1 and a_2. If the value of a_2 obtained from Eq. (3.19) is negative, it means that the effective crack length is $\underline{a} = a_0 + (a_1$, with $a_1 \leq 0.3a_0$. Therefore, the expression of Δ_F in such a case is given by:

$$\Delta_F = \frac{2}{E}\left\{\int_0^{a_0} K_{IP,0}\left(\frac{\partial K_{IF,0}}{\partial F}\right)_{F=0} dx + \int_0^{a_0+a_1\cos\theta}\left[K_{IP,1}\left(\frac{\partial K_{IF,1}}{\partial F}\right)_{F=0} + K_{IIP,1}\left(\frac{\partial K_{IIF,1}}{\partial F}\right)_{F=0}\right]dx\right\} \tag{3.20}$$

and a_1 is determined from the following equation by employing an iterative procedure:

$$E = \frac{6S}{C_u W^2 B}\left\{a_0 V\left(\frac{a_0}{W}\right) + \left[\cos^6\frac{\theta}{2} + \sin^2\frac{\theta}{2}\cos^4\frac{\theta}{2}\right]\left[(a_0 + a_1\cos\theta)\, V\left(\frac{a_0 + a_1\cos\theta}{W}\right) - a_0 V\left(\frac{a_0}{W}\right)\right]\right\} \tag{3.21}$$

Finally, the critical stress-intensity factor under mixed mode, $K^s_{(I+II)C}$, is computed through Eqs. (3.6) and (3.14a), by employing the above effective critical crack lengths.

3.5 Conclusion

The present chapter was devoted to the application of the fracture mechanics approaches in the cementitious materials. In particular, this chapter started with a general application of fracture mechanics and earlier approaches of the LEFM. Then, it reviewed the applications of the LEFM in fracture study of cementitious materials. It was found that LEFM is not sufficient for fracture study of concrete since the latter one is a quasi-brittle material in which the fracture parameters of concrete are related to the size effect and the fracture process zone. These parameters are linked to non-linear deformation of concrete.

The non-linear fracture models based on the finite element method or the modified LEFM concept have been proved to be more effective in the determination of the fracture parameters for the cementitious materials.

The two parameter model TPM has proven that the stress intensity factor (SIF) and the crack opening displacement (CMOD) are the only parameters controlling the fracture properties for any geometry of the specimen.

The modified two parameter model MTPM was found to be more accurate in the case of the large deflection of the crack propagation path.

CHAPTER 4

Characterization of materials and Experimental Program

4.1 Introduction

The second chapter dealt with the influence of various constituents on the formulation and the properties of different types of mortars and concretes. Furthermore, In this work, the identification of different constituents that have been utilized in the formulation of cement-based materials (cement, aggregates, fibers) is essential. This chapter presents the details about the experimental campaign conducted for characterizing these materials, through their morphological, physic-chemical and mechanical properties. Moreover, this chapter describes the methods which were applied in preparing and testing the cementitious composites.

4.2 Characterization of materials

4.2.1 Cement

Limestone Portland cement CEM II/A-LL 42.5 R, conforms to **EN 197-1 [93]** is used in this study. This cement was provided by Buzzi Unicem S.p.A. The technical performance of cement provided by the manufacture are the following: it contains from 80% to 94% of clinker and 6% to 20% of limestone, the Blaine specific surface of the ce-

ment is ranged between 3100 to 4400 cm^2/g, an initial setting time from 130 min, and a minimum compressive strength at 28 days of 47 MPa **[94]**. A sample from this cement powder was destined to the cement laboratory of Ain Kbira (Setif) for the purpose of analyzing the chemical composition of this cement,the results obtained are listed in table 4.1. The Physical properties of the cement were tested in the laboratory , the clinker composition calculated using Bogue equations. These results are summarized in table 4.2

Table 4.1: Chemical composition of cement

Chemical composition	CaO	SiO_2	Al_2O_3	Fe_2O_3	MgO	K_2O	SO_3	Cl	LoI	Insoluble residual
Quantity (%)	61.345	19.635	4.26	2.17	2.555	0.83	2.905	0.04	6.003	0.257

Table 4.2: Physical and mineralogical composition of cement

Physical properties	
Blaine/BET specific surface area (cm^2/g)	4085
Compressive strength MPa (28 days)	54.1
Specific density (g/cm^3)	3.08
Bulk density (g/cm^3)	0.98
Bogue composition (clinker) (%)	
C_3S	65.0
C_2S	13.0
C_3A	8.0
C_4AF	8.0

4.2.2 Aggregates

In this study, the silica sand with a grain size distribution of 0/2 mm was used. This sand of gray color is in accordance with the standard **NF P 18-545 [95]**, It is provided by the company Bacchi S.P.A . It was extracted from the Po river from northern Italy (see Figure 4.1)

4.2.2.a Particle size analysis

The particle size analysis was done to determine the size and the respective weight percentages of different grain of the sand specimen. In order to prepare cement mortar according to the European recommendation **EN 196-1 [96]**, the particle size distribution of the sand was corrected to obtain such curve similar to that of standardized sand

Figure 4.1: Sand 0/4 mm

conform to the standard **EN 196-1 [96]**. For this purpose, silica sand with two different grain size distribution (classic sand 0.125/2 mm and fine sand 0/0.6mm) was utilized to obtain a reconstituted sand conform to **EN 196-1** standard, The grain size distribution of the reconstituted sand is summarized in the table 4.3. The grain size distribution curve fine sand , classic sand and the reconstituted sand are presented in Figure 4.2.

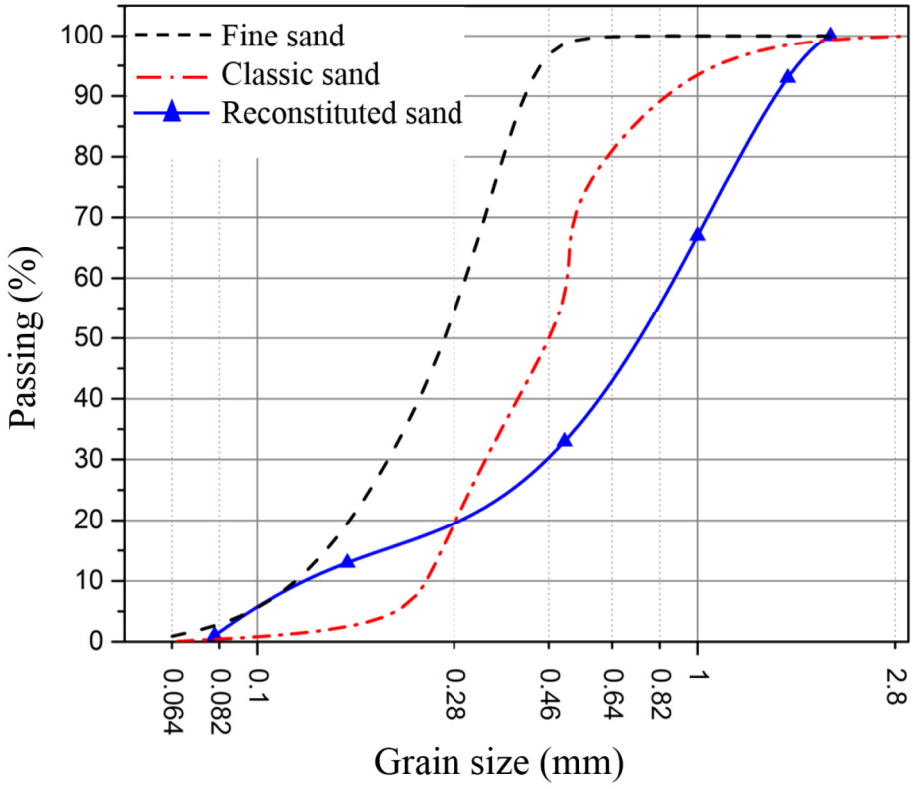

Figure 4.2: Particle size curve of the sand

4.2.2.b Chemical composition

The chemical composition of the sand is available in the technical sheet provided by the company Bacchi S.P.A. It is represented in table 4.4 **[97]**.

Table 4.3: Grain size distribution of the sand 0/2

Sieve diameter (mm)	Particular quantity of remaining sand (%)
2 - 1.6	7
1.6 - 1	26
1 - 0.5	34
0.5 - 0.16	20
0.16 - 0.08	12
<0.08	1

Table 4.4: Chemical analysis of sand

Chemical composition	Quantity (%)
Silicon dioxide (SiO_2)	79.8
Iron oxide (Fe_2O_3)	2.42
Aluminum oxide (Al_2O_3)	3.28
Calcium oxide (CaO)	4.6
Magnesium oxide (MgO)	2.18
Sodium oxide (Na_2O)	2
Potassium oxide (K_2O)	1.96
PH	7

4.2.2.c Density and water absorption

The bulk density was determined using an apparatus with a sieve funnel and tripod, a unit weight measure of 1-liter capacity, a spatula, a straight edge, and an aluminum scoop. The absolute density of the sand was determined according to **EN 1097-6 [98]**. This test allows to measure the absorption coefficient of the aggregates, the results of the different physical characteristics of the sand are summarized in the table 4.5

Table 4.5: Physical characteristics of sand

	Reconstituted sand
Nature	siliceous
Size (mm)	0 - 2
Bulk density (g/cm^3)	1.43
Specific density (g/cm^3)	2.62
Water absorption coefficient (%)	0.25
Finesses modulus	2.2

4.2.3 Admixtures

The high water reducer superplasticizer based on natural and synthetic polymers was used in this study. It was added to the mortar mixtures with a content of 1% of cement weight for getting good workability in fresh state of mortar composites the used superplasticizer is commercialized under the name of Concretan200l and produced by Ruredil **[99]**.

4.2.4 Water

The utilized water in this study is a tap water, the quality of water is conformed to the standard.

4.2.5 Date palm fibers

The date palm tree (Figure 4.3) is a member of date palm tree family (phoenix dactylifera). It is found in the middle east, Northern Africa, the canary Islands, Pakistan, India, and in the United states (California). There are more than 100 million date palm tree in the world and each tree can grow for more than 100 years. In Algeria, there are more than 18 million tree, this amount generates yearly 200 000 tones of wastes, the fibers used in this study are a part of these wastes.

The DPMFs used in the present study are obtained from Deglet- Noor date palms (Deglet-Noor date is one of the most appreciated variety in the world) from the oasis of Tolga (Biskra, Algeria). The DPMFs are the fibers surrounded the stem of the date palm tree.

Figure 4.3: Components of the date palm tree.

The preparation process of the DPMFs from the tree into single fibers is presented in figure 4.4 and it summarized in the following points:

1. The extraction of the woven mat in form of a sheet of a length, width dimensions about 300 mm, 500 mm respectively. It is covered by the petioles(the beginning of the branches). Therefore, after cutting the petiole edges, it is easy to pull out the rectangular sheet of the DPMFs.
2. The woven mat sheet consists of single fibers crossing each other, in order to separate them into single fibbers, the Date palm sheet emerged in water, then the Interlocking fibers were easy separated into single fibers that have a length of 20 to 50 mm. Then let them dry in laboratory oven at a temperature degree of 75 °C until reaching a constant weight. The fibers reached a constant weight after two days of being dried.
3. The single fibers then were cut into desired length of 7 to 10 mm by using a paper cutter with metallic support to fix the Cutting distance of fibers.

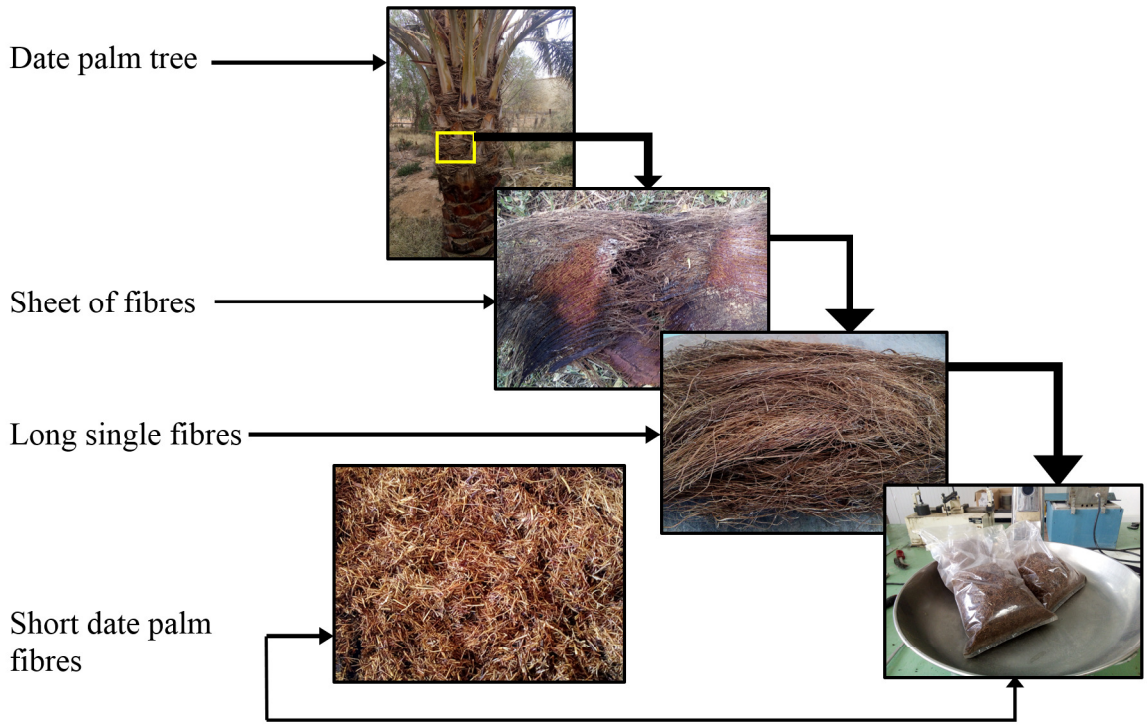

Figure 4.4: Extraction process of date palm fibers

4.2.5.a Chemical characteristics of DPMFs

As seen in chapter 2, the most dominant component in the chemical composition of the Date palm fibers is the cellulose, there is two other components which found in a significant amount, they are the hemicellulose and the lignin. The fractions of theses three components varied in the literature according to many researchers. This varia-

tion could be attributed to which part of tree these fibers come from and the origin of the date palm tree. For instance, according to (AL-KHanbashi et al. 2005) **[100]**, the fractions of the cellulose, lignin, and hemicellulose are 46%, 20%, and 18%, respectively. The cellulose particle found in higher fraction of 54% in the study of (Julkapli et al. 2015) **[101]**. Whereas in the characterization study of (Bendahou et al. 2007) **[102]**, the cellulose component found in lower fractions of 33.5% in the leaves and 44% in the spine. The chemical analysis of the date palm fibers according to multiple researchers are listed in table 4.6

Table 4.6: Chemical composition of date palm fibers

Element(%)	(Al-Khanbashi et al. 2005) **[100]**	(Bendahou et al. 2007)[102]	(Julkapli et al. 2015) **[101]**	(Sbiai et al. 2011) **[17]**	(Mohanty et al. 2014) **[103]**	(Haddadou et al. 2015) **[104]**
Cellulose	46	44	54.71	35	54.75	47.31
Lignin	20	14	15.30	27	15.3	15.67
Hemicellulose	18	n.a	20	28	20	25.72
Water content	5	n.a	6.5	n.a	n.a	n.a
other	11	28	2.45	n.a	n.a	n.a

4.2.5.b Physical and mechanical properties of date palm fibers

The geometrical sizes and physical properties, listed in Table 4.7, are taken from the literature **[31]**, since the fibers used in the present research work come from the same geographic area as those employed by (Kriker et al.2005) **[31]**. It can be observed that the variability in diameter is significant (equal to 50.4%), which is typical of natural fibers. The mechanical properties listed in Table 4.8 are also taken from **[31]**.

Table 4.7: Geometrical sizes and physical properties of DPMF **[31]**

Property	Min.	Max.
Diameter [mm]	0.1	0.8
Bulk density [Kg/m^3]	512	1089
Specific density [Kg/m^3]	1300	1450
Natural moisture content [%]	9.5	10.5
Water absorption to saturation [%]	97	203

Table 4.8: Mechanical properties of DPMF **[31]**.

Property	Length [mm]		
	100	60	20
Tensile strength [MPa]	170 ± 40	240 ± 30	290 ± 20
Elongation [%]	16 ± 3	12 ± 2	11 ± 2
Elastic Modulus [GPa]	4.74 ± 2	5.00 ± 2	5.25 ± 2

4.3 Methods of characterization for mortar composites

4.3.1 Specimens preparation and curing conditions

The mixture proportions adopted for both plain and reinforced cement-based mortar are cement:water:sand (by weight)= $1 : 0.55 : 3$. The ratio between water and cement is fixed after performing a workability test with the flow table according to the European standard **EN 1015-3 [105]**. In particular, the content of water in the mixture shall be enough to produce a flow of about 110% by jolting the flow table 15 times in approximately 15s. The above mortar mix design is prepared according to European Recommendation **EN 196-1 [96]**, and the mortar mixture composition is listed in Table 4.9.

Table 4.9: Mortar mix composition.

Material	Dosage [Kg/m3]
Cement 42.5	580
Water	320
Sand (0-2 mm)	1750
Superplasticizer	6

The mixing process is important in which it has a significant effect on the fresh and hardened properties of the material. It is mandatory to be adapted to mixture nature to obtain a good homogeneity. The mortar specimens with and without DPMF were prepared according to European Standard **EN 196-1:2005** . In the initial phase of specimen preparation, the DPMFs are submerged in water at room temperature for 24 hours and then dried in air, before being added to the mixture(see Figure 4.5).

These operations are needed in order to avoid that fibers absorb an excessive amount of mixing water during the casting. Subsequently, the DPMFs are added in the cement-based mortar matrix, with a fiber content equal to 2, 4, 6, 8 and 10% by volume (Table 4.10).

Figure 4.5: Components of the date palm tree.

Table 4.10: DPMF percentage and weight in the reinforced mortar.

Mixture	DPMF	
	Fiber amount [%]	In weight [Kg/m^3]
PM	-	-
RM_2	2	28
RM_4	4	56
RM_6	6	84
RM_8	8	112
RM_{10}	10	140

This procedure is performed slowly in order to avoid the possible clumping of fibers. Then a superplasticizer (named Concretan200l and produced by Ruredil), with a content of 1% of cement weight, is added to the mixture in order to achieve the desired self-compacting properties. The fresh slurry is hence placed in molds on a conventional vibrating table (the time of vibration is of 30s for each mold). Each mold consists of a beam with prismatic shape, whose sizes depend on the test type being performed. For instance, the $40 \times 40 \times 160mm$ specimens were used for the flexural test. Whereas, the $15 \times 30 \times 160mm$ were used for the fracture tests (see Figure 4.6), more details about these tests conduction is explained in sections 4.3.5 and 4.3.6.

Finally, the specimens are cured in laboratory for 24 hours under normal climatic conditions (temperature equal to 21°C and relative humidity of 50%) and, after demolding, are submerged in water at an ambient temperature for 28 days (see Figure 4.7).

Figure 4.6: mortar molds for flexural and fracture tests.

Figure 4.7: Cementitious composites specimens: (a). Cured specimens submerged in water; (b). Specimens after 28 days

The reinforced mortar specimens are referenced by the notation RM_n, where n is the fiber percentage being examined (i.e. $n = 2, 4, 6, 8$ and 10). Moreover, the plain cement-based mortar specimens are named with the notation PM in the following. Accordingly, six different types of mixtures are formulated.

4.3.2 Workability of cementitious composites

The workability of the mortars was measured by the test with the flow vibrating table according to **EN 1015-3 [105]**. This test measures the spreading diameter of mortar

placed in a frustoconical mold subjected on the top of a shaking table. This table applies 15 shocks each corresponding to a fall of 10 mm (see Figure 4.8). In particular, the content of water in the mixture shall be enough to produce a flow of about 110% by shaking the flow table 15 times in approximately 15s.

Figure 4.8: Workability test

4.3.3 Density of mortar composites

For each specimen, density is determined after curing, according to **EN 1015-10 [106]**. Firstly, the weight of each water saturated specimen is recorded. Then, the specimen is maintained at 105 °C in oven until one weight variation is further recorded. Finally, density is computed according to the above UNI EN Recommendation , and the density mean values, ρ, measured on nine specimens for each of the six mortar mix types.

4.3.4 Compressive test

The compressive test has been done after performing the bending test. Thus, the broken ($40 \times 40 \times 160$ mm) specimens coming from the experimental campaign of bending test were cut into formal specimens of ($40 \times 40 \times 40$ mm). This test was conducted with an electromechanical press machine with a load cell higher than 250KN and a load speed of 2.4 $KN.s^{-1}$, according to EN 196-1. The formal ($40 \times 40 \times 40$ mm) specimens are placed in the center of the machine tray (Figure 4.9). The compressive strength is calculated as the following equation:

$$R_c = \frac{F_{c,\max}}{B.W} \tag{4.1}$$

Where:

- R_c is the compressive strength in [MPa]
- $F_{c,\max}$ is the peak load causing the failure in [N]
- B, W are the width and the depth of specimen respectively [$B = W = 40$ mm].

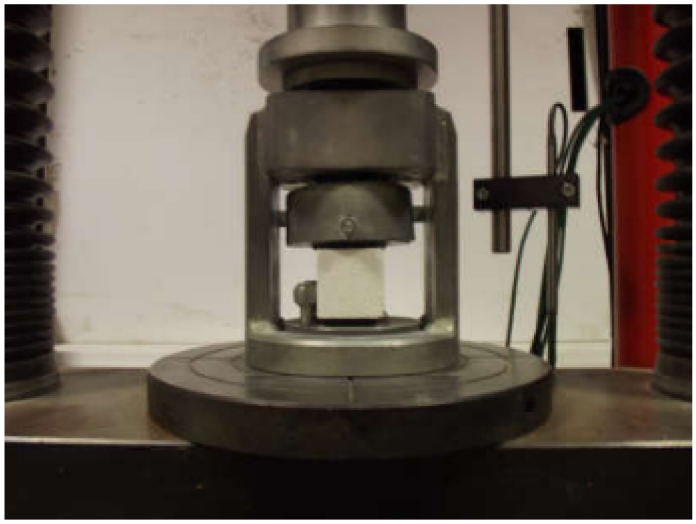

Figure 4.9: Compressive test on composite mortar specimen.

4.3.5 Three-point bending tests on unnotched beams: Flexural strength

The three-point bending tests on unnotched specimens are carried out according to UNI EN 196-1:2005 European standard, which deals with the standard test method to evaluate compressive and flexural properties of cement-based mortar. The tested specimens are characterized by the following geometrical sizes: width (B) $\times$ depth (W) $\times$ length (L)= 40 $\times$ 40 $\times$ 160 mm, and support span (S)= 120 mm. The tests are performed under load control with a rate equal to 44Ns1 according to the ASTM C348-14 Standard (see Figure 4.10). More precisely, the applied load is measured by means of a load cell, whereas the deflection of the specimen is evaluated through the measurement of the head displacement. As is shown in Figure 4.11, each specimen is monotonically loaded up to failure.
The flexural strength R_f can be computed according to the following equation and the experimental results in terms of peak load P_f (see a typical load against deflection curve in Figure 4.11):

$$R_f = \frac{1.5 \cdot P_f \cdot S}{W^3} \tag{4.2}$$

where S and W are the support span and the specimen depth, respectively, both in mm

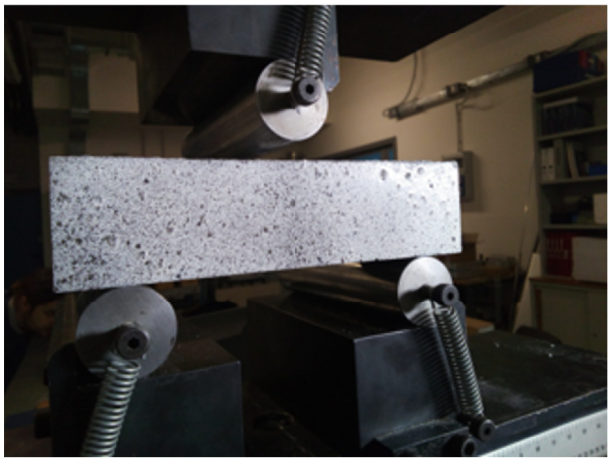

Figure 4.10: loading configuration for three-point bending test

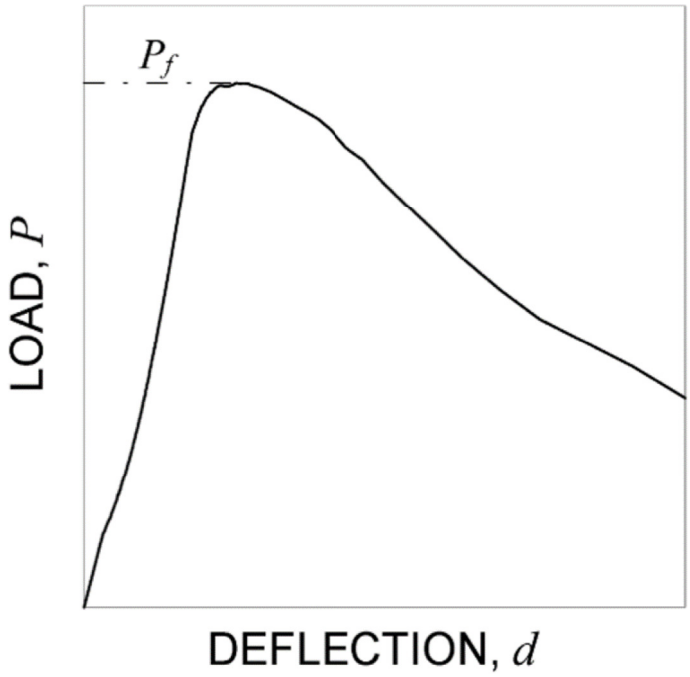

Figure 4.11: Typical load against deflection curve for the tested unnotched mortar specimens

4.3.6 Three-point bending tests on notched beams: Fracture toughness

The three-point bending tests on notched specimens are carried out according to the TPM **[87]** and the RILEM recommendations **[107, 108]**, which deal with the standard test method to evaluate fracture parameters of mortar and concrete. The tested specimens present a notch in the lower part of the middle cross-section, and are characterized by the following geometrical sizes: specimen depth-width ratio $= W/B = 2$; support span-specimen depth ratio$= S/W = 4$; notch length-specimen depth ratio$=$

$a_0/W = 1/3$, and notch width$< 3.175mm$. In more detail, each specimen consists of a beam 15mm $\times$ 30mm $\times$ 160mm ($B \times W \times L$) and, consequently, $S = 120mm$ and the notch length a_0 is equal to about $10mm$ (Figure 4.12).

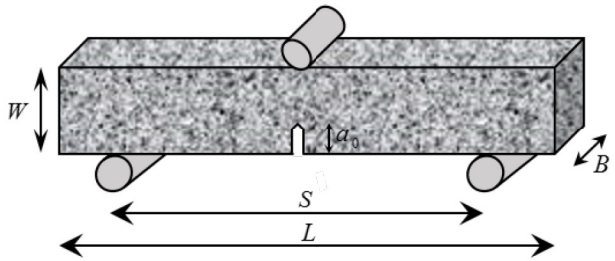

Figure 4.12: Geometrical sizes and loading configuration for three point bending test on notched specimens

The tests are performed under Crack Mouth Opening Displacement (CMOD) control, employing a clip gauge at an average rate equal to 0.1mmh^1 (Figure 4.13). Moreover, the applied load is measured by means of a load cell.

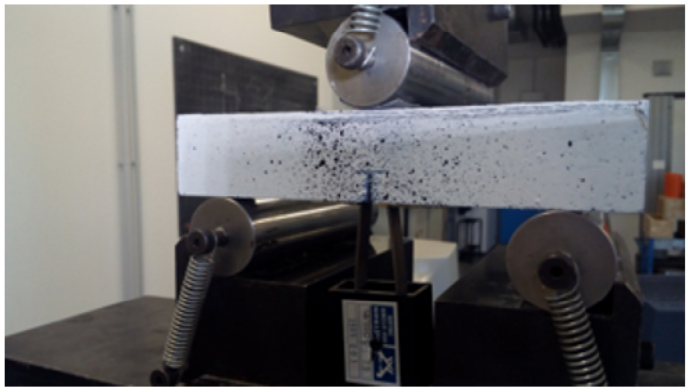

Figure 4.13: Loading configuration for three-point bending test on notched beam.

As is shown in Figure 4.14, each specimen is monotonically loaded. After the peak load P_{max} is achieved, the post-peak stage follows and, when the load is equal to about 95% of P_{max}, the specimen is fully unloaded (up to a load value equal to about zero) by proceeding under load control. Finally, the specimen is reloaded up to failure under CMOD control with the same initial average rate.

On the basis of the experimental results in terms of peak load P_{max}, initial (C_i) and unloading (C_u) linear elastic compliances (see a typical load against CMOD curve in Figure 4.14), elastic modulus E, and fracture toughness $K^S_{(I+II)C}$ (i.e. the critical mixed mode SIF) are computed according to the equations related to the Modified Two-Parameter Model (MTPM), reported in Refs. **[90, 109, 110]**. It should be highlighted that the modified version of the TPM is here employed instead of the original one since cracks are experimentally observed to generally grow under mixed mode

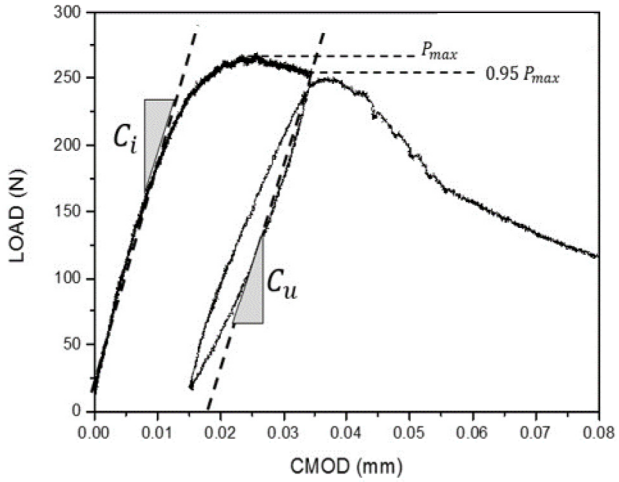

Figure 4.14: Typical load against Crack Mouth Opening Displacement (CMOD) curve for the tested notched specimens.

(Mode I together with Mode II). As is shown in Figure 4.15 for one specimen of each tested type, crack starting from the notch tip deflects (kinked crack) due to the inhomogeneities (i.e. aggregates and DPMFs) embedded in the mortar matrix. As a matter of fact, fracture toughness would be overestimated by considering crack propagation under pure Mode I loading (that is, by using the TPM).

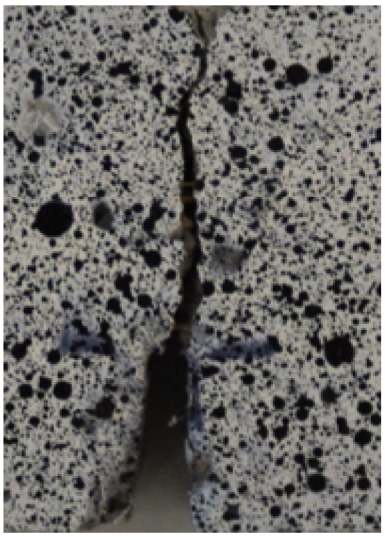

Figure 4.15: Crack path for Composite mortar specimen.

4.3.7 Calibration of Digital Image Correlation (DIC)

The two-dimensional (2D) displacement fields are directly detected from the digital images of the surface of a specimen. Figure 4.16(a) shows an example of an experimental setup for the 2D digital image correlation. The front surface of the specimen is captured usually by a charge-coupled device (CCD) camera with an imaging lens. Then, the images of the front surface of the specimen, before and after deformation, are captured, and stored in a computer as digital images. The first image was taken as a reference, then all the remaining images are compared to the first image by detecting the displacement of a matched point from one image to another. To find the matched point, an area with multiple pixels (such as 19 x 19 pixels) is used to perform the matching process. This area is called a subset, it has a unique light intensity (gray scale) distribution inside the subset itself. It is considered that the light intensity distribution does not change during the test application **[111]**.

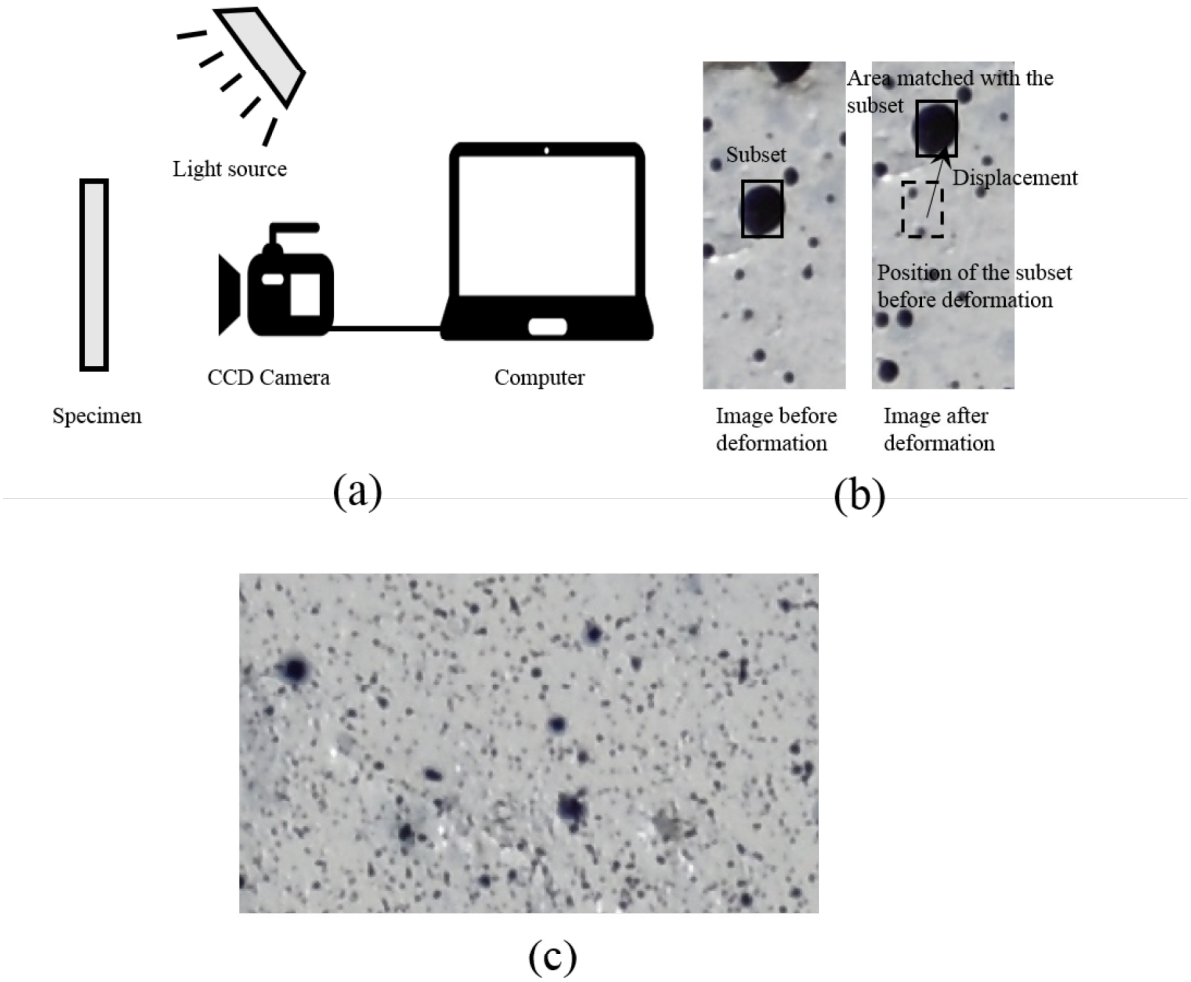

Figure 4.16: (a) Setup for displacement measurement using digital image correlation. (b) Matching the subset before and after deformation. (c) Typical example of random pattern on specimen surface.

The setup used in the laboratory during the three-point bending test is presented in Figure 4.17

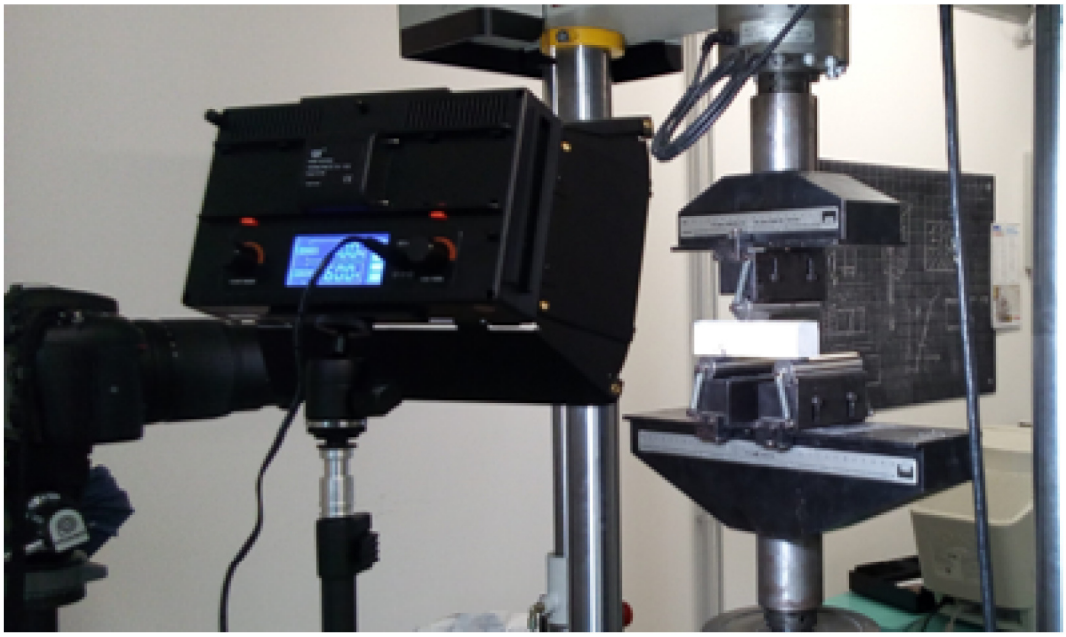

Figure 4.17: Setup for the DIC test.

Figure 4.16(b) shows a part of the region of interest (ROI) in the digital image before and after deformation. The displacement of the subset can be found after deformation by following the same gray pixels in the subset. Once its location is found, the displacement of this subset can be determined. In order to reach this object, the surface of the specimen must have a feature that allows the subset being matched between the selected images. This feature on the front surface of the specimen can be applied artificially (Figure 4.16 (c)), by using random pattern on the surface of specimen produced by black and white spraying paints. This concept is common among other techniques in digital image correlation **[111]**.

On the highlight of the basic concept mentioned above, several functions exist to match the subset between two successive images, the first one is the magnitude of gray intensity value difference as:

$$R\left(x,y,x^{*},y^{*}\right)=\sum\left|F\left(x,y\right)-G\left(x^{*},y^{*}\right)\right| \tag{4.3}$$

And the other one is the normalized cross-correlation as:

$$C\left(x,y,x^{*},y^{*}\right)=\frac{\sum F\left(x,y\right)G\left(x^{*},y^{*}\right)}{\sqrt{\sum F(x,y)^{2}\sum G(x^{*},y^{*})^{2}}} \tag{4.4}$$

where $F\left(x,y\right)$ and $G\left(x^{*},y^{*}\right)$ represent the gray levels within the subset of the undeformed and the deformed images, (x,y) and (x^{*},y^{*}) represent the coordinates of the

pixels in the subset before and after deformation, respectively. The summation symbol represents the sum of the values within the subset. There are several functions except Equations (4.2) and (4.3), however, the normalized cross-correlation (Equation (4.2)) is widely used in the digital image correlation analysis **[111]**.

The utilization of the DIC technique was performed by VIC-2D software™ provided by correlated solution. The steps required for the analysis of each specimen are summarized in the following points:

- The first image is added as a reference image.
- The remaining images are added as deformed images.
- The measurement scale of the reference image is defined for getting the results in metric unit instead of pixel.
- The definition of the ROI, which represents the zone where the crack propagates (Figure 4.18).
- The definition of subset's dimensions, this step is very important because smaller or bigger subset will influence badly the matching for the displacement computation.
- The start of analysis, and exportation of the results.

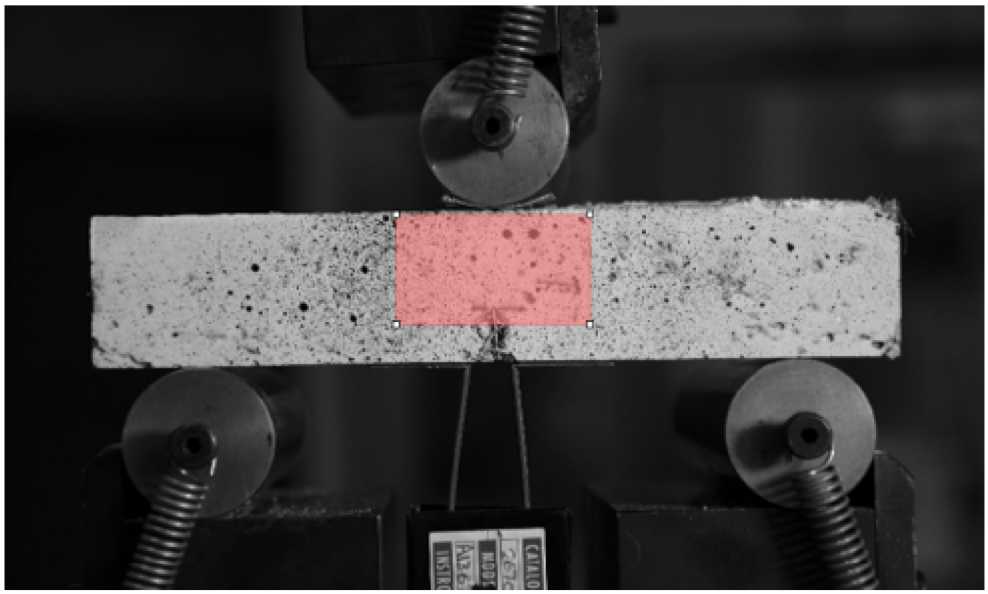

Figure 4.18: ROI for the tested specimen.

4.4 Conclusion

The main characteristics of the materials used and the methods of preparing the cementitious composites could be summarized in the following points;

- The sand used in this study was silica sand of grain distribution of 0/2 mm. its chemical composition is mainly composed of silicion dioxide (SiO2).
- The cement used in this study was a limestone Portland cement CEM II/A-LL 42.5 R contains more than 80% of clinker. It has a Blaine surface of 4085 cm2/g , the mineralogical composition of cement is mainly composed of C3S (65%), C2S (13%), C3A (8%)and C4AF (8%)
- The date palm fibers used in this study are delivered from the oasis of Biskra region, it was the mesh mat surrounding the trunk of the date palm tree. The main chemical composition of these fibers provided by other studies for a similar date palm fibers was the cellulose (35% to 54%) . The fibers diameter ranged from 0.1 to 0.8 mm and with a tensile strength of about 170 MPa.
- To reach the objectives declared in chapter 1, cubic and prismatic specimens were prepared after optimizing the W/C ratio for the cement composites. The flexural and compressive tests were carried out according to the European recommendations using an Instron machine 8862. Whereas, the fracture tests were performed according to the Two parameter model
- A CCD camera was used to capture multiple images during the three-point bending test for the DIC analysis.

CHAPTER 5

Results and discussion

5.1 Introduction

After the identification of the materials employed and the description of the methods used for preparing the mortar composites. This chapter presents the results of our experimental program on mortar composites. Moreover, it is followed by results discussion and comparison between the recent previous research works were done on this subject.

The fresh state properties of mortar composites were first presented , for the purpose of determining the optimum water and superplasticizer content for the composites formulation, Thereafter, the prepared mortar composites with and without different amount of DPMF were investigated in terms of the mechanical properties in dry state, in which, compressive strength , flexural strength and fracture properties of cement mortar composites were discussed. Furthermore, the density of mortar composites and their correlation with the mechanical behavior is presented.

5.2 Properties of fresh mortars modified with DPMF

5.2.1 Workability

The flow results of plain mortar and reinforced mortars with DPMF amounts of 0%, 2%, 4%, 6%, 8% and 10% are presented in Table 5.1 and illustrated in Figure 5.1. It

can be remarked that the flow of the reinforced mortars decreased with the increase of DPMF content. This decrease can be neglected at the scale of the rheological characteristic of mortar. This result is in accordance with the **EN 1015-3 [105]** standard. As a matter of fact, the utilization of the DPMF in the wet state was beneficial on the flow property of the fresh reinforced mortar, as wet fibers are already saturated, then do not influence the matrix ingredients, specially the water. A similar result was found in literature **[25]**, the authors found that the addition of vegetable fibers in wet state has no negative effect on the flow of the composite mortar. The small decrease with the DPMF volume fraction of 10% is attributed to the agglomeration phenomenon of the fibers which is very hard to be avoided at a high reinforcement ratio, the presence of small DPMF pellets in the mortar slurry makes the flowability of mortar to be lower compared to the flow of plain mortar.

Table 5.1: Flow of Unreinforced and reinforced mortars with different amount of DPMF.

Fiber content [%[	Flow [%]	Decrease [%]	Flow required by EN 1015-3 [%]
0	110.92	–	
2	110.5	0.42	
4	109.85	1.07	
6	109.50	1.42	110±5
8	108.24	2.68	
10	106.42	4.5	

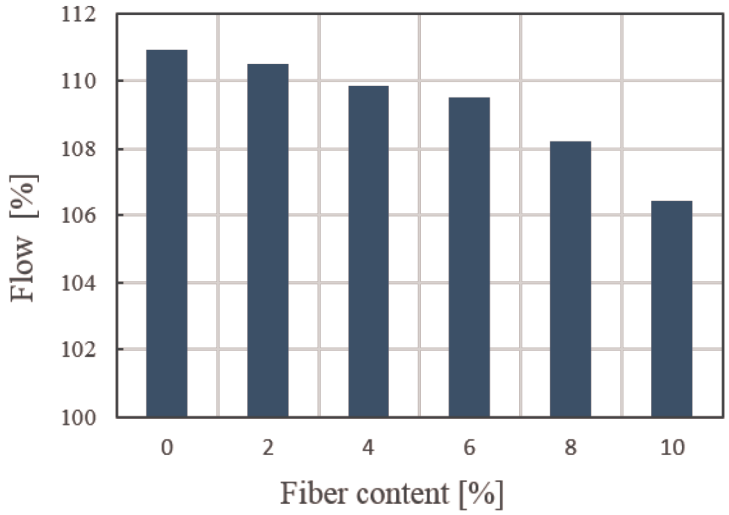

Figure 5.1: Flow of the unreinforced and reinforced mortars with different amount of DPMF.

5.3 Properties of hardened mortars modified with DPMF

5.3.1 Mortar Density

The measured values of the mortar density, ρ, are listed in Table 5.2 and illustrated in Figure 5.2. It can be observed that the density of the reinforced mortars gradually decreases by increasing the dosage of DPMF. Such a decrease with respect to plain mortar ranges from 0.74% (RM_2) to 9.8% (RM_{10}), and is due to (i) increase of porosity by including fibers, and (ii) alveolar structure of fibers. Similar results were found by Xiaoli et al **[112]**, in which the bulk density decreased by up to 37.3% and 35.3% when using a reinforcement of Rice fiber and Bamboo fibers, respectively. It can be observed also that the standard deviation increases up to 70.65 kg per 1 m^3 by increasing the DPMF content, this phenomenon could be attributed to the distribution of fibers in mortar mix slurry during preparation of samples, which produces such a variance in the weight of the specimens at 28 days of being cured in air.

Table 5.2: Density mean value measured on nine specimens for each mortar mix.

Mortar mix	Density, ρ [kg/m^3]	SD, [kg/m^3]	COV, [%]
PM	2297.44	27.35	1.19
RM2	2280.43	30.61	1.34
RM4	2236.42	36.59	1.64
RM6	2172.46	39.95	1.84
RM8	2136.16	58.24	2.73
RM10	2071.93	70.95	3.42

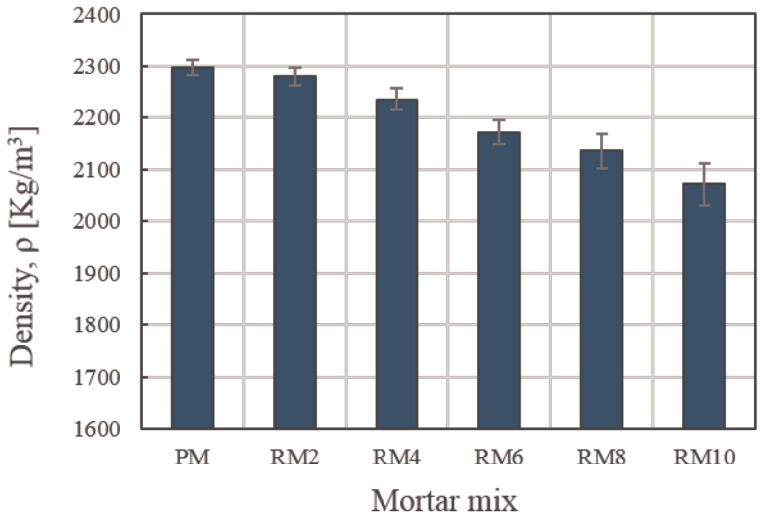

Figure 5.2: Density mean value measured on nine specimens for each mortar mix.

5.3.2 Compressive strength

The cubic $40 \times 40 \times 40$ of unreinforced and reinforced specimens with multiple fractions of DPMF were tested under a compression load at the age of 28 days of being cured in water. The compressive strength results of the mortar composites are summarized in the Figure 5.3 , it can be seen that the compressive strength decreases by up to 50% with the increase in the DPMF content (up to 10% of DPMF) , this decrease was from about 49 MPa for the plain mortar to about 24 MPa for the composite mortar reinforced by 10% of DPMF.

The aforementioned results are in accordance with literature, in which Nora et al **[113]** recorded a compressive strength loss of 15.8-51.9%. other researchers found loss rate of lower than the mentioned results, Benmansour et al **[20]** recorded a loss rate in the compressive strength of about 82% at fiber reinforcement ratio of 5%. This behavior is attributed to the fact that the increase of fibers content leads to the decrease the density of the reinforced specimens. As a matter of fact, a high content of fibers caused in the formation of fibers pellets which makes voids introduced into the mortar composites. The best compressive strength result obtained for reinforced mortar specimens was 36 MPa, at a fiber reinforcement ratio of 2%, which still lower than that of plain mortar by 25.40%.

Generally, the incorporation of the date palm fibers into the cementitious matrices would reduce the compressive strength of cementitious composite. The major factor behind this decrease is the increased porosity in the composite materials, which is in agreement with many researchers in literature **[20, 30, 113]**. The possible reasons of the fall in the compressive strength can be summarized in the following points :

- The porous structure of the vegetable fibers which creates more voids in the composite specimens.
- The capillarity of the vegetables fibers.
- The low density of the vegetables fibers compared with that of matrix **[30, 113]**.
- The variance in the real amount of water between the reinforced mortar mixes, as it has been mentioned in the previous chapter, the DPMF were used in wet state, for the reasons of saving the water of hydration not absorbed by the fibers. Though this mixing process has a good results on the flowability of the mortar mixes, it has a negative effect on the compressive behavior of the composites.

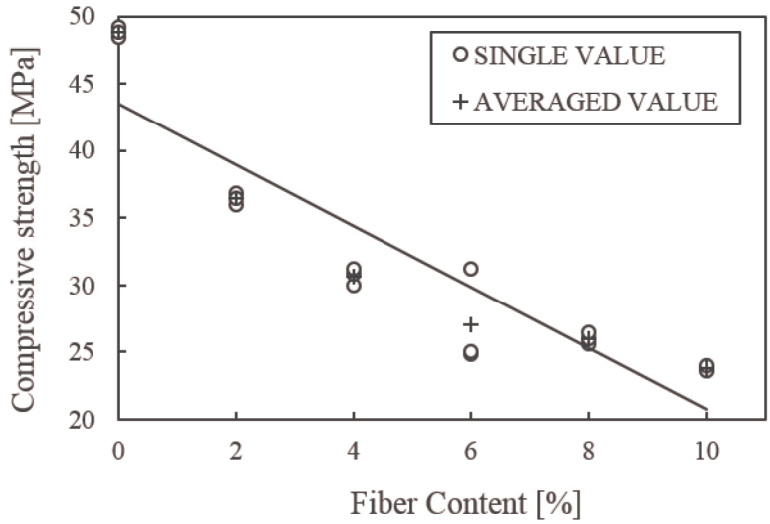

Figure 5.3: Compressive strength of the plain and the reinforced mortars with DPMF.

5.3.3 Compressive strength and density correlation $[R_c \ \& \ D]$

In order to show up the influence of the apparent density on the compressive strength of composite mortar, a relationship trending curve is plotted in the Figure 5.4. In particular, the following equation was obtained for the prediction of the compressive strength from the measured density values related to each fiber reinforcement ratio.

$$R_c = 0.0748e^{0.0027\rho}; \qquad R^2 = 0.824 \tag{5.1}$$

it is well indicated in the figure that the compressive strength decreases by the decrease rate of the density (increasing content of the fibers). Generally, the loss of density by the utilization of natural fibers always be accompanied by a loss in the compressive strength **[20, 112, 113, 114]**

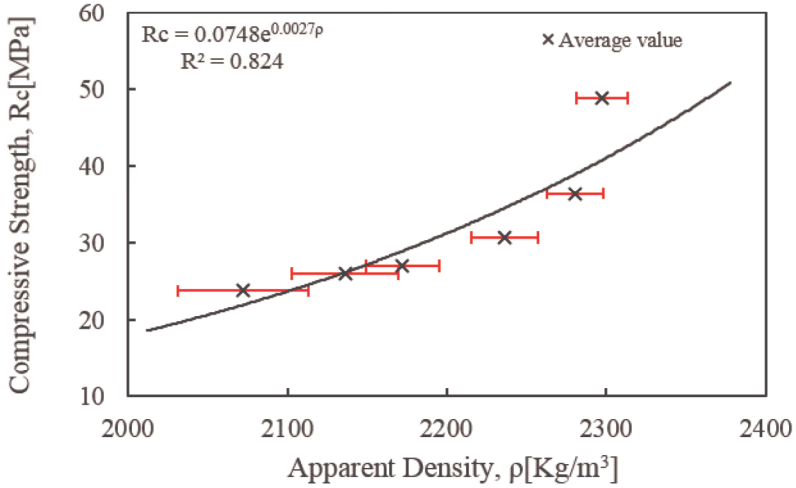

Figure 5.4: Relationship between the Compressive strength and the apparent density.

5.3.4 Flexural strength

By examining the experimental load-deflection curves obtained from the experimental campaign described in Sub-Section 4.3.5, it can be noticed that, by increasing the fiber percentage, the value of the peak load decreases (as is shown in Figure 5.5 for plain mortar specimens and mortar specimens reinforced with DPMF). Such a behavior may be induced by the increase of porosity with the fiber dosage, this increase is due to the inclusion of air during processing, limited wettability of fibers and low ability of fibers to be more compact **[115]**.

On the other hand, it can be observed that the use of DPMF improves the post-peak behavior, and delays the failure of the reinforced specimens in comparison with the plain mortar specimens. Such a behavior is mainly related to the fiber-bridging mechanism, which consists in the transmission of additional tensile stresses caused by the DPMF across the crack surfaces.
The obtained results are listed in Table 5.3 for each tested specimen. In more detail, the measured values of peak load P_f and the results in terms of flexural strength (see Figure 5.6) R_f determined according to Eq. (4.1) are reported.

Table 5.3: Flexural strength of different mortar composites.

Specimen type	P_f[kN]	R_f[MPa]
PM (3)	2.15	6.05
	2.37	6.66
	2.16	6.08
RM_2 (3)	2.17	6.11
	1.98	5.56
	1.90	5.35
RM_4 (3)	1.656	4.658
	1.87	5.26
	1.57	4.40
RM_6 (3)	1.294	3.64
	1.43	4.03
	1.40	3.93
RM_8 (3)	1.22	3.44
	1.13	3.17
	1.24	3.49
RM_{10} (3)	1.04	2.93
	1.20	3.37
	0.96	2.69

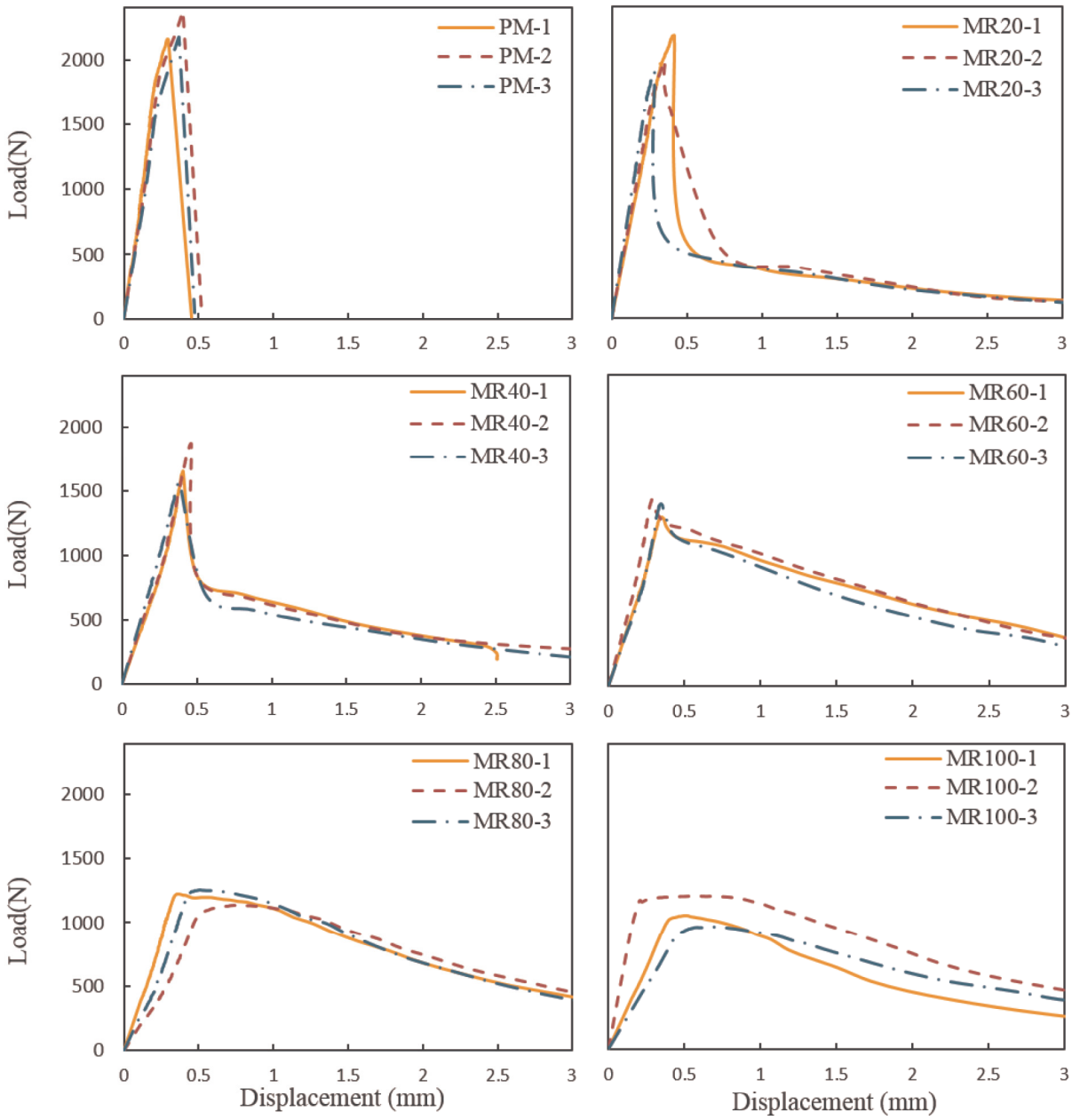

Figure 5.5: Typical load-deflection curves for studied mortar composites (PM and RM)

It can be remarked that the best performance in terms of flexural strength is generally achieved for plain mortar specimens: the R_f value for PM specimens is, for instance, about two times greater than the corresponding value for RM_{10} specimens, that is, an increase of the DPMF content does not produce a beneficial effect on flexural strength. As was observed by Boumhaout and co-workers **[116]**, such a result is mainly due to the addition of DPMF to the mortar matrix, which promote the creation of pores. Therefore, the porosity of the DPMF reinforced specimens increases and, consequently, the compactness and the cohesion of the composite material are significantly reduced. Moreover, the decrease in flexural strength is also related to a poor bonding at the fiber-matrix interface **[20]**. Note that different chemical surface treatments (such as alkali and acid treatments) can be adopted in order to improve the

fiber-matrix interfacial bonding **[117]**.

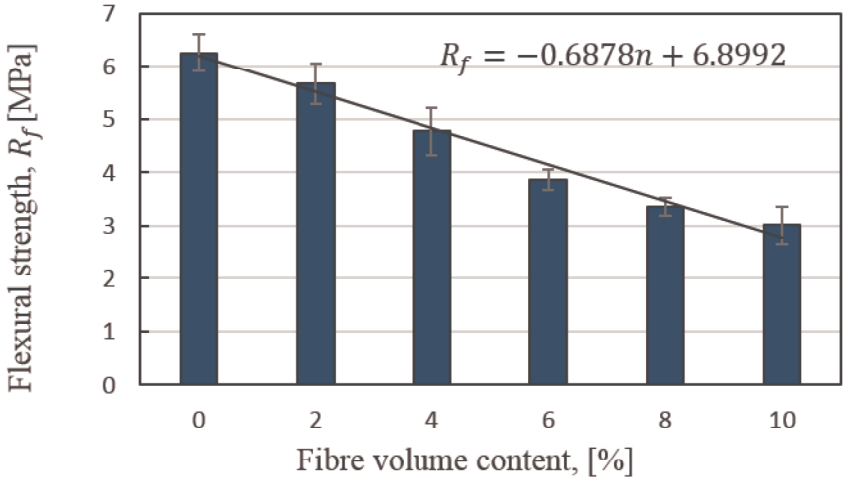

Figure 5.6: Relation of flexural strength, R_f with fiber content, %

5.3.5 Fracture Toughness

By examining the experimental load-CMOD curves coming from the experimental campaign described in Sub-Section 4.3.6, it can be observed that the use of DPMF generally improves the softening behavior in comparison with that related to PM specimens. For instance, as far as the load-CMOD curves for both plain mortar and mortar reinforced with 8% of DPMF are concerned (Figure 5.7), a significant load-bearing capability increase in the post-peak behavior can be noticed, even in the case of large values of CMOD. By increasing the DPMF percentage, this trend is much more pronounced due to the effectiveness of fibers.

From the visual inspection of the crack path in each tested specimen, it is observed that the crack starting from the notch tip generally deflects, as is shown in Figure 5.8 for one specimen of each tested amount of reinforcement. Such a deflection is the result of inhomogeneities embedded in the cementitious matrix. In particular, inhomogeneities can be represented by aggregates and DPMF for plain and reinforced mortar specimens. Therefore, a Mixed Mode loading occurs at the tip of the crack.

The results deduced through the MTPM are listed in Table 5.4 for each tested specimen. More specifically , the measured values of peak load $P_{\max}$ and the results determined for elastic modulus E and critical mixed mode SIF $K^S_{(I+II)C}$ are reported in such a Table(5.4).

In agreement with other studies available in the literature **[38, 118, 119]**, the values of both elastic modulus and fracture toughness decrease with an increase of the DPMF content (Table 5.4). For instance, the effect of fiber content is evaluated in terms of

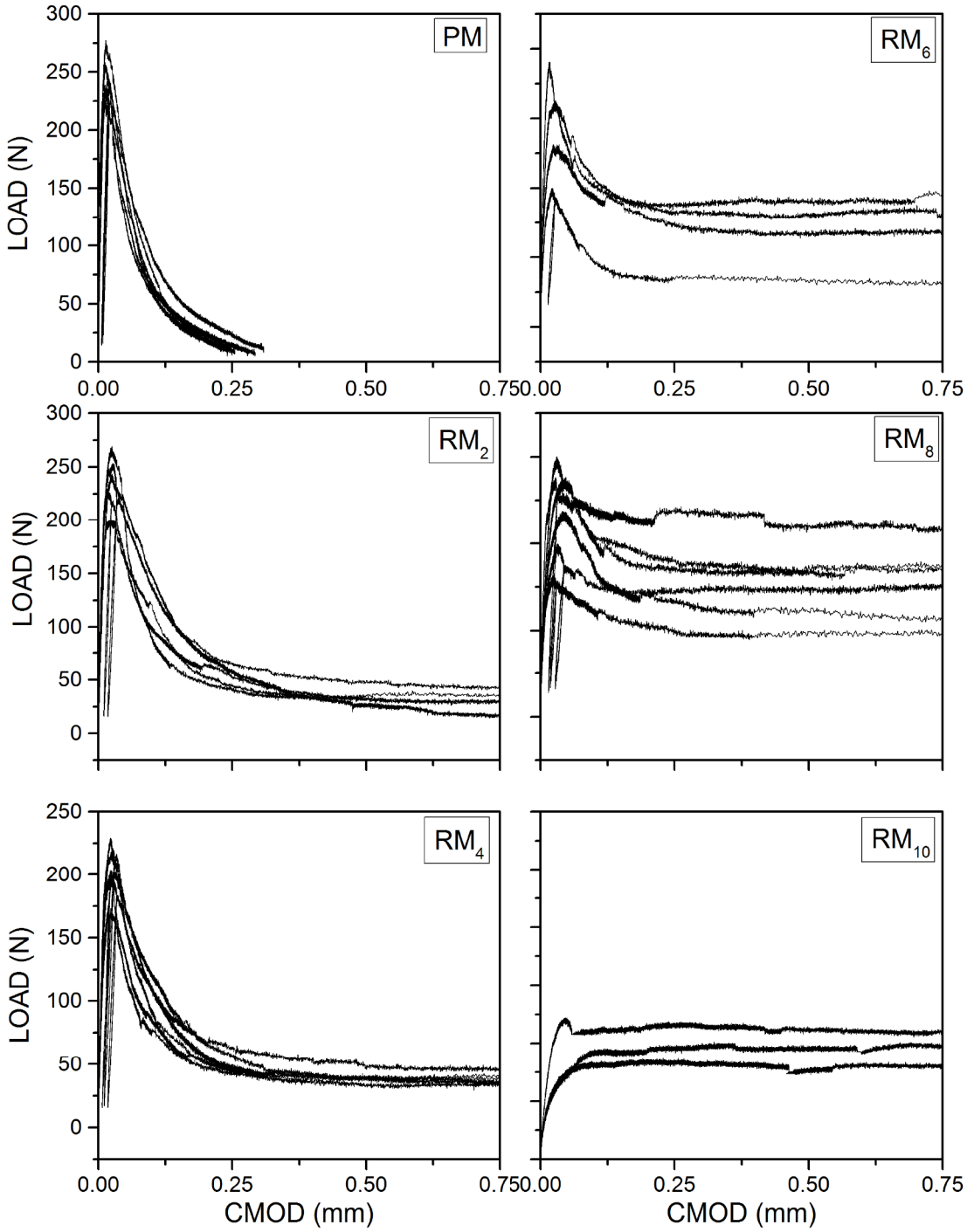

Figure 5.7: Typical load-CMOD curves for plain mortar specimens and reinforced mortar specimens with DPMF.

elastic modulus E and critical mixed mode SIF $K^S_{(I+II)C}$ by interpolating the averaged experimental values of such parameters for the five different values of fiber content being examined (Figure 5.7).

Such a decrease in the critical mixed mode SIF $K^S_{(I+II)C}$ with respect to plain mortar ranges from 7% (RM_2) to 66% (RM_{10}), and can be considered to be significant only for high fiber contents: from RM_6 (decrease equal to 32%) to RM_{10} (decrease equal to 58%).

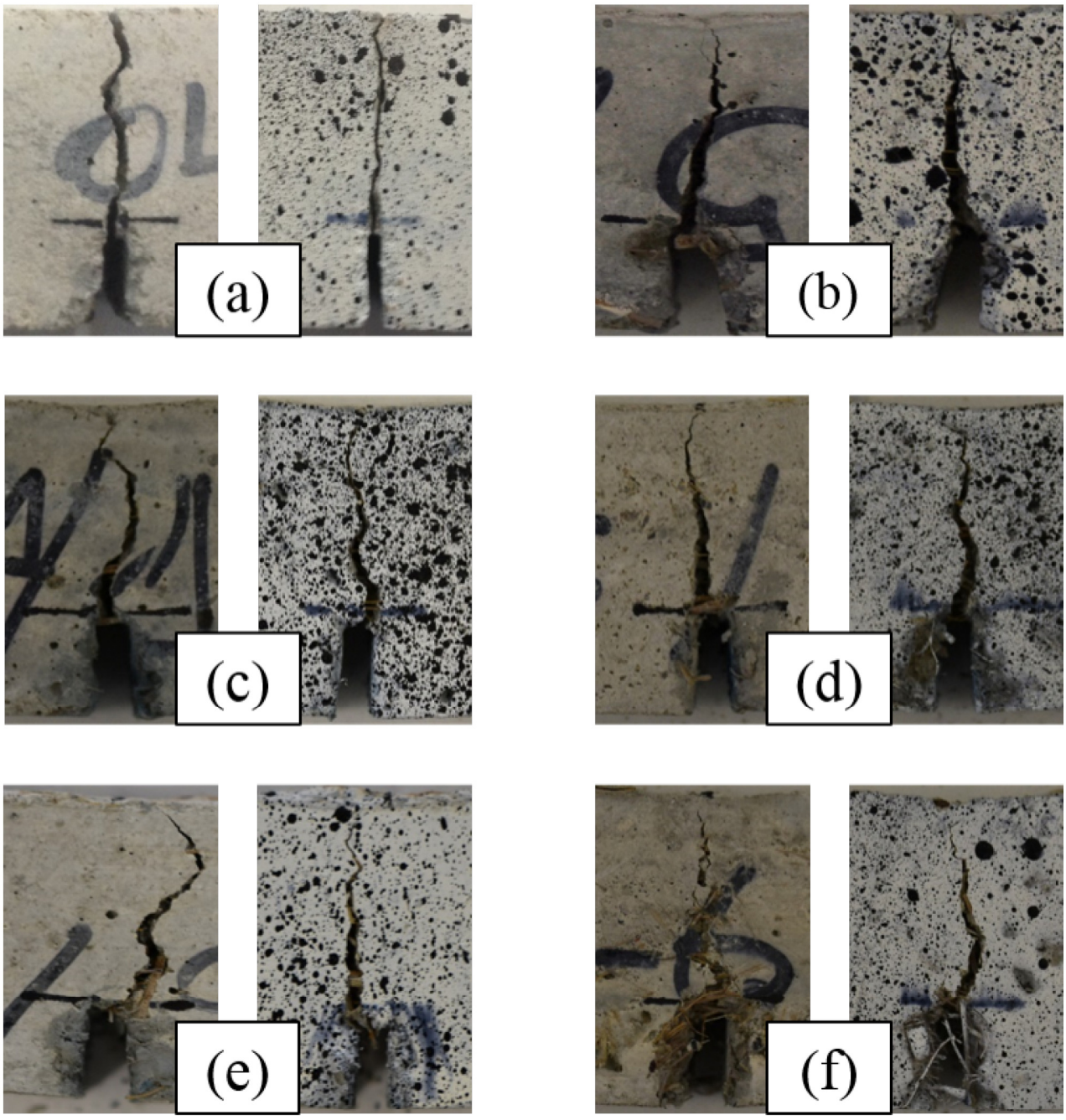

Figure 5.8: Crack path for one notched mortar specimen of each tested type: (a) PM; (b) RM_2; (c) RM_4; (d) RM_6; (e) RM_8; (f) RM_{10}.

Table 5.4: Peak load, $P_{\max}$, elastic modulus, E, and critical SIF, $K^S_{(I+II)C}$, for each notched specimen being considered. The number of tested specimens for each type is reported in round brackets.

Specimen Type	$P_{\max}$ [kN]	E [MPa]	$K^S_{(I+II)C}$ [MPa(m)$^{0.5}$]
PM (6)	0.249	22028.759	0.710
	0.215	24761.043	0.565
	0.240	21350.979	0.615
	0.263	21539.808	0.676
	0.227	20622.030	0.587
	0.226	31261.008	0.878
RM_2 (5)	0.230	12529.312	0.543
	0.238	19499.225	0.621
	0.221	16133.067	0.544
	0.259	19144.118	0.706
	0.187	17732.783	0.575
RM_4 (6)	0.191	17668.427	0.512
	0.209	15106.863	0.578
	0.196	11673.816	0.480
	0.222	17702.556	0.683
	0.193	16260.402	0.650
	0.166	11917.614	0.429
RM_6 (4)	0.162	12725.507	0.439
	0.087	12146.371	0.314
	0.153	9876.432	0.417
	0.109	11715.699	0.363
RM_8 (6)	0.085	5201.028	0.199
	0.106	10756.276	0.364
	0.073	4756.530	0.154
	0.133	6412.145	0.287
	0.127	6897.511	0.327
	0.139	9728.548	0.380
RM_{10} (3)	0.093	2170.236	0.193
	0.115	5876.341	0.276
	0.076	3089.028	0.185

In particular, the following expressions are obtained:

$$E = -1885.7n + 22474.4 \tag{5.2}$$

$$K^S_{(I+II)C} = -0.05n + 0.69 \tag{5.3}$$

where n is the fiber percentage. Note that the single values related to E and $K^S_{(I+II)C}$ are also reported in Figure 5.9.

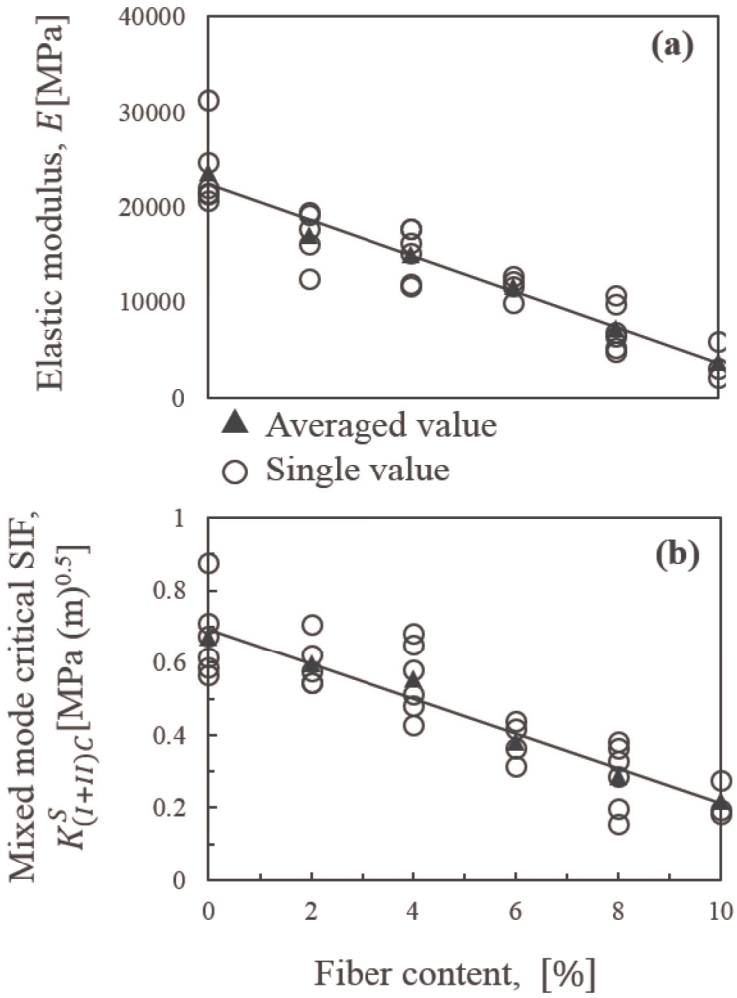

Figure 5.9: DPMF content effect on: (a) elastic modulus, E; (b) critical SIF under mixed mode stress state, $K^S_{(I+II)C}$.

For DPMF content equal to 2% (RM_2 specimen type), the above equations estimate an E decrease equal to about 17% and a $K^S_{(I+II)C}$ decrease equal to about 14% with respect to the values related to PM specimens. This behaviour can be explained as follows:

- The lower elastic modulus of the vegetable fibers when compared with the matrix elastic modulus;

- The incorporation of air during the mixing phase, that increases with the amount of DPMF.

Note that the mortar specimens characterized by a low content of DPMFs present fracture toughness values similar to those related to cement-based composites reinforced with traditional fibers. For instance, the averaged value of $K^S_{(I+II)C}$ related to RM_2 specimen type (0.598 MPa $\cdot m^{1/2}$) is in agreement with that determined by Carpinteri et al. **[110]** for concrete specimens reinforced with 2.5% of polypropylene fibers (0.658 MPa $\cdot m^{1/2}$).

As a conclusion, although the increase of fiber content reduces the fracture properties of reinforced mortar with respect to those of plain mortar, the $K^S_{(I+II)C}$ values obtained for low concentration of fibers (that is, DPMF content equal to 2% by volume) are good enough, and enable the use of these materials for non-structural and low-cost civil constructions.

5.3.6 Toughness Index

The toughness index of cementitious materials is directly related to the area under the load-deflection or the load-CMOD curves. In literature, the toughness index is usually refers to the area under the load-deflection curve **[120]**. For instance, **ASTM C1018 [121]** defines the toughness index of the unnotched beams as the ratio between the area under the load deflection curve up to a prescribed deflection and the area under the same curve up to the first crack deflection, where the prescribed deflections are defined as multiples of the first crack deflection value. Other researchers use this concept for the definition of toughness index for notched beams also **[122]**. It can be noticed that the above indexes depend on the deflection value at the first crack load, which is difficult to be defined from the load-deflection curves. In this case, it can be determined graphically only by assuming the first crack load is equal to the load where the curve starts to deviate from the linearity. In order to facilitate this process, Bryans et al **[123]** have proposed recently a toughness index based on the area under load-CMOD curve up to the first peak of notched specimen. This concept is simpler and more objective way than that based on the first crack value and corresponds to the end of the cementitious matrix dominant response **[120]**.

The toughness index I_t is herein measured by following a similar approach reported in the works by Gopalaratnam et al **[124]** and Jamet et al **[125]**. It is defined as the ratio between the area under load-CMOD curve up to a prescribed multiplier m of $CMOD_{peak}$(which is the CMOD value at the peak load) and the area under the same curve up to $CMOD_{peak}$ (Figure 5.10) Now five different values of the multiplier m are

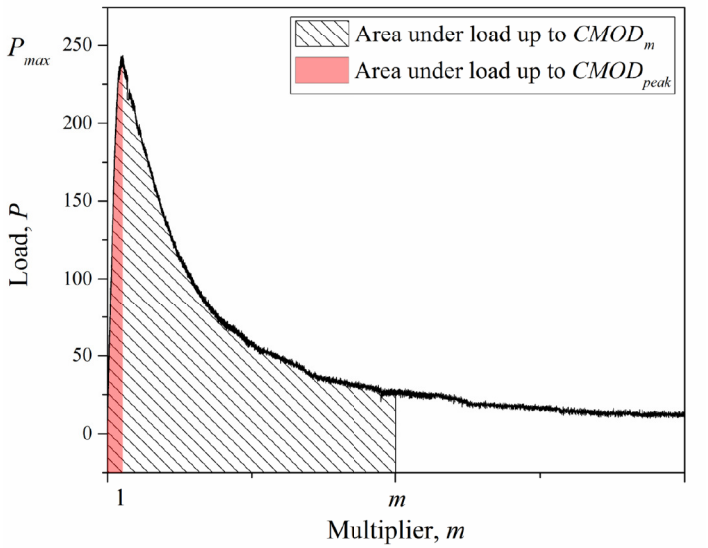

Figure 5.10: Definition of the toughness index .I_t.

examined (1, 3, 5, 10 and 15), and the toughness index is computed as the average of the values related to six beams, for each of the six mortar mix types (PM, RM_2, RM_4, RM_6, RM_8, RM_{10}). The results obtained are plotted in Figure 5.11, it can be remarked that the toughness index increases with the increase of both the multiplier and the fiber's content. For instance, the plain mortar indicates a maximum toughness value corresponds to a $CMOD_{peak}$ multiplier equal to 15 of 5.36, as, for reinforced mortar with 10% of DPMF, the toughness index reaches a maximum value of 19.08 corresponds to the same multiplier. It can be also remarked that where the curves overlap with each other up to a CMOD value equal to about 3 times $CMOD_{peak}$. Such a behavior denotes that inclusion of DPMF starts to significantly delay the growth of macroscopic crack from CMOD = 3 $\times$ $CMOD_{peak}$.This analysis suggests that the DPMF inclusion produces an increase of the required energy for the beam collapse.

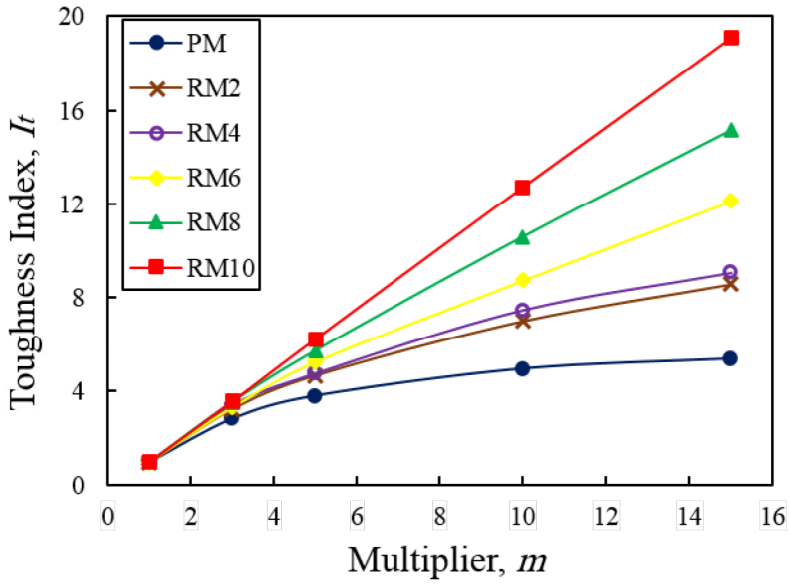

Figure 5.11: Toughness index I_t as a function of the multiplier m, for each mortar mix examined.

5.3.7 DIC displacement fields (2D) of notched beams

The DIC measurement of the displacement field (2D) are herein presented in this section. For each image, the rectangular region of interest was selected above the notch, which is known also as the fracture process zone. The (2D) horizontal displacement are presented for three different regions in the load application: (a). The pre-peak region with a load application of 50% and 95% of the peak load, respectively; (b). The peak load region; (c). The post-peak region which is represented by a CMOD value three times greater than the CMOD value corresponding to the peak load region. These region selections were chosen for the evaluation of the crack extension for different amount of DPMF content. To make the discussion succinct, only one specimen is presented for each fibers content.

Figure 5.12 shows the horizontal displacement (2D) of the plain mortar specimen. It can been seen that the horizontal displacement near the notch tip is almost imperceptible for the pre-peak region and the peak load region, with values ranged between $4 \times 10^{-3} mm$ and $8 \times 10^{-3} mm$,whereas for the post-peak region, it can be noticed that the horizontal displacement reached a value of $16 \times 10^{-3} mm$. Moreover, it can be remarked that the horizontal displacement around the notch tip was developed in an unstable manner, in which there is a sudden jump in the displacement value after peak load region.

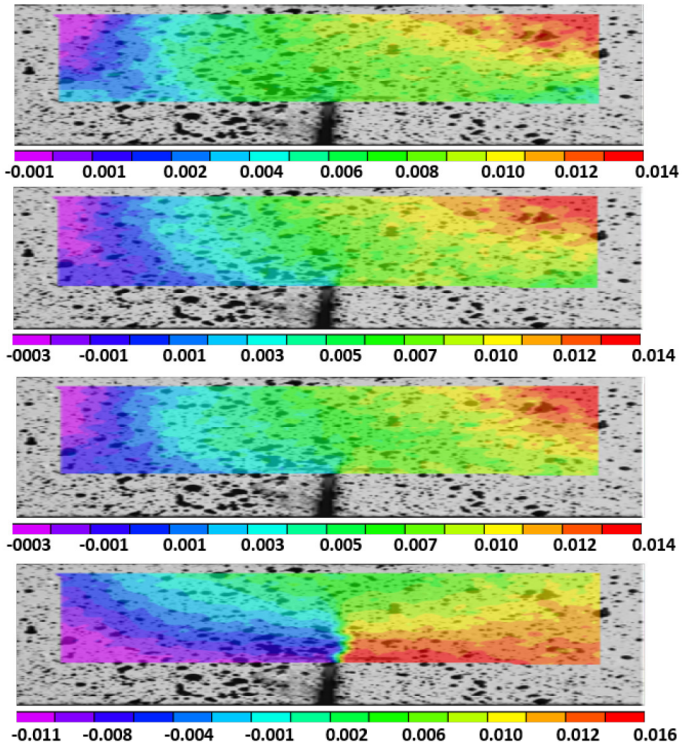

Figure 5.12: Horizontal displacement fields at: (a) 50% Peak load, (b) 95% Peak load, (c) Peak load, and (d) Post-peak load, for plain mortar specimen.

The horizontal displacement (2D) of the reinforced mortar specimen with 2% of DPMF is presented in the Figure 5.13. It can be observed that when the load application rate was 50% of the peak load, the 2D H-displacement near the tip notch was very low (0.0018 mm). For the pre-peak and peak regions, the crack is visible as the distinct displacement-jump at the tip of the notch. The h-displacement near the tip of the notch was $6 \times 10^{-3} mm$ and $8 \times 10^{-3} mm$ under a load application corresponding to 0.95 of peak load, and the peak load, respectively. The last image is related to the post-peak region in the load application, it can be seen that the extent of displacement-jump at the tip of the notch is clearly visible, the crack propagates in an unstable manner, and the h-displacement reached a higher value compared to the plain mortar specimen ($40 \times 10^{-3} mm$)

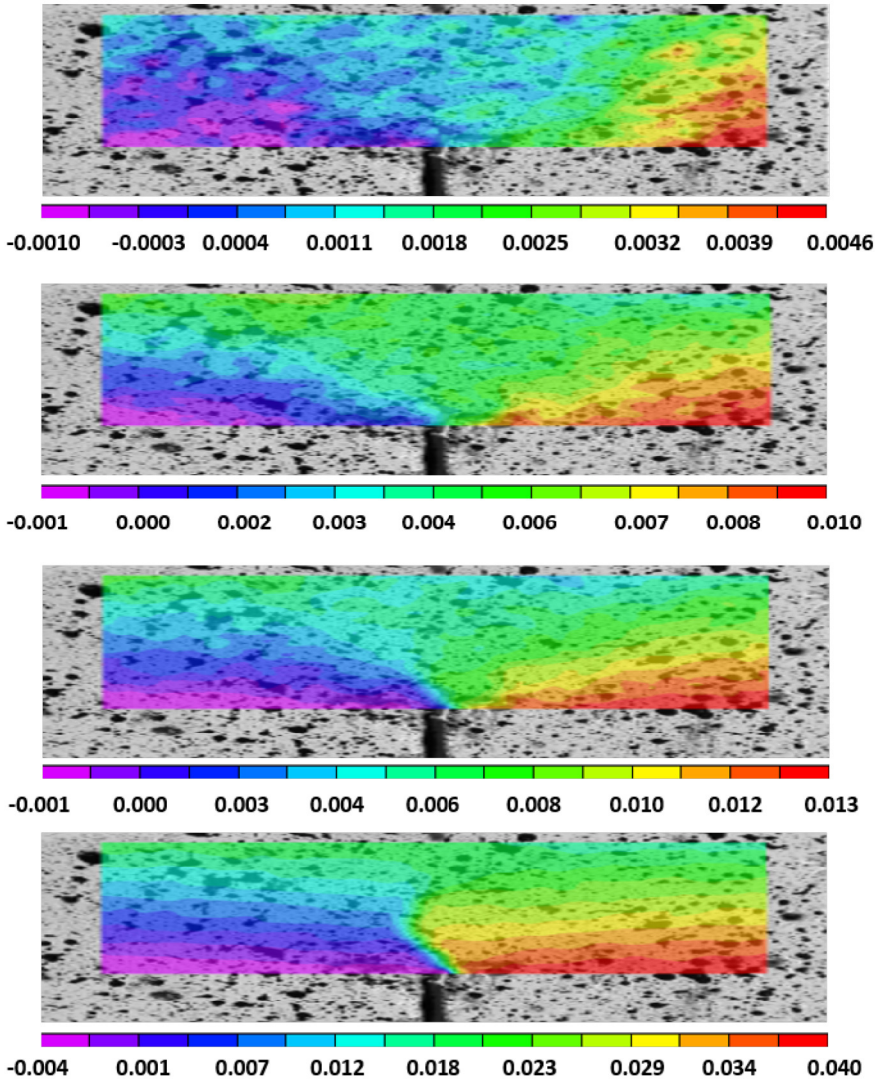

Figure 5.13: Horizontal displacement fields at: (a) 50% Peak load, (b) 95% Peak load, (c) Peak load, and (d) Post-peak load, for reinforced mortar specimen with 2% of DPMF.

Figure 5.14 shows the h-displacement of the reinforced mortar specimen with 4% of DPMF. By examining these images, it can be clearly seen as the same for the previous figure that, for load application equal to 50% of the peak load, there is no crack visible, and the displacement-jump is almost imperceptible. When the load applied by 95% of peak load , we noticed a h-displacement value of $6 \times 10^{-3} mm$ near the tip of the notch. A significant increase in the h-displacement was observed which makes the crack visible and the extent in the displacement-jump reaches $12 \times 10^{-3} mm$ at the tip. Finally, in the post-peak region, it was noticed the same gradual increase in the distinct displacement jump, it is reached with this amount of DPMF a value of $41 \times 10^{-3} mm$

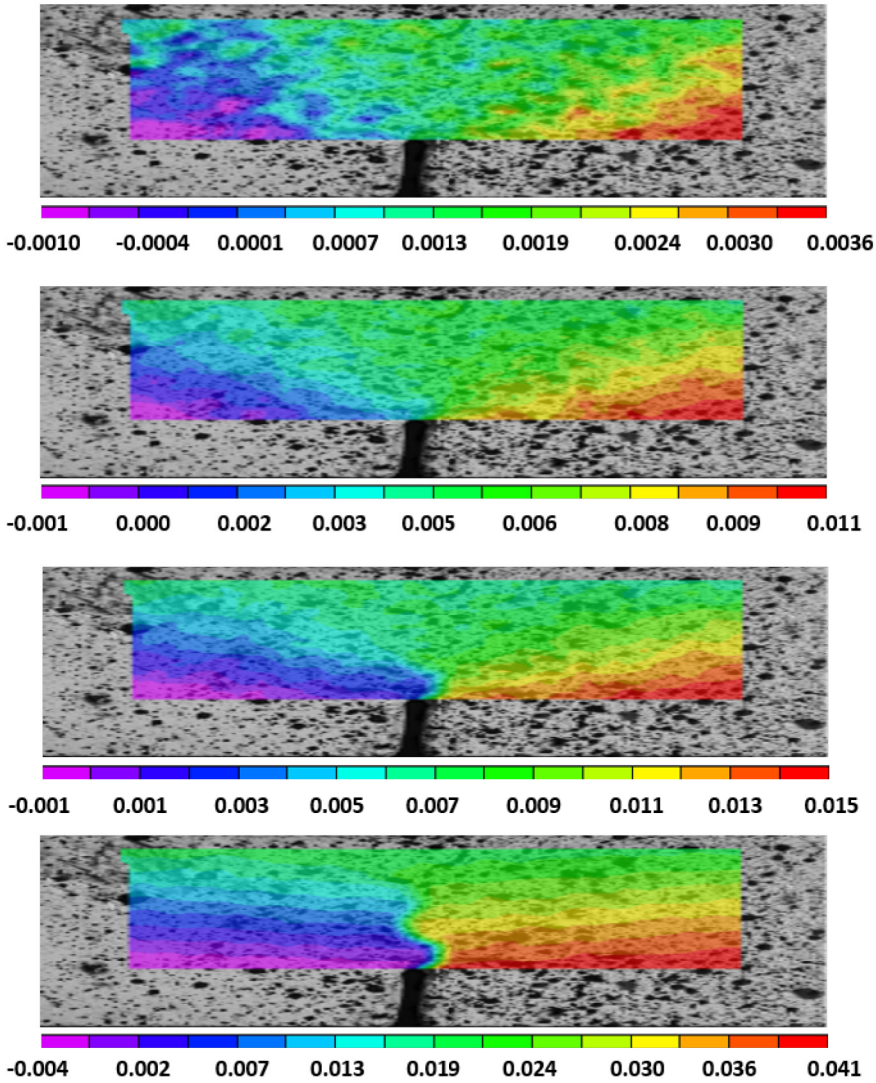

Figure 5.14: Horizontal displacement fields at: (a) 50% Peak load, (b) 95% Peak load, (c) Peak load, and (d) Post-peak load, for reinforced mortar specimen with 4% of DPMF.

Figure 5.15 shows the h-displacement corresponding to the reinforced mortar specimen with 6% of DPMF. For the first image, it can be noticed that, by applying 50% of the peak load, a low distinct displacement-jump was observed on the right side of the tip of notch ($3.5 \times 10^{-3} mm$). This trend was not observed in the previous figures for the same load rate applied related to small reinforcement ratio. For the second and the third image, the displacement-jump near the tip of notch becomes critical ($14 \times 10^{-3} mm$ and $15 \times 10^{-3} mm$ for load applied by 95% peak load and peak load, respectively), the crack can be visible according to the shape of the color map on the images. For the last image, the h-displacement reaches a value of $50 \times 10^{-3} mm$ near the tip of notch, which can be concluded that the high rate ratio of fibers reinforcement contributed to the improvement of the post-peak behavior

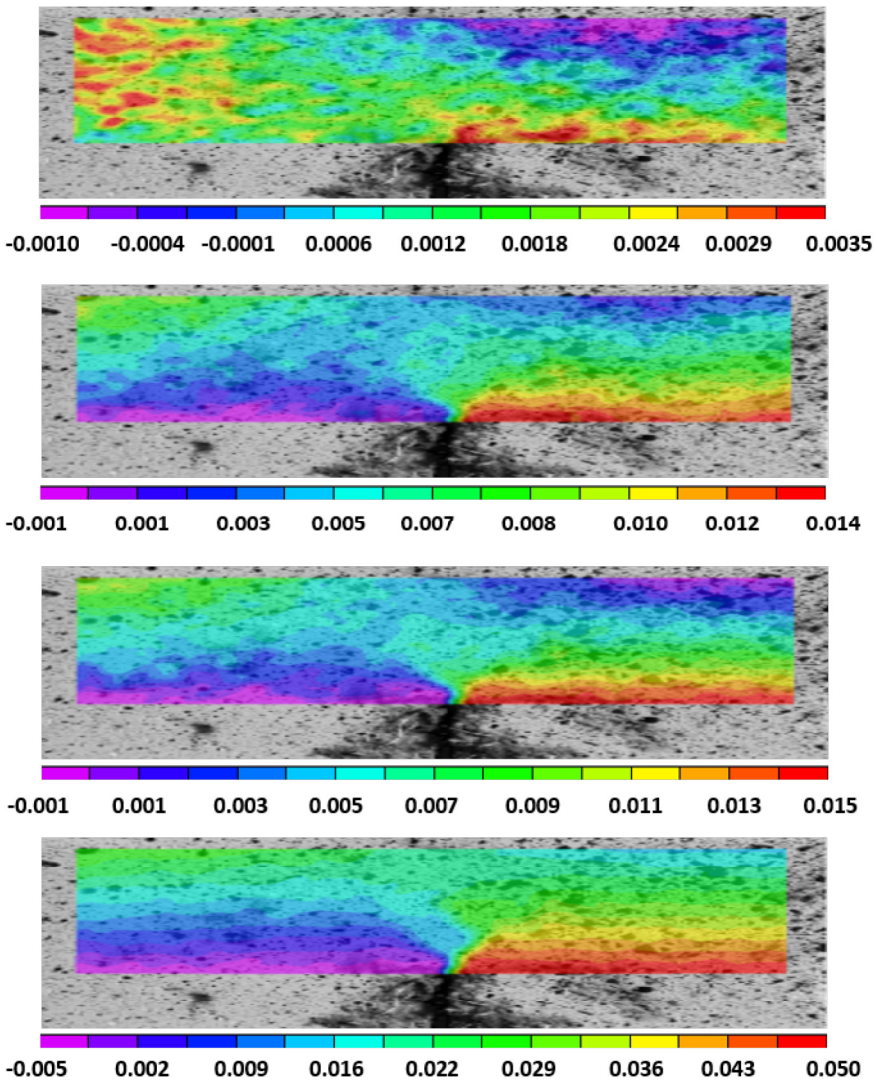

Figure 5.15: Horizontal displacement fields at: (a) 50% Peak load, (b) 95% Peak load, (c) Peak load, and (d) Post-peak load, for reinforced mortar specimen with 6% of DPMF.

Regarding the high reinforcement ratio, the h-displacement of mortar specimen reinforced with 8% of DPMF is presented in Figure 5.16. The first thing that can be remarked is that, the scale of these images is far bigger than the previous images. Even for the lowest applied load (50% of peak load), the h-displacement is almost $6 \times 10^{-3} mm$ near the tip of notch, By approaching to the peak region, the h-displacement reaches a value of $24 \times 10^{-3} mm$ by applying 95% of peak load, and it reaches $31 \times 10^{-3} mm$ under the peak load. In the post-peak region, the h-displacement reaches the highest value ($82 \times 10^{-3} mm$), as a matter of fact, the high rate displacement observed in the mortar specimen reinforced with high amount of fibers is mainly due to the fiber bridging mechanism, which allows the two broken pieces of the specimen to remain stuck to each other by the presence of the fibers.

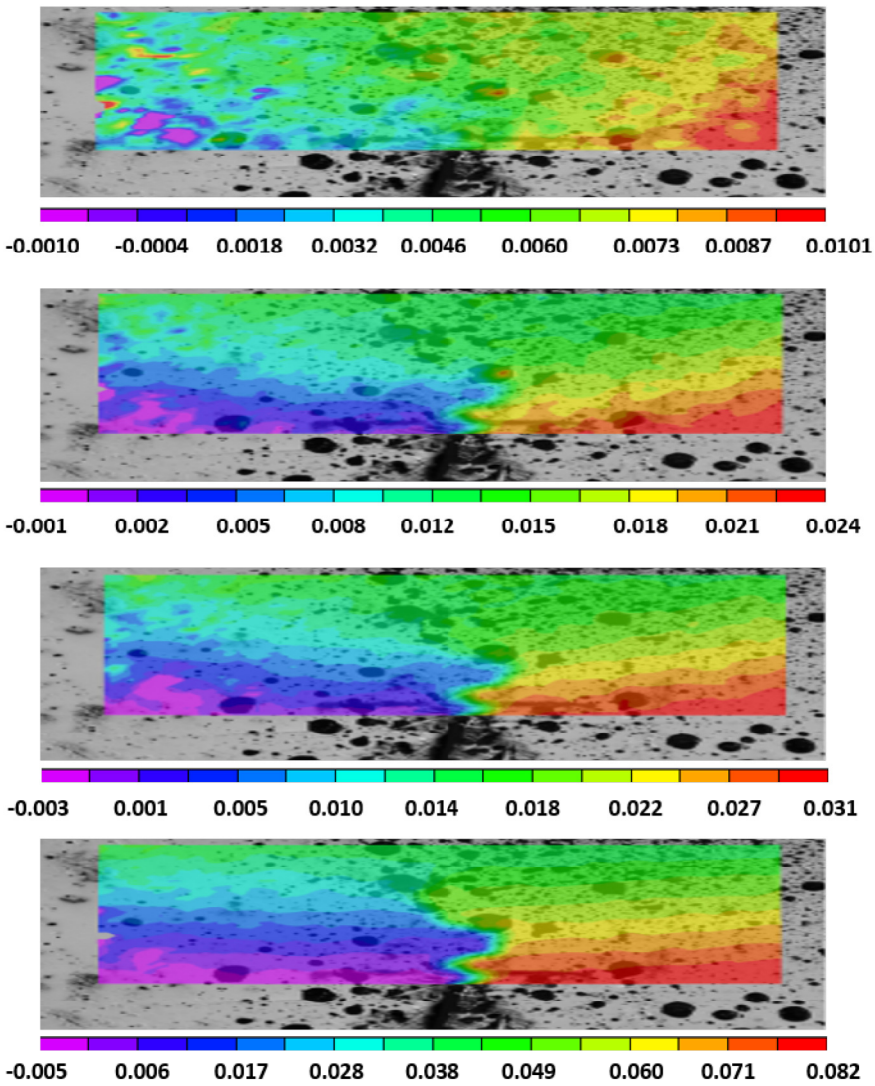

Figure 5.16: Horizontal displacement fields at: (a) 50% Peak load, (b) 95% Peak load, (c) Peak load, and (d) Post-peak load, for reinforced mortar specimen with 8% of DPMF.

Figure 5.17 shows the h-displacement of the last reinforced specimen with 10% of DPMF. The displacement jump distinct can be observed from the first image corresponding to the 50% of the load application, it can be recorded a h-displacement value of $10 \times 10^{-3} mm$ near the tip of notch. For a load application of 95% of peak load, and peak load, a similar trend can be noticed in the value of the h-displacement near the tip of notch ($23 \times 10^{-3} mm$ and $31 \times 10^{-3} mm$ for 95% of peak load and peak load, respectively). In addition, it can be observed that another minor crack was created on the left side of the main crack, that could be due to high fiber concentration in the specimen which deliver more stiffness to the mortar matrix. For the last image which corresponds to the post-peak region, the h-displacement reaches the highest value ($91 \times 10^{-3} mm$) compared to all specimen, and this result suits the fibers content used for this specimen.

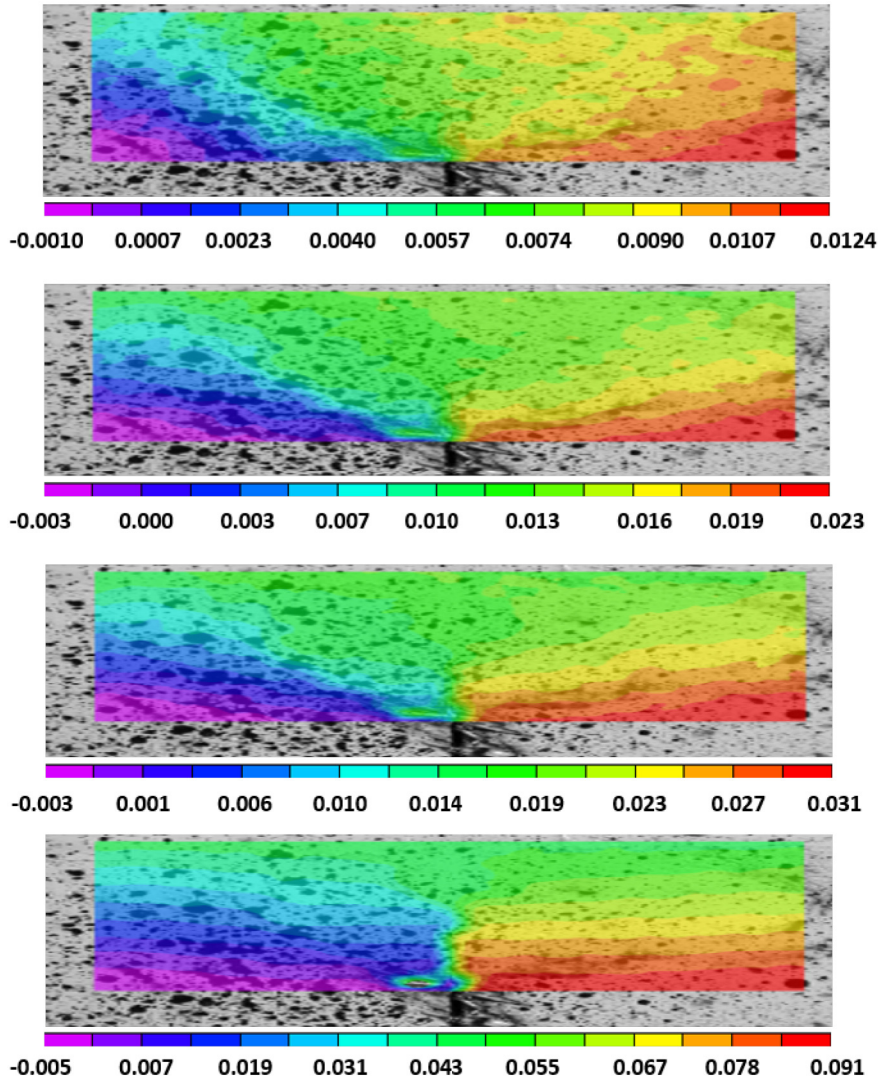

Figure 5.17: Horizontal displacement fields at: (a) 50% Peak load, (b) 95% Peak load, (c) Peak load, and (d) Post-peak load, for reinforced mortar specimen with 10% of DPMF.

On the highlight of these results, the main points that can be summarized are the following:

- The unreinforced mortar specimens showed no distinct h-displacement before and while reaching the peak region.
- There is no crack visible before and by reaching the peak region of the reinforced mortar specimens.
- The displacement jump after the total failure was small for the unreinforced mortar specimens.
- The h-displacement distinct was increasing gradually with the increase of the fiber ratio.
- The extent jump of the h-displacament near the tip of notch was higher for high reinforcement ratio.
- For the high reinforcement ratio, The CMOD was found to be very large before the total failure of the specimens.

The DPMF found to be an adequate reinforcement for improving the softening behavior of the reinforced mortar specimens. These results obtained by the DIC technique have been proved to be in accordance with the experimental results obtained from the three-point bending test.

5.3.8 DIC displacement fields (3D) of notched beams

The colored map figures of the (2D) displacements fields could give a good overview on the state of specimen during the load application, however, in order to provide a better estimation on the crack length extension (Δa) and the crack tip opening displacement (CTOD), the h-displacement field is herein plotted in 3D, based on the specimen's results presented in section 5.3.7, each figure consists of four images correspond to: (a). Load application equal to 50% of peak load; (b). 95% of peak load; (c). Peak load; (d). Post peak load corresponds to a CMOD value equal to three times of the CMOD critical.

Figure 5.18 shows the 3D h-displacement plot for the plain mortar specimen. As can be seen, the CTOD and Δa can be determined directly from the images using the DIC technique. For the first image corresponds to load applied by 50% of peak load, there is no CTOD visible, and there is no crack extension visible. The surface of the h-displacement is slightly twisted which reflects the beginning of the specimen deformation. By reaching the peak load region, the CTOD and Δa recorded values of $7 \times 10^{-3} mm$ mm and $4mm$, respectively, under a peak load. In the post-peak region, it can be observed a sudden increase in the CTOD and Δa of the plain mortar specimen (CTOD and Δa: $27 \times 10^{-3} mm$ and $12mm$, respectively).

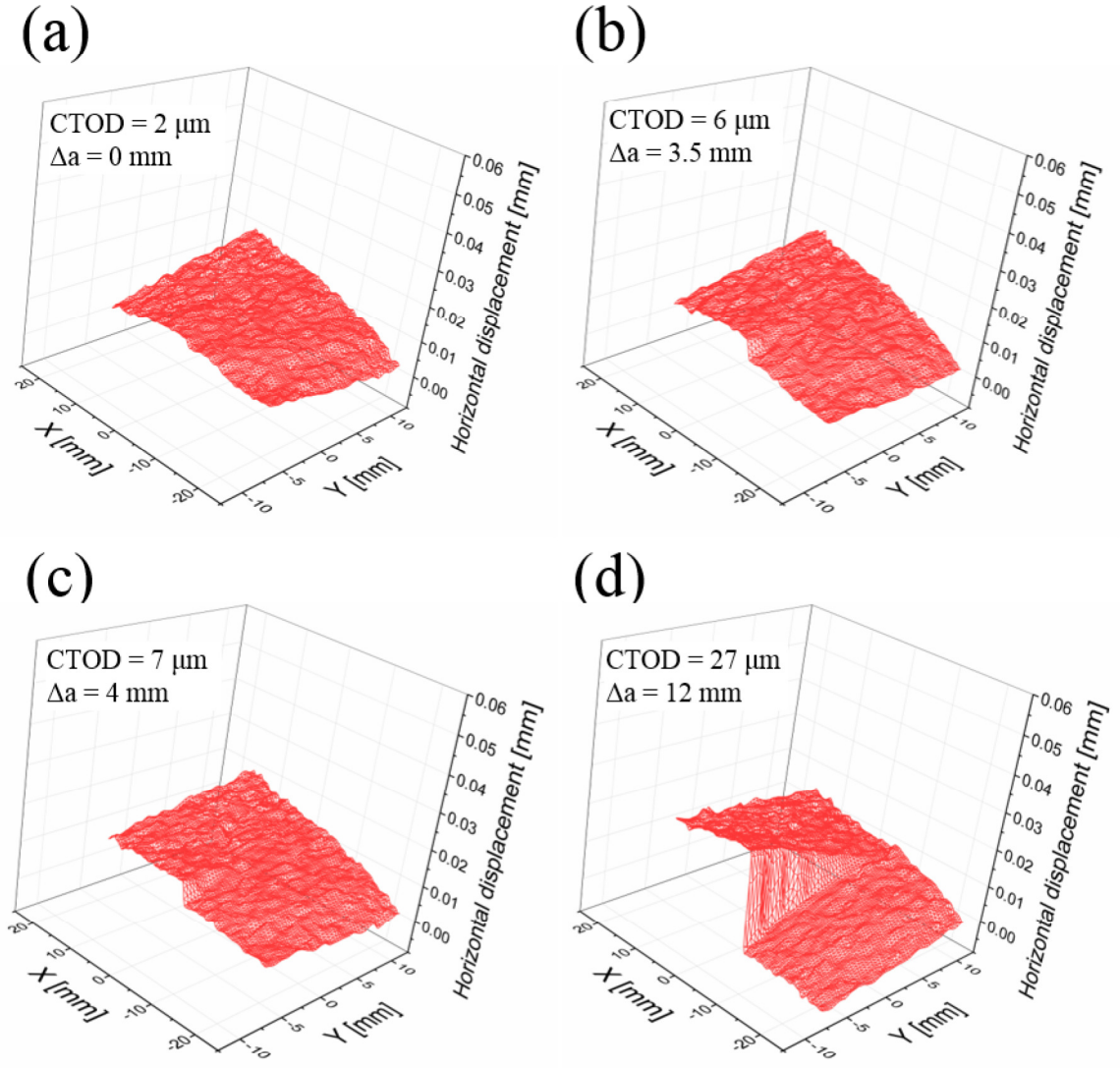

Figure 5.18: 3D plot of the h-displacement fields at: (a) 50% Peak load, (b) 95% Peak load, (c) Peak load, and (d) Post-peak load, for plain mortar specimen.

For the reinforced mortar specimen with 2% of DPMF, the 3D h-displacement plot is shown in the Figure 5.19. Regarding the CTOD, it can be noticed that the CTOD increases gradually with the load enhancement. For instance, it recorded 0.003 mm, 0.008 mm, 0.009 mm, and 0.046 mm under an applied load of 0.5 Peak load, 0.95 Peak load, Peak load, and post-peak load, respectively. It can be concluded that for 2% of DPMF reinforcement, the critical CTOD corresponds to the peak load application increases by 27% compared to plain mortar specimen, while the CTOD before the final failure increases by 70% compared to plain mortar specimen. Regarding the crack extension Δa, for the first stage of loading (50% of peak load), the crack extension Δa does not appear in the 3D plot. While for the other stages, the Δa extents as the CTOD increases, it reached 5 mm, 6 mm, 15.5 mm in the pre-peak, peak, and post-peak region, respectively.

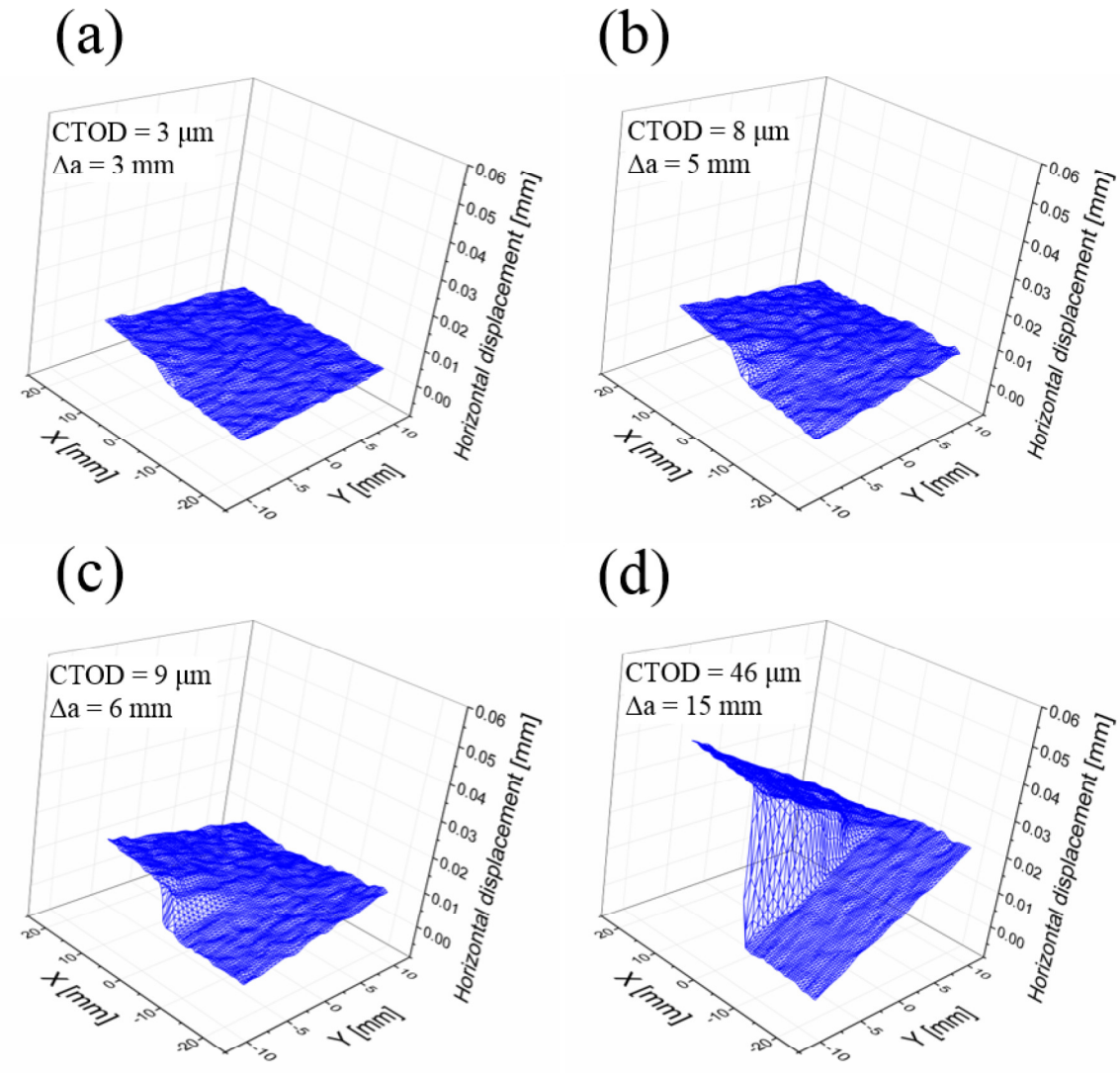

Figure 5.19: 3D plot of the h-displacement fields at: (a) 50% Peak load, (b) 95% Peak load, (c) Peak load, and (d) Post-peak load, for reinforced mortar specimen with 2% of DPMF.

The 3D h-displacement plot of the reinforced specimen with 4% of DPMF is shown in Figure 5.20. It can be seen that for the first stage, there is no CTOD, and Δa visible. For the pre-peak region close to the peak load (95% of peak load), a small crack extent can be observed (CTOD, and Δa equal to 0.006 mm, and 4.5 mm, respectively). By reaching the peak region, a distinct jump in the CTOD and Δa can be observed, (CTOD, and Δa equal to 0.013 mm, and 7 mm, respectively). Finally, for the last stage corresponds to the post-peak region, the CTOD and Δa reached values equal to 0.048 mm, and 16 mm, respectively. The increase rate in the CTOD and Δa is equal to 70% and 33.34%, respectively. This result is in accordance with the increase rate in the fiber ratio.

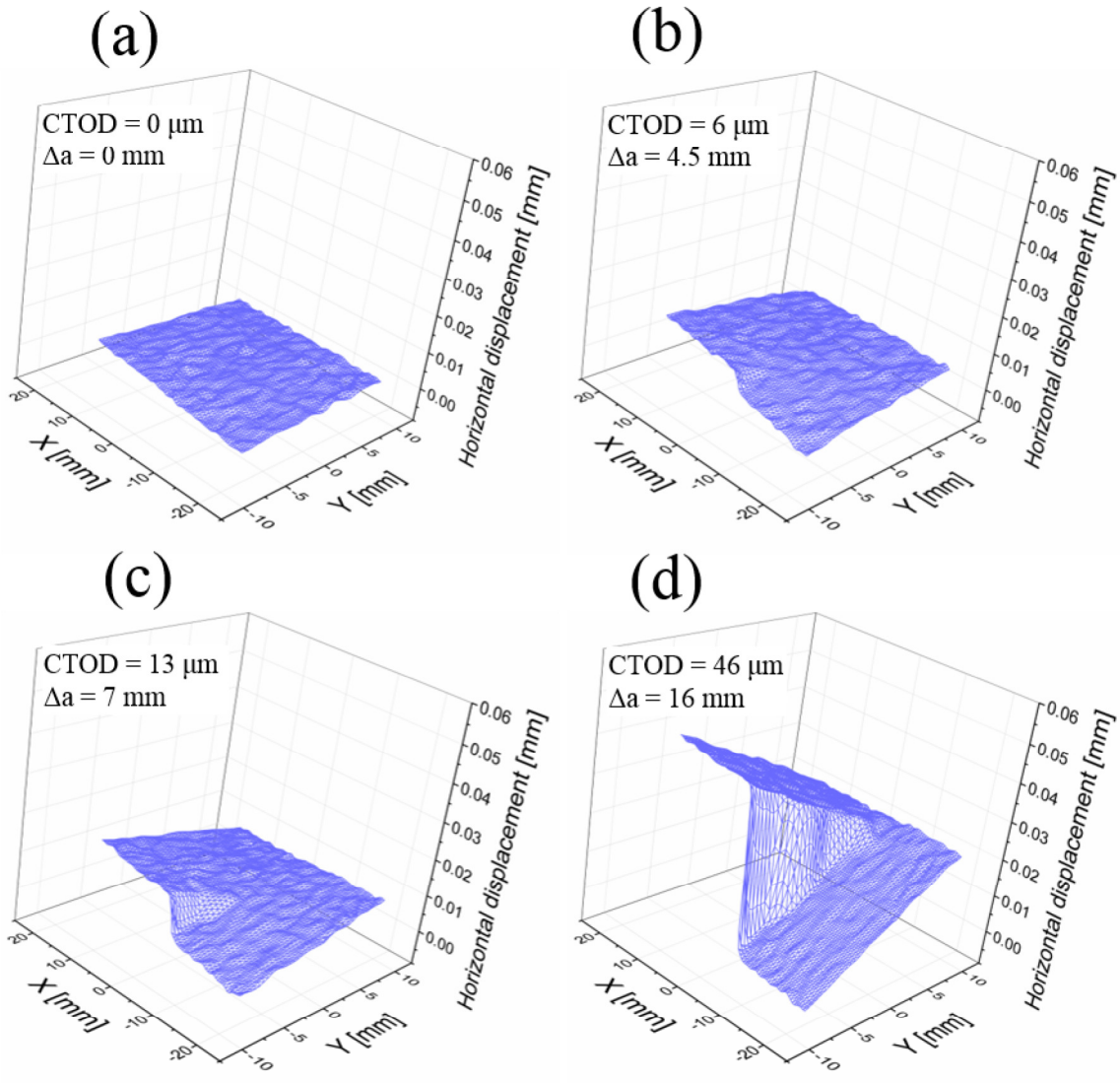

Figure 5.20: 3D plot of the h-displacement fields at: (a) 50% Peak load, (b) 95% Peak load, (c) Peak load, and (d) Post-peak load, for reinforced mortar specimen with 4% of DPMF.

For the reinforced mortar specimen with 6% of DPMF, te 3D h-displacement is shown in Figure 5.21. In the first stage of load application (50% of peak load), a similar trend was found for the previous specimens discussed. By getting close to the peak region (95% of peak load and peak load), a significant opening in the CTOD and Δa was noticed (CTOD and Δa equal to 0.015 mm and 6 mm, respectively for 95% peak load, and 0.018 mm and 8 mm, respectively for peak load). In the post-peak region, the CTOD and Δa have recorded values of 0.059 mm, and 16 mm, respectively.

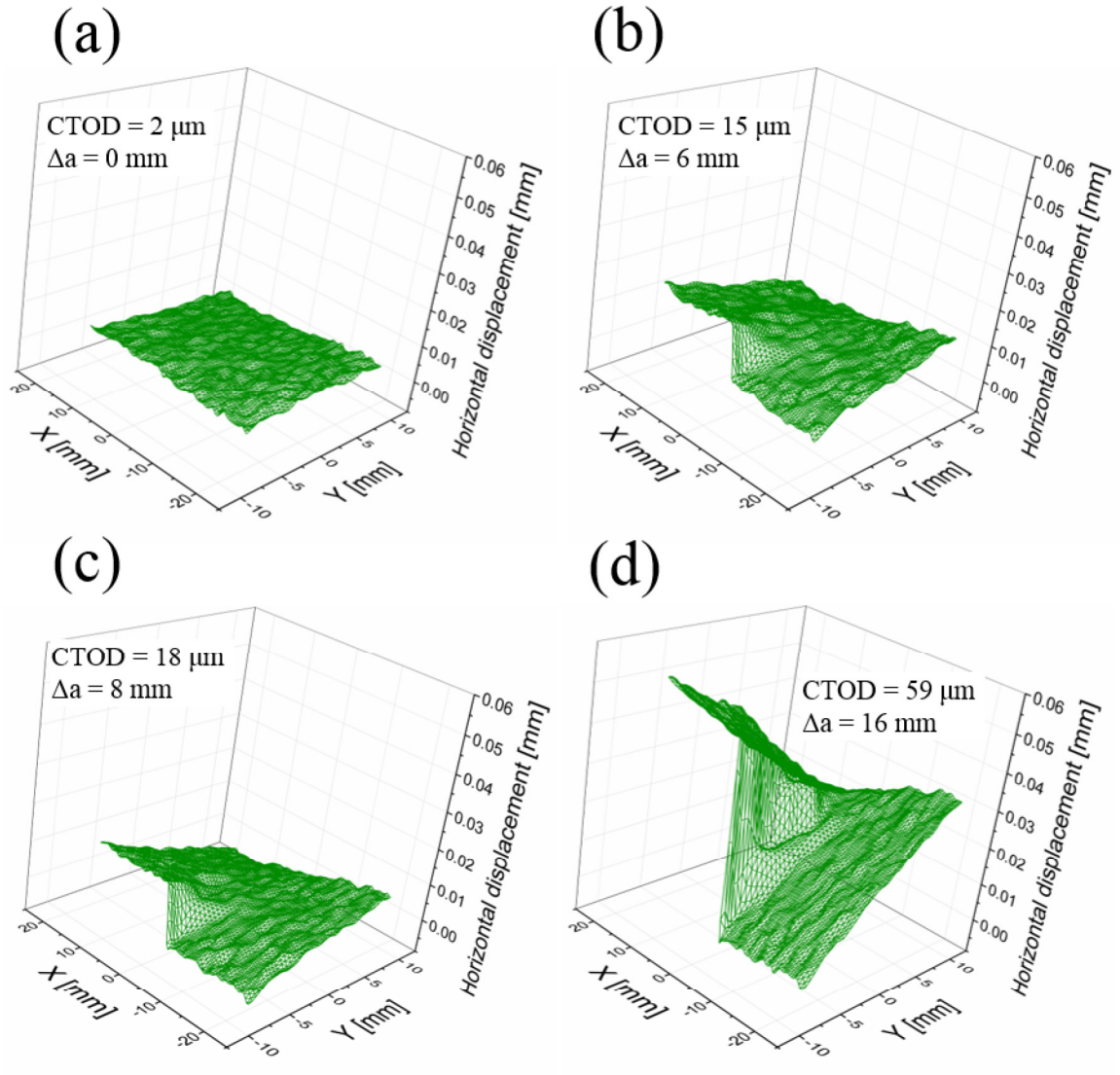

Figure 5.21: 3D plot of the h-displacement fields at: (a) 50% Peak load, (b) 95% Peak load, (c) Peak load, and (d) Post-peak load, for reinforced mortar specimen with 6% of DPMF.

Figure 5.22 shows the 3D plot results of the h-displacement of the reinforced mortar specimen with 8% of DPMF. For the first image, the surface plot of the h-displacement seems that it is peaked in many points, which is the result of many small deformations began to be created. The CTOD and Δa found to be bigger than those corresponding to the small reinforcement ratio. For instance, the CTOD and Δa for the Peak load region are 0.034 mm, and 11 mm, respectively. For the post-peak region, they reached 0.090 mm, and 18 mm respectively.

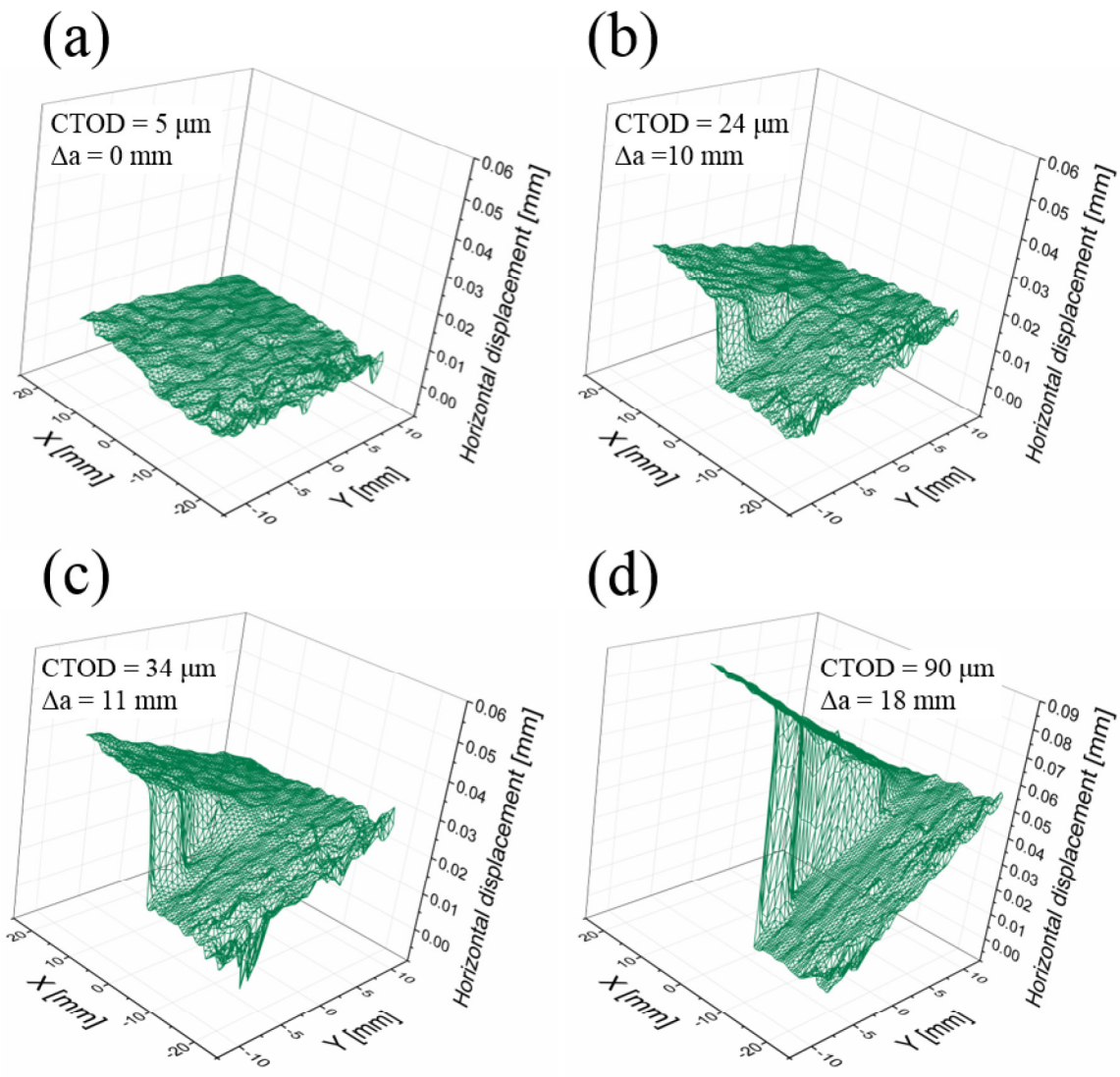

Figure 5.22: 3D plot of the h-displacement fields at: (a) 50% Peak load, (b) 95% Peak load, (c) Peak load, and (d) Post-peak load, for reinforced mortar specimen with 8% of DPMF.

The results correspond to the high reinforcement ratio of 10% of DPMF are shown in Figure 5.23. The variance in the 3D plot h-displacement can be observed since the first stage (50% of peak load). The CTOD and Δa are equal to 0.01 mm, and 6 mm, respectively. As a matter of fact, the CTOD and Δa have recorded their maximum values for this ratio of DPMF reinforcement, For instance, they are equal to 0.035 mm, and 12 mm, respectively, for the peak load application. Moreover, they are equal to 0.096 mm, and 19 mm respectively, for the post-peak load application.

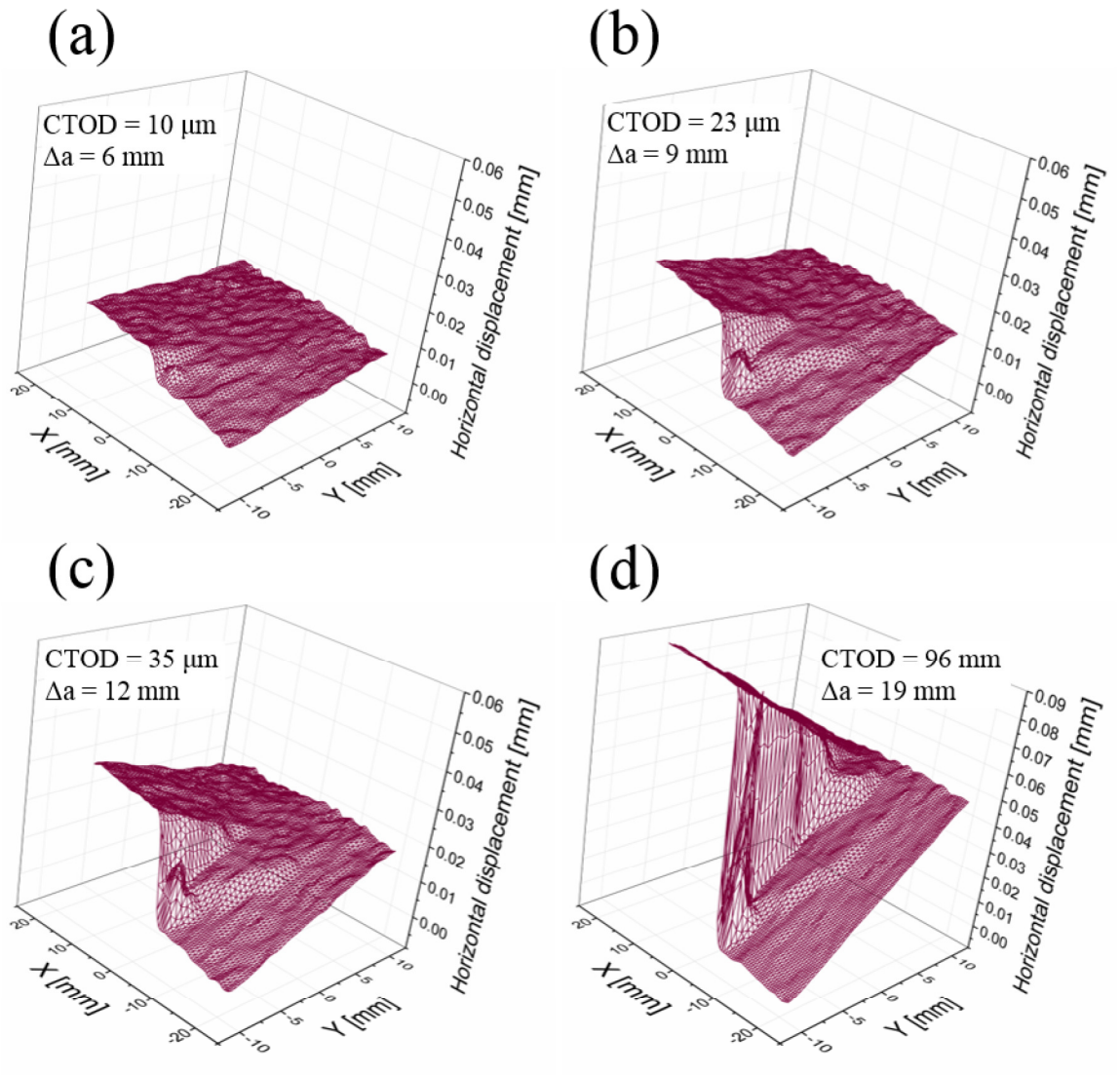

Figure 5.23: 3D plot of the h-displacement fields at: (a) 50% Peak load, (b) 95% Peak load, (c) Peak load, and (d) Post-peak load, for reinforced mortar specimen with 10% of DPMF.

5.4 Conclusion

The results obtained from the experimental campaign can be expressed in the following points :

- Since the fibers were added in wet state to mortar mixture, the workability of reinforced mortar was not affected by the presence of the DPMF until a reinforcement ratio of 10%.
- The flexural strength of mortar composites decreased gradually with the addition of the DPMF.
- The post-peak behavior obtained from the load-deflection curves was significantly improved by the presence of fibers (up to 10% of fibers reinforcement).
- The fracture toughness of fiber reinforced mortar was generally decreased with high increase in fibers content. However, the use of 2% of DPMF showed a similar values of that of concrete reinforced with 2% of synthetic fibers.
- The elastic modulus of composite mortar specimens was gradually decreased by the presence of fibers and that was reported to lower elastic modulus of the vegetable fibers compared with matrix elastic modulus.
- Despite the drop in the compressive and the density (decreased up to 50% compared to the plain mortar) of composites mortar when 10% of DPMF used, this reinforcement ratio (10% of DPMF) contributed to the best performances in terms of ductility and energy absorption in which the complete failure is delayed. Furthermore, it could be used as a thermal insulator as it was mentioned by many researchers in literature.
- The toughness index demonstrated a significant improvement in the ductility of composite mortars for a reinforcement ratio up to 10% of DPMF.
- The horizontal displacement fields obtained by the DIC technique demonstrated high displacements rate around the tip notch of the specimens when the DPMF used for high reinforcement ratios (up to 10% of fibers reinforcement).
- The DIC proved to be a powerful tool for the determination of CTOD and the δa, the high reinforcement ratio (10% of fibers reinforcement) showed the maximum values of in the CTOD and the Δa, which concluded that the high reinforcement ratio improved significantly the ductility of the reinforced mortars.

Conclusion and Perspectives

General Conclusion

The addition of date palm fibers in the cementitious materials has opened a promising path toward the production of new lightweight green material. It could improve such properties of cement-based materials and this depends on the characteristics of the fibers itself such as elastic modulus , the size of fibers, surface modification, volume fractions of fibers. These parameters influence directly the mechanical characteristics of the cement-based composites (water absorption, compressive strength, flexural strength, fracture toughness). The conception of such green composite material passes through the investigation of all of these parameters.

Within the first chapter of this thesis, the different methods on the characterization of the vegetable fibers have been reviewed, The incorporation of the vegetable fibers in the cementitious materials was for the aim of delaying the first crack and controlling the crack propagation for getting such a ductile material. A composite material reinforced with fibers continues to support more load even after failure. Furthermore, the vegetable fibers could improve such mechanical behavior such as flexural, fracture and the fatigue. The improvement of these behaviors is directly related to the volume fractions, the nature and the mechanical behavior of fiber itself. Regarding to this literature review, the vegetable fibers could be a promising alternative to the traditional synthetic fibers. These fibers have multiple beneficial advantages such as low cost, environmental impact and its incorporation could improve the cost and satisfy the mid-range requirement for the flexural and fracture behavior and also impact resistance. On the highlights of the literature review and for the suitable valorization of the local materials, an investigation on the utilization of date palm fibers in cementitious materials is hence required. For the best knowledge of authors , no studies related to the fracture behavior of cement-based composites reinforced with DPMF are available in the literature. Therefore, the present work deals with the mechanical and physical properties of a cement-based mortar reinforced with short DPMF including

the fracture, flexural and compressive strength.

The next chapter was an overview on the available approaches of the fracture mechanics in the appplication of cementititous materials. In particular, a general application of fracture mechanics and earlier approaches of the LEFM was presented. Then, the applications of the LEFM in the fracture study of cementitous materials was reviewed. It was found that LEFM is not sufficient for fracture study of concrete since the later one is a quasi-brittle material in which the fracture parameters of concrete are related to the size effect and the fracture process zone. These parameters are linked to non-linear deformation of concrete. The non-linear fracture models based on the finite element method or the modified LEFM concept have been proved to be more effective in the determination of the fracture parameters the cementitious materials. The two parameter model TPM has proven that the stress intensity factor (SIF) and the crack opening displacement (CMOD) are the only parameters controlling the fracture properties for any geometry of specimen. The Modified two parameter model MTPM was found to be more accurate in case the large deflection of the crack propagation path.

The main characteristics of the materials used and the methods of preparing the cementitious composites were mentioned after in chapter 4. The sand used in this study was silica sand of grain distribution of 0/2 mm. Its chemical composition is mainly composed of silicion dioxide (SiO2). The cement used in this study was a limestone Portland cement CEM II/A-LL 42.5 R contains more than 80% of clinker. It has a Blaine surface of 4085 cm2/g. The date palm fibers used in this study are delivered from the oasis of Biskra (a city in Algeria), it was the mesh mat surrounding the trunk of the date palm tree. To reach the objectives declared in chapter 1, cubic and prismatic specimens were prepared after optimizing the W/C ratio for the cement composites. The flexural and compressive tests were carried out according to the European recommendations using an Instron machine 8862. Whereas, the fracture tests were performed according to the Two parameter model.

The results obtained from the experimental campaign can be summarized in the following points : Since the fibers were added in wet state to mortar mixture, the workability of reinforced mortar was not affected by the presence of the DPMF. The flexural strength of mortar composites decreased gradually with the addition of the DPMF. The post-peak behavior obtained from the load-deflection curves was significantly improved by the presence of fibers. The fracture toughness of fiber reinforced mortar was generally decreased with high increase in fibers content. However, the use of 2% of DPMF showed a similar values of that of concrete reinforced with 2% of synthetic fibers. The elastic modulus of composite mortar specimens was gradually decreased by the presence of fibers and that was reported to lower elastic modulus of the vegetable fibers compared with matrix elastic modulus. The compressive strength

and the density of mortar composites were decreased up to 50% by the addition of 10% of DPMF , these results are in accordance with other studies in literature. These results also indicate that the compressive strength of DPMF reinforced mortar is directly related to the density of the later one. The toughness index demonstrated a significant improvement in the ductility of composite mortars.

Perspectives

On the highlights of the present thesis , multiple perspectives could be drawn for the future work

- Adopt some fibers treatments methods such as pulp and kraft processes in order to improve the fibers stiffness.
- Adopt a better preparation process for the composite materials in the casting by removing the excess water from the specimens.
- Develop a numerical model in order to validate the experimental results on the fracture toughness measurement by using the MTPM.
- Study the long terms mechanical behavior of composite materials.
- Study the fatigue behavior of the composite materials reinforced with date palm fibers.

Bibliography

[1] M. Ardanuy, J. Claramunt, and R. D. Toledo Filho, "Cellulosic fiber reinforced cement-based composites: A review of recent research," *Construction and Building Materials*, vol. 79, pp. 115–128, 2015.

[2] A. A. Griffith and M. Eng, "VI. The phenomena of rupture and flow in solids," *Phil. Trans. R. Soc. Lond. A*, vol. 221, no. 582-593, pp. 163–198, 1921.

[3] A. Carpinteri, G. Fortese, C. Ronchei, D. Scorza, and S. Vantadori, "Mode I fracture toughness of fibre reinforced concrete," *Theoretical and Applied Fracture Mechanics*, vol. 91, pp. 66–75, 2017.

[4] R. R. Bhansali, "Date palm cultivation in the changing scenario of Indian arid zones: challenges and prospects," in *Desert plants*, pp. 423–459, Springer, 2010.

[5] B. Agoudjil, A. Benchabane, A. Boudenne, L. Ibos, and M. Fois, "Renewable materials to reduce building heat loss: Characterization of date palm wood," *Energy and Buildings*, vol. 43, no. 2-3, pp. 491–497, 2011.

[6] R. D. S. G. Campilho, *Natural fiber composites*. CRC Press, 2015.

[7] A. K. Bledzki, V. E. Sperber, and O. Faruk, *Natural and wood fibre reinforcement in polymers*, vol. 13. iSmithers Rapra Publishing, 2002.

[8] K. R. Hakeem, M. Jawaid, and U. Rashid, "Biomass and bioenergy: Processing and properties," *Biomass and Bioenergy: Processing and Properties*, vol. 9783319076, pp. 1–367, 2014.

[9] M. Jawaid and H. P. Abdul Khalil, "Cellulosic/synthetic fibre reinforced polymer hybrid composites: A review," *Carbohydrate Polymers*, vol. 86, no. 1, pp. 1–18, 2011.

[10] F. M. Al-Oqla and M. S. Salit, "Materials selection for natural fiber composites," *Materials Selection for Natural Fiber Composites; Elsevier: Amsterdam, The Netherlands*, pp. 107–168, 2017.

[11] D. D. Stokke, Q. Wu, and G. Han, *Introduction to wood and natural fiber composites*. John Wiley & Sons, 2013.

[12] T. Väisänen, A. Haapala, R. Lappalainen, and L. Tomppo, "Utilization of agricultural and forest industry waste and residues in natural fiber-polymer composites : A review," vol. 54, pp. 62–73, 2016.

[13] K. G. Satyanarayana, G. G. Arizaga, and F. Wypych, "Biodegradable composites based on lignocellulosic fibers-An overview," *Progress in Polymer Science (Oxford)*, vol. 34, no. 9, pp. 982–1021, 2009.

[14] C. Baley, *Fibres naturelles de renfort pour matériaux composites*. Ed. Techniques Ingénieur, 2005.

[15] B. Chabert, *Fibres de renfort pour matériaux composites*. Ed. Techniques Ingénieur, 1988.

[16] R. Rowell, "A New Generation of Composite Materials from Agro-Based Fiber," in *Polymers and Other Advanced Materials SE - 68*, pp. 659–665, Springer, 1995.

[17] A. Sbiai, "des fibres de palmier dattier : effet de l ' oxydation au DATTIER : EFFET DE L ' OXYDATI ON AU TEMPO," 2012.

[18] F. Ahmad, H. S. Choi, and M. K. Park, "A Review : Natural Fiber Composites Selection in View of Mechanical , Light Weight , and Economic Properties," pp. 10–24, 2015.

[19] D. Kocak and S. I. Mistik, "The use of palm leaf fibres as reinforcements in composites," *Biofiber Reinforcements in Composite Materials*, pp. 273–281, 2015.

[20] N. Benmansour, B. Agoudjil, A. Gherabli, A. Kareche, and A. Boudenne, "Thermal and mechanical performance of natural mortar reinforced with date palm fibers for use as insulating materials in building," *Energy and Buildings*, vol. 81, pp. 98–104, 2014.

[21] A. Bentur and S. Mindess, *Fibre reinforced cementitious composites*. CRC Press, 2014.

[22] C. Sawsen, K. Fouzia, B. Mohamed, and G. Moussa, "Effect of flax fibers treatments on the rheological and the mechanical behavior of a cement composite," *Construction and Building Materials*, vol. 79, pp. 229–235, 2015.

[23] P. P. M. A. Aziz and S. L. Lee, "Prospects for natural fibre reinforced concretes in construction," *International Journal of Cement Composites and Lightweight Concrete*, vol. 3, pp. 123–132, may 1981.

[24] B. Çomak, A. Bideci, and Ö. Salli Bideci, "Effects of hemp fibers on characteristics of cement based mortar," *Construction and Building Materials*, vol. 169, pp. 794–799, apr 2018.

[25] S. Chakraborty, S. P. Kundu, A. Roy, R. K. Basak, B. Adhikari, and S. B. Majumder, "Improvement of the mechanical properties of jute fibre reinforced cement mortar: A statistical approach," *Construction and Building Materials*, vol. 38, pp. 776–784, 2013.

[26] O. Onuaguluchi and N. Banthia, "Plant-based natural fi bre reinforced cement composites : A review," *Cement and Concrete Composites*, vol. 68, pp. 96–108, 2016.

[27] AMERICAN CONCRETE INSTITUTE (ACI), "Report on Fiber Reinforced Concrete," *Report on Reinforced Concrete (Reapproved). ACI Committee 544. Detroit,*, vol. 96, no. Reapproved 2009, pp. 1–66, 2009.

[28] T. Tioua, A. Kriker, G. Barluenga, and I. Palomar, "Influence of date palm fiber and shrinkage reducing admixture on self-compacting concrete performance at early age in hot-dry environment," *Construction and Building Materials*, vol. 154, pp. 721–733, 2017.

[29] W. N. Al-Rifaie and M. Al-Niami, "Mechanical performance of date palm fibre-reinforced gypsums," *Innovative Infrastructure Solutions*, vol. 1, no. 1, p. 18, 2016.

[30] N. G. Ozerkan, B. Ahsan, S. Mansour, and S. R. Iyengar, "Mechanical performance and durability of treated palm fiber reinforced mortars," *International Journal of Sustainable Built Environment*, vol. 2, no. 2, pp. 131–142, 2013.

[31] A. Kriker, G. Debicki, A. Bali, M. M. Khenfer, and M. Chabannet, "Mechanical properties of date palm fibres and concrete reinforced with date palm fibres in hot-dry climate," *Cement and Concrete Composites*, vol. 27, no. 5, pp. 554–564, 2005.

[32] R. Belakroum, A. Gherfi, M. Kadja, C. Maalouf, M. Lachi, N. El Wakil, and T. H. Mai, "Design and properties of a new sustainable construction material based on date palm fibers and lime," *Construction and Building Materials*, vol. 184, pp. 330–343, 2018.

[33] R. Hamzaoui, S. Guessasma, B. Mecheri, A. M. Eshtiaghi, and A. Bennabi, "Microstructure and mechanical performance of modified mortar using hemp fibres and carbon nanotubes," *Materials and Design*, vol. 56, pp. 60–68, 2014.

[34] H. Tian, Y. X. Zhang, C. Yang, and Y. Ding, "Recent advances in experimental studies of the mechanical behaviour of natural fibre-reinforced cementitious composites," *Structural Concrete*, vol. 17, no. 4, pp. 564–575, 2016.

[35] P. R. L. Lima, R. D. Toledo Filho, and J. A. Melo Filho, "Compressive stress-strain behaviour of cement mortar-composites reinforced with short sisal fibre," *Materials Research*, vol. 17, no. 1, pp. 38–46, 2014.

[36] Ö. Andiç-Çakir, M. Sarikanat, H. B. Tüfekçi, C. Demirci, and Ü. H. ErdoÇğan, "Physical and mechanical properties of randomly oriented coir fiber-cementitious composites," *Composites Part B: Engineering*, vol. 61, pp. 49–54, 2014.

[37] D. SEDAN, *Etude des interactions physico-chimiques aux interfaces fibres de chanvre/ciment. Influence sur les propriétés mécaniques du composite.* PhD thesis, 2007.

[38] R. S. P. Coutts and P. G. Warden, "Sisal pulp reinforced cement mortar," *Cement and Concrete Composites*, vol. 14, no. 1, pp. 17–21, 1992.

[39] O. Benaimeche, A. Carpinteri, M. Mellas, C. Ronchei, D. Scorza, and S. Vantadori, "The influence of date palm mesh fibre reinforcement on flexural and fracture behaviour of a cement-based mortar," *Composites Part B: Engineering*, vol. 152, no. July, pp. 292–299, 2018.

[40] M. G. Le Hoang, T., M. Boutouil, F. Khadraoui, "Mechanical and microstructural characterization of flax fibreâĂŚreinforced cement composite," in *Proceedings of the 11th JapanâĂŚKoreaâĂŚ FranceâĂŚCanada Joint Seminar on Geoenvironmental Engineering*, vol. 11, pp. 131–136, 2012.

[41] Z. P. Bazant and J. Planas, "Fracture and Size Effect in Concrete and Other Quasi-Brittle Materials, 1998."

[42] X. Zhou, S. H. Ghaffar, W. Dong, O. Oladiran, and M. Fan, "Fracture and impact properties of short discrete jute fibre-reinforced cementitious composites," *Materials and Design*, vol. 49, pp. 35–47, 2013.

[43] A. Razmi and M. M. Mirsayar, "On the mixed mode I/II fracture properties of jute fiber-reinforced concrete," *Construction and Building Materials*, vol. 148, pp. 512–520, 2017.

[44] J. M. L. Reis, "Fracture and flexural characterization of natural fiber-reinforced polymer concrete," *Construction and Building Materials*, vol. 20, no. 9, pp. 673–678, 2006.

[45] J. M. L. Reis, "Sisal fiber polymer mortar composites: Introductory fracture mechanics approach," *Construction and Building Materials*, vol. 37, pp. 177–180, 2012.

[46] P. K. Rastogi and E. Hack, *Optical methods for solid mechanics: a full-field approach*. John Wiley & Sons, 2012.

[47] M. A. Sutton, "Computer vision-based, noncontacting deformation measurements in mechanics: a generational transformation," *Applied Mechanics Reviews*, vol. 65, no. 5, p. 50802, 2013.

[48] F. Hild and S. Roux, "Digital image correlation: from displacement measurement to identification of elastic propertiesâĂŞa review," *Strain*, vol. 42, no. 2, pp. 69–80, 2006.

[49] M. Grédiac and F. Hild, *Full-field measurements and identification in solid mechanics*. Wiley Online Library, 2013.

[50] B. D. Lucas and T. Kanade, "An iterative image registration technique with an application to stereo vision," 1981.

[51] M. A. Sutton, J. J. Orteu, and H. Schreier, *Image correlation for shape, motion and deformation measurements: basic concepts, theory and applications*. Springer Science & Business Media, 2009.

[52] T. C. Chu, W. F. Ranson, and M. A. Sutton, "Applications of digital-image-correlation techniques to experimental mechanics," *Experimental mechanics*, vol. 25, no. 3, pp. 232–244, 1985.

[53] M. A. Sutton, W. J. Wolters, W. H. Peters, W. F. Ranson, and S. R. McNeill, "Determination of displacements using an improved digital correlation method," *Image and vision computing*, vol. 1, no. 3, pp. 133–139, 1983.

[54] L. C. S. Nunes and J. M. L. Reis, "Estimation of crack-tip-opening displacement and crack extension of glass fiber reinforced polymer mortars using digital image correlation method," vol. 33, pp. 248–253, 2012.

[55] E. Dildar, E. Tsangouri, K. Spiessens, G. D. Schutter, and D. G. Aggelis, "ScienceDirect Digital image correlation (DIC) on fresh cement mortar to quantify settlement and shrinkage," vol. 19, pp. 205–214, 2019.

[56] S. Das, M. Aguayo, V. Dey, R. Kachala, B. Mobasher, G. Sant, and N. Neithalath, "Cement & Concrete Composites The fracture response of blended formulations containing limestone powder : Evaluations using two-parameter fracture model and digital image correlation," vol. 53, pp. 316–326, 2014.

[57] G. L. Golewski, "Measurement of fracture mechanics parameters of concrete containing fly ash thanks to use of Digital Image Correlation (DIC) method," vol. 135, pp. 96–105, 2019.

[58] A. Madadi, H. Eskandari-Naddaf, R. Shadnia, and L. Zhang, "Digital image correlation to characterize the flexural behavior of lightweight ferrocement slab panels," *Construction and Building Materials*, vol. 189, pp. 967–977, 2018.

[59] M. Ghahremannejad, M. Mahdavi, A. E. Saleh, S. Abhaee, and A. Abolmaali, "Experimental investigation and identification of single and multiple cracks in synthetic fiber concrete beams." 2018.

[60] H. Nguyen, V. Carvelli, E. Adesanya, P. Kinnunen, and M. Illikainen, "High performance cementitious composite from alkali-activated ladle slag reinforced with polypropylene fibers," *Cement and Concrete Composites*, 2018.

[61] M. Kuna, *Finite elements in fracture mechanics*. Springer, 2013.

[62] C. E. Inglis, "Stresses in a plate due to the presence of cracks and sharp corners," *Trans Inst Naval Archit*, vol. 55, pp. 219–241, 1913.

[63] G. R. Irwin, "Fracturing of metals," *ASM, Cleveland*, vol. 147, p. 19, 1948.

[64] G. R. Irwin, "Onset of fast crack propagation in high strength steel and aluminum alloys," tech. rep., 1956.

[65] G. R. Irwin, "Analysis of stresses and strains near the end of a crack traversing a plate," *J. appl. Mech.*, 1957.

[66] H. M. Westergaard, "Bearing pressures and cracks," *Journal of applied mechanics*, vol. 6, no. 2, pp. A49–A53, 1939.

[67] T. L. Anderson, *Fracture mechanics: fundamentals and applications*. 2017.

[68] D. Broek, "Elementary engineering fracture mechanics.pdf," 1986.

[69] H. Tada, P. C. Paris, and G. R. Irwin, "The Stress Analysis of Cracks Handbook, Third Edition," *Handbook, Del Research Corporation*, 1985.

[70] I. Genois, "FRACTURE RESISTANCE OF MICRO-FIBER REINFORCED CEMENT COMPOSITES," no. October, 1995.

[71] M. F. Kaplan, "Crack propagation and the fracture of concrete," in *Journal Proceedings*, vol. 58, pp. 591–610, 1961.

[72] S. Kumar and S. V. Barai, *Concrete Fracture Models and Applications*. 2011.

[73] J. Glucklich, "Fracture of plain concrete," *Journal of the Engineering Mechanics Division*, vol. 89, no. 6, pp. 127–138, 1963.

[74] D. J. Naus and J. L. Lott, "Fracture toughness of Portland cement concretes," in *Journal Proceedings*, vol. 66, pp. 481–489, 1969.

[75] S. P. Shah and F. J. McGarry, "Griffith fracture criterion and concrete," *Journal of the Engineering Mechanics Division*, vol. 97, no. 6, pp. 1663–1676, 1971.

[76] P. F. Walsh, "Fracture of plain concrete," *Indian Concrete Journal*, vol. 46, no. 11, 1972.

[77] J. H. Brown, "Measuring the fracture toughness of cement paste and mortar," *Magazine of Concrete Research*, vol. 24, no. 81, pp. 185–196, 1972.

[78] C. E. Kesler, D. J. Naus, and J. L. Lott, "Fracture mechanics-its applicability to concrete," in *Proceedings of the Society of Materials Science Conference on the Mechanical Behavior of Materials.*, no. Conf Paper, 1972.

[79] J. H. Brown and C. D. Pomeroy, "Fracture toughness of cement paste and mortars," in *ICF3, Munich (Germany) 1973*, 1973.

[80] P. F. Walsh, "Crack initiation in plain concrete," *Magazine of Concrete Research*, vol. 28, no. 94, pp. 37–41, 1976.

[81] A. Hillerborg, M. Modéer, and P.-E. Petersson, "Analysis of crack formation and crack growth in concrete by means of fracture mechanics and finite elements," *Cement and concrete research*, vol. 6, no. 6, pp. 773–781, 1976.

[82] G. I. Barenblatt, "The formation of equilibrium cracks during brittle fracture. General ideas and hydrotheses: Axially-symmetric cracks," *J. Appl. Math. Mech.*, vol. 23, pp. 622–636, 1959.

[83] G. I. Barenblatt, "The mathematical theory of equilibrium cracks in brittle fracture," in *Advances in applied mechanics*, vol. 7, pp. 55–129, Elsevier, 1962.

[84] Z. P. Bažant, "Concrete fracture models : testing and practice," vol. 69, pp. 165–205, 2002.

[85] R. D. Recommendation, "Determination of the fracture energy of mortar and concrete by means of three-point bend tests on notched beams," *Materials and structures*, vol. 18, no. 106, pp. 285–290, 1985.

[86] A. Hillerborg, "Analysis of fracture by means of the fictitious crack model, particularly for fibre reinforced concrete," *International journal of cement composites*, vol. 2, no. 4, pp. 177–184, 1980.

[87] Y. Jenq and S. P. Shah, "Two Parameter Fracture Model for Concrete," *Journal of Engineering Mechanics*, vol. 111, no. 10, pp. 1227–1241, 1985.

[88] S. P. Shah, "Determination of fracture parameters (K(Formula presented.) and CTODc) of plain concrete using three-point bend tests," *Materials and Structures: Matériaux et Construction*, vol. 23, no. 6, pp. 457–460, 1990.

[89] S. R. Ratanalert and M. Wecharatana, "Evaluation of existing fracture models in concrete," *Special Publication*, vol. 118, pp. 113–146, 1990.

[90] A. Carpinteri, F. Berto, G. Fortese, C. Ronchei, D. Scorza, and S. Vantadori, "Modified two-parameter fracture model for bone," *Engineering Fracture Mechanics*, vol. 174, pp. 44–53, 2017.

[91] B. Cotterell and J. Rice, "Slightly curved or kinked cracks," *International journal of fracture*, vol. 16, no. 2, pp. 155–169, 1980.

[92] H. Kitagawa, R. Yuuki, and T. Ohira, "Crack-morphological aspects in fracture mechanics," *Engineering Fracture Mechanics*, vol. 7, no. 3, pp. 515–529, 1975.

[93] E. 197-1, "Composition, spécifications et critères de conformité des ciments courants," in *Ciment*, 2001.

[94] "https://www.buzziunicem.it/web/italia/-/tipo-ii-a-ll-42-5-r," 2019.

[95] XP, "P 18-545, Granulats Éléments de définition, conformité et codification," tech. rep., 2004.

[96] UNI, "EN 196-1:2005 European Recommendation. Methods of testing cement - Part 1: determination of strength," tech. rep., 2005.

[97] C. Po, "Sabbia silicea umida del fiume po," tech. rep., Bacchi. S.P.A, 2015.

[98] E. 1097-6, "Détermination de la masse volumique réelle et du coefficient d'absorption d'eau," in *Essais pour déterminer les caractéristiques mécaniques et physiques des granulats*, 2001.

[99] C. 200 L, "Retardated high range water reducer - superplasticiser for ready mixed concrete," tech. rep., Ruredil S.p.A., 2009.

[100] A. Al-Khanbashi, K. Al-Kaabi, and A. Hammami, "Date palm fibers as polymeric matrix reinforcement: Fiber characterization," *Polymer Composites*, vol. 26, no. 4, pp. 486–497, 2005.

[101] M. S. Salit, M. Jawaid, N. B. Yusoff, and M. E. Hoque, "Manufacturing of natural fibre reinforced polymer composites," *Manufacturing of Natural Fibre Reinforced Polymer Composites*, pp. 1–383, 2015.

[102] A. Bendahou, A. Dufresne, H. Kaddami, and Y. Habibi, "Isolation and structural characterization of hemicelluloses from palm of Phoenix dactylifera L.," *Carbohydrate Polymers*, vol. 68, no. 3, pp. 601–608, 2007.

[103] J. R. Mohanty, S. N. Das, H. C. Das, and S. K. Swain, "Effect of chemically modified date palm leaf fiber on mechanical, thermal and rheological properties of polyvinylpyrrolidone," *Fibers and Polymers*, vol. 15, no. 5, pp. 1062–1070, 2014.

[104] J. Pan, S. Qi, Y. Lu, J. Fan, X. Zhang, J. Zhou, and J. Peng, "Intraventricular craniopharyngioma: Morphological analysis and outcome evaluation of 17 cases," *Acta Neurochirurgica*, vol. 153, no. 4, pp. 773–784, 2011.

[105] E. 1015-3, "Détermination de la consistance du mortier frais," in *Méthodes d'essai des mortiers pour maçonnerie*, 1999.

[106] E. 1015-10, "Determination of dry bulk density of hardened mortar," in *Methods of test for mortar for masonry*, 2007.

[107] D. R. RILEM, "50-FMC Committee Fracture Mechanics of Concrete,âĂIJDetermination of the fracture energy of mortar and concrete by means of three-point bending tests on notched beamsâĂİ," *Materials and Structures*, vol. 85, no. 85, pp. 285–290, 1985.

[108] .-F. RILEM Technical Committee, "Determination of fracture parameters (KsIC and CTODc) of plain concrete using three-point bend tests, proposed RILEM draft recommendations," *Materials and structures*, vol. 23, pp. 457–460, 1990.

[109] S. Vantadori, A. Carpinteri, G. Fortese, C. Ronchei, and D. Scorza, "Mode I fracture toughness of fibre-reinforced concrete by means of a modified version of the two-parameter model," *Procedia Structural Integrity*, vol. 2, pp. 2889–2895, 2016.

[110] A. Carpinteri, G. Fortese, C. Ronchei, D. Scorza, and S. Vantadori, "Mode I fracture toughness of fibre reinforced concrete," *Theoretical and Applied Fracture Mechanics*, vol. 91, pp. 66–75, 2017.

[111] S. Yoneyama and G. Murasawa, "Digital image correlation," *Experimental mechanics*, vol. 207, 2009.

[112] X. Xie, Z. Zhou, M. Jiang, X. Xu, Z. Wang, and D. Hui, "Cellulosic fibers from rice straw and bamboo used as reinforcement of cement-based composites for

remarkably improving mechanical properties," *Composites Part B: Engineering*, vol. 78, pp. 153–161, 2015.

[113] F. N. A. Farah Nora, S. M. Bida, N. A. M. Nasir, and M. S. Jaafar, "Mechanical properties of lightweight mortar modified with oil palm fruit fibre and tire crumb," *Construction and Building Materials*, vol. 73, pp. 544–550, 2014.

[114] G. Araya-Letelier, F. C. Antico, M. Carrasco, P. Rojas, and C. M. García-Herrera, "Effectiveness of new natural fibers on damage-mechanical performance of mortar," *Construction and Building Materials*, vol. 152, pp. 672–682, 2017.

[115] K. Pickering, M. A. Efendy, and T. Le, "A review of recent developments in natural fibre composites and their mechanical performance," *Composites Part A: Applied Science and Manufacturing*, vol. 83, pp. 98–112, apr 2016.

[116] M. Boumhaout, L. Boukhattem, H. Hamdi, B. Benhamou, and F. Ait Nouh, "Thermomechanical characterization of a bio-composite building material: Mortar reinforced with date palm fibers mesh," *Construction and Building Materials*, vol. 135, pp. 241–250, 2017.

[117] A. Alawar, A. M. Hamed, and K. Al-Kaabi, "Characterization of treated date palm tree fiber as composite reinforcement," *Composites Part B: Engineering*, vol. 40, no. 7, pp. 601–606, 2009.

[118] H. Savastano, P. G. Warden, and R. S. Coutts, "Mechanically pulped sisal as reinforcement in cementitious matrices," *Cement and Concrete Composites*, vol. 25, no. 3, pp. 311–319, 2003.

[119] P. Soroushian, Z. Shah, and J. P. Won, "Optimization of wastepaper fiber-cement composites," *Materials Journal*, vol. 92, no. 1, pp. 82–92, 1995.

[120] S. Vantadori, A. Carpinteri, L. P. Guo, C. Ronchei, and A. Zanichelli, "Synergy assessment of hybrid reinforcements in concrete," *Composites Part B: Engineering*, vol. 147, no. April, pp. 197–206, 2018.

[121] A. C1018, "Standard test method for flexural toughness and first-crack strength of fiber-reinforced concrete (using beam with third-point loading)," in *Annual book of ASTM standards*, 2002.

[122] B. I. G. Barr and E. B. D. Hasso, "A study of toughness indices," *Magazine of concrete research*, vol. 37, no. 132, pp. 162–174, 1985.

[123] L. Bryars, R. Gettu, B. Barr, and A. Ariño, "Size effect in the fracture of fiber-reinforced high-strength concrete," *Fracture and damage in quasi-brittle structures. E & FN Spon, London*, pp. 319–326, 1994.

[124] V. S. Gopalaratnam, R. Gettu, S. Carmona, and D. Jamet, "Characterization of the toughness of fiber reinforced concretes using the load-CMOD response," *Proceedings FRAMCOS-2, edited by Wittmann, FH, AED1FICATIO Publishers, Freiburg*, pp. 769–782, 1995.

[125] D. Jamet, "Toughness of fiber-reinforced high-strength concrete from notched beam tests," *Special Publication*, vol. 155, pp. 23–40, 1995.